Extracellular Respiration by *Geobacter sulfurreducens*:

Electron pathways are optimized at the inner membrane and substrate interface

A DISSERTATION SUBMITTED TO THE
GRADUATE FACULTY OF
THE UNIVERSITY OF MINNESOTA

By

Lori Ann Zacharoff

IN PARTIAL FULFILLMENT OF THE REQUIREMENTS FOR THE DEGREE OF
DOCTOR OF PHILOSPHY

Advisor: Daniel Bond

September 2016

Acknowledgments

Science would not be science without criticism. Because of that it is easy to be overly critical of oneself. I would not have made it to graduate school in the first place without the mentorship of Dr. Janet Dubinsky. I will be forever grateful of her support, guidance and confidence building. As I embark on my own career in science I will do my best to make you proud of my conduct and of the challenges I take on.

Next of course, I would like to thank my advisor for taking me in. I will never forget the first few weeks of graduate school. Daniel Bond introduced me to a new world, and new questions and a new level of enthusiasm for pursing the unknown through science. The unwavering enthusiasm is what made the last five years special.

Though I only traveled to the University of East Anglia recently, I am very grateful to Dr. Julea Butt for the opportunity to learn the chemistry of multiheme cytochromes from the professionals. I am particularly thankful for the wisdom and patience of Dr. Marcus Edwards, Dr. Tony Blake, Dr. Jessica Van Wonderen.

I liked to thank my committee for the inestimable patience and guidance. Particularly, Dr. John Lipscomb, Dr. Jeffrey Gralnick and Dr. Burckhard Seelig for input on the composition of this document.

My dissertation work is obviously built on the shoulders of giants. None of this would have been possible without the help of Dr. Caleb Levar, Dr. Chi Ho Chan, Dr. Jon Badalementi and Dr. Misha Mehta.

And last but not least, my family, Mom, Dad and Amy, my friends through thick and thin: Emily, Lindsey, Shelly and Dana.

Abstract

Iron is the fourth most abundant element in the Earth's crust. Part of the biogeochemical cycling of iron occurs in stratified ecological zones in the anoxic layer in a process aided by dissimilatory metal reducing bacteria. *Geobacter sulfurreducens* is a model organism for this respiratory process. This organism harnesses respiratory energy from the metabolism of substrates with a low amount of available free energy. Since metal reduction occurs extracellularly, metabolic electrons have to be transferred distances that are measured in micrometers. The final step of metal respiration requires *G. sulfurreducens* to make direct contact with extracellular metals and then transfer electrons to extracellular metals through insulating membrane barriers. The metals respired add another level of complexity to respiration. For example, insoluble iron oxides change electrical potential and degree of solubility while being reduced. Currently, the molecular mechanism of the metal reducing processes has yet to be elucidated but multiheme cytochromes are known to be involved.

This dissertation focuses on the inner membrane cytochrome CbcL. The goal was to find a protein that is capable of coupling the movement of electrons to the generation of a proton motive force in the inner membrane. Physiological and electrochemical approaches described in this dissertation support the conclusion that CbcL is an inner membrane protein important for extracellular metal respiration. CbcL functions in a way that is specific to the redox potential of the terminal electron acceptor. This provides a mechanism for precisely coupling energy harvesting to the amount of free energy provided by the extracellular terminal electron acceptor.

Further, this dissertation contains evidence that the final step of electron transfer to metals involves the protein PgcA. Using biochemical, electrochemical and phenotypic analyses, PgcA adheres to insoluble metals, has apparent electron

shuttling properties and is required by *G. sulfurreducens* only for reduction of insoluble metals and not soluble ferric citrate or poised electrodes.

Table of Contents

List of Tables

Chapter 1

Chapter 2

Chapter 3

Chapter 5

List of Figures

Chapter 1

Chapter 2

Chapter 3

Chapter 4

Chapter 5

Chapter 6

List of Equations

Chapter 1

Chapter 2

Chapter 5

Chapter 1: Introduction

1.1 Geobacter sulfurreducens

1.1.1 Fundamental features of *Geobacter sulfurreducens* and its native habitat

The entirety of the Earth's surface exists as stratified ecological zones, and one of the most important is the oxic-anoxic interface. The location of this interface is determined by characteristics of the soil or sediment, but in all cases, it supports a wide diversity of energetic strategies. Microorganisms thrive in these anaerobic environments by employing respiratory systems based on prevalent terminal electron acceptors such as humic substances, nitrate, sulfate, ferric iron oxide species and insoluble manganese oxides (Lovley and Phillips, 1986; Thamdrup 2000; Canfield, Rosing, and Bjerrum 2006; Nealson and Saffarini 1994). Dissimilatory metal reducing bacteria, such as those found in the genus *Geobacter*, are ubiquitous in ferruginous anoxic zones common to marine and freshwater sediments, as well as soils, anaerobic digestors, and deep subsurface sites. The organism examined in this dissertation, *Geobacter sulfurreducens,* was originally isolated from sediments in a near-surface ditch in Norman, Oklahoma (Caccavo et al. 1994).

Since most iron- and manganese- containing minerals are insoluble at neutral pH, dissimilatory metal reduction is an extracellular process that requires respiratory electrons to be transferred out of the bacterium to the terminal electron acceptor (Weber, Achenbach, and Coates, 2006). While some bacteria, such as *Shewanella oneidensis* (Canstein et al 2008), *Pseudomonas aeruginosa* (Rabaey et al. 2004) and *Geothrix fermentans* (Mehta-Kolte and Bond 2012; Kelly P Nevin and Lovley 2002) are known to use secreted electron shuttles, the biochemical systems for metal reduction in *G. sulfurreducens* are clearly different (contrasted in Figure 1.1). Evidence that direct contact was essential for reduction by *Geobacter* was first observed with metal oxides, (Nevin and Lovley 2002; Nevin and Lovley 2000) and

was later observed with cells attached to electrodes (Bond et al. 2002; Reguera et al. 2006; Marsili, Sun, and Bond 2010). This requirement for contact-mediated direct electron transfer makes *G. sulfurreducens* one of the most important models for this mode of long-range electron transfer, and may explain why *Geobacter* is so adept at using poised electrodes as electron acceptors (Nevin et al. 2008).

There is an intense interest in deciphering the respiratory mechanism of the anaerobic environmental bacterium *Geobacter sulfurreducens.* The novelty of the respiratory system in *G. sulfurreducens* is not only linked to the bacterium's ability to use iron and manganese (Caccavo et al. 1994), uranium (Gorby and Lovley 1993; Wall and Krumholz 2006), and poised electrodes (Bond et al. 2003) as terminal electron acceptors, but also to its ability to form conductive biofilms. While other organisms can transfer electrons to poised electrodes, *G. sulfurreducens* can form a conductive layer of cells, allowing electrons to travel micron-scale distances and support current densities over ten times higher than cells that grow as monolayers (Bond et al. 2003; Marsili, Sun and Bond 2010; Schrott et al 2014; Snider et al. 2012).

The molecular mechanism of respiration and electron transfer by *Geobacter* representatives remains elusive. Past research focused on extracellular electron transfer and outer membrane proteins has only hinted at the molecular mechanism that relays metabolic electrons to terminal electron acceptors. Moreover no research has revealed proteins involved in coupling electron transfer to energy conservation at the inner membrane, until the research presented here.

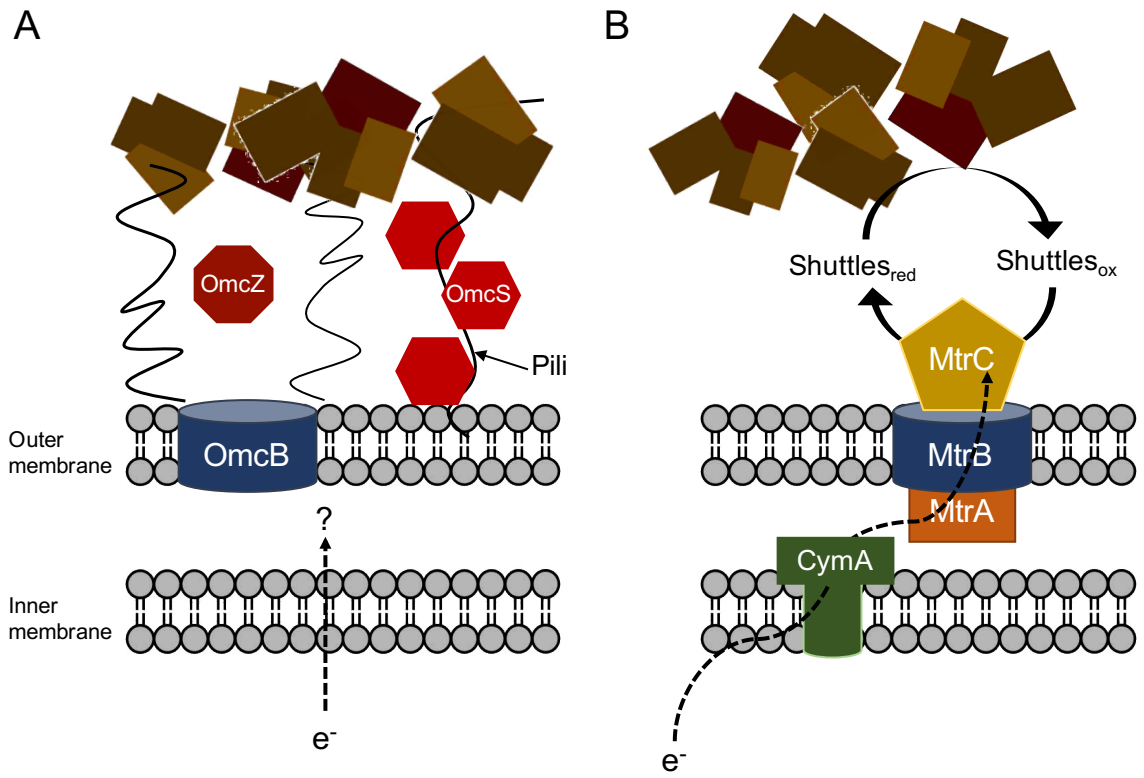

Figure 1.1 *Comparison of molecular models of* G. sulfurreducens *extracellular respiration and* S. oneidensis *extracellular respiration.* A. The direct contact method of *Geobacter sulfurreducens*. This organism produces a complex extracellular matrix that includes multiheme *c*-type cytochromes (such as OmcS, OmcZ) and pili. B. *Shewanella oneidensis* diffusible redox mediator method. Respiratory electrons traverse the inner membrane using CymA. CymA then relays the electrons to an Mtr system such as MtrABC. This complex reduces secreted redox active shuttles.

1.1.2 Three mysteries of metal respiration and electrode respiration by *Geobacter sulfurreducens*

The respiratory strategy of *Geobacter sulfurreducens* presents many energetic mysteries. It is not known how the respiratory mechanisms in *G. sulfurreducens* are able to overcome these challenges at the molecular level. For example:

1. The energy available to provide a driving force for respiration is relatively small, with the available free energy based on the electron acceptor (such as iron oxides ranging from -0.3 V to 0.3 V) being only a fraction of that of

oxygen (at an accepting potential of 0.82 V). As negatively charged electrons leaving the cell to reduce metals represents net dissipation of the proton motive force, energy conservation at the inner membrane has to be highly efficient.

2. The terminal electron acceptors themselves are highly complex and variable. Insoluble Fe(III) oxides alone are known to exist in 15 different forms that have a range of redox potentials, particles sizes, crystallinities, and doping structures (Thamdrup 2000; Cornell and Schwertmann 2003; Majzlan, 2012). If metals change redox potential and form while being reduced, different energetic strategies may need to be employed during reduction of a single mineral (Nealson and Saffarini 1994).
3. The distance that electrons must travel during respiration is far: physiologically relevant between-protein and between-redox centers electron transfer events span distances measured in angstroms (Gray and Winkler 2009). Respiratory electrons from *G. sulfurreducens* must travel across electrically insulating membranes, periplasmic spaces, and in some cases through micrometers of biofilm in order to reach the terminal acceptor.

I address the first two problems here by reporting the discovery and characterization of the multiheme protein CbcL. The third mystery is approached through new evidence for a role for the protein PgcA in metal reduction, and a comparison of this protein to known extracellular shuttles. The details of these experiments and rationale are at the end of this introduction, after a review of relevant literature and techniques that will put the three mysteries of *G. sulfurreducens* respiration in context.

1.1.3 Multiheme insoluble metal respiratory complex of *Shewanella oneidensis*.

Shewanella oneidensis MR-1 has the most well-described extracellular metal respiration pathway, to date (Figure 1.1B). Under anaerobic conditions, *S.*

oneidensis expresses the inner membrane tetraheme *c*-type cytochrome CymA, which serves as an electron hub, receiving metabolic electrons from the menaquinone pool and then transferring those electrons to periplasmic carriers (McMillan et al. 2013; Marritt, McMillan, et al. 2012; Marritt, Lowe, et al. 2012). For nearly every extracellular terminal electron acceptor provided, terminal electrons will first pass through CymA (Coursolle and Gralnick 2012; Myers and Myers 2000). The outer membrane electron transfer event then occurs via multiheme *c*-type cytochrome – porin complexes: primarily MtrABC and its paralog MtrDEF. The recently solved crystal structure of MtrF revealed a chain of 10 hemes, all within 6 Å of each other, sufficient for rapid electron transfer through the protein. Together with a decaheme protein on the inner face of the membrane, these complexes create a pathway for crossing the ~20 nm wide outer membrane. The isolated MtrABC protein complex will reduce a variety of electron acceptors, such as ferric citrate, goethite (and insoluble iron oxide), and flavin mononucleotide (FMN). As FMN is secreted by *Shewanella* into the extracellular space, and reduced FMN can be oxidized by other insoluble metals and electrodes, flavin-based shuttling is used by *Shewanella* to access acceptors not in contact with the cell membrane (Kotloski and Gralnick 2013; Hartshorne et al. 2009) (and reviewed extensively, for example (Richardson et al. 2012)).

1.1.4 Known functionality of *Geobacter sulfurreducens* multiheme *c*-type cytochromes.

There are many biochemical studies of *G. sulfurreducens* multiheme *c*-type cytochromes. The most definitive studies have focused on periplasmic and extracellular cytochromes which are highly abundant and soluble. Two extracellular cytochromes, OmcZ and OmcS, have both biochemical and phenotypic data available. The midpoint reduction potential of the octaheme protein OmcZ is centered at -220 mV versus the standard hydrogen electrode (SHE), but spans a very wide window (-420 to -60 mV). The purified protein can be oxidized by ferric citrate, Mn(IV) oxide, Au(III), and Cr(VI) but not Fe(III) oxides.

When the gene for OmcZ is disrupted, current production on poised electrodes is decreased, but reduction of Fe(III)-oxides is unaffected (Nevin et al 2008; Inoue et al. 2010).

The hexaheme cytochrome OmcS has a midpoint potential of -212 vs. SHE, and is reduced over a window more narrow than OmcZ (−360 to −40 mV). OmcS can reduce the same metals as OmcZ, but also reduces Fe(III) oxides (Leang et al. 2010; Qian et al. 2011). Expression of *omcS* is increased during growth with Fe(III) oxides compared to Fe(III) citrate, and deletion of *omcS* diminishes Fe(III)-oxide but not Fe(III) citrate reduction (Coppi et al 2008). These phenotypes, along with the observation that OmcS is found extracellularly and aligned along Type IV pili (Leang et al 2010), make OmcS a candidate for involvement in the terminal steps of insoluble metal reduction by *G. sulfurreducens*. The phenotype and extracellular localization of OmcZ suggests a role in electron transfer during poised electrode reduction. More recently, evidence has been acquired supporting the hypothesis that the outer membrane protein OmcB, along with other proteins (OmbA, OmbB), functions as an outer membrane conduit in a manner similar to the Mtr system of *S. oneidensis* (Liu et al. 2014).

While detailed information, and possible roles for these three cytochromes is available, this is only a fraction of the cytochromes in the genome (Methé et al. 2003), and most *G. sulfurreducens* cytochromes lack homologs in other any other organism. Transposon mutagenesis experiments were very successful in identifying metal reduction pathways in *S. oneidensis*, such as the original Tn*phoA* mutant unable to reduce Fe(III)-citrate that led to discovery of the CymA inner membrane cytochrome (Myers and Myers 1997). However, when a similar transposon mutagenesis approach was conducted with *G. sulfurreducens* (Rollefson et al. 2009) few cytochrome genes essential for specific growth conditions were found. A hypothesis for why this approach failed can be seen in data from gene disruption of specific cytochromes in *G. sulfurreducens*, where

many partial or leaky phenotypes are reported (Aklujkar et al. 2013; Leang, Coppi, and Lovley 2003; Mehta et al. 2005). It is possible that due to the complexity of multiheme cytochromes expressed by *G. sulfurreducens*, many phenotypes are not sufficiently negative, so as to be selected, during screening. This dissertation work narrows down these complications by examining more closely a subset of putative inner membrane multiheme cytochromes.

1.1.5 Proton motive force in the energetic extremes

The establishment of a chemiosmotic gradient by electron transfer or redox-coupled reactions is used by most forms of life to drive ATP synthesis by ATP synthase (Nicholls and Ferguson 2002). The chemiosmotic hypothesis originally proposed by Mitchell in 1961 (Mitchell 1961) has been reviewed extensively (Mitchell 1979; Richardson and Sawers 2002; Simon, van Spanning, and Richardson 2008). As formalized by Mitchell, the side of the membrane where protons, or positive charge, accumulate is denoted as the "P" side, while the opposite or negative face is the "N" side. In neutrophilic bacteria, the cytosolic compartment, N side, typically has a net negative charge and a slightly more alkaline pH compared to the external growth medium, allowing proton or sodium ion influx that drives ATP synthesis via the F_1F_0 ATPase (Nicholls 2002). Thus, electron flow during respiration by an organism such as *Geobacter* is the net movement of protons and positive charge out of the cell, to establish proton motive force (*pmf*). The potential energy that can be harvested at the membrane can be mathematically expressed as the total voltage difference across a membrane, with both an electrical charge term, ψ, and a pH term (Equation 1.1), at 25 °C:

$$pmf\ (mV) = \Delta\psi - 59\Delta pH \qquad \text{(Eq. 1.1)}$$

As most measurements of *pmf* in respiratory bacteria are around -150 mV, and those for mitochondria are as high as -200 mV (Nicholls and Ferguson 2002), the free energy change of a redox reaction attempting to translocate a proton out of

the cell must exceed this value, on a per electron basis, and be significantly in excess if rapid reactions are to take place. For example, based on a ΔE of 240 mV (a common acceptor potential used by metal reducers) per electron under standard conditions, the coupling of the two-electron oxidation of NADH linked to menaquinone reduction represents enough energy to support the translocation of two to four protons out of the cell. However, small changes to the redox potential of the terminal electron acceptor could easily lower the ΔE to barely 100 mV, and limit this stoichiometry under physiological conditions.

This chain of redox reactions requires a terminal electron acceptor that has more oxidizing potential than its electron donor. Mitochondria exclusively use oxygen as the terminal electron acceptor. This is in contrast to bacteria, which are able to use a range of electron acceptors (Bird, Bonnefoy, and Newman 2011). Also typically required for a respiratory chain to function is a pool of lipid soluble redox mediators. The most common couples are ubquinone/ubiquinol (UQ/UQH_2) and menaquinone/menaquinol (MK/MKH_2), which shuttle electrons between inner membrane proteins (Simon, van Spanning, and Richardson 2008). Electrons generated from intracellular metabolism, such as the NAD^+/NADH couple (Figure 1.2) can be moved across the membrane and up the electrical gradient through redox cofactors including flavins (FMN and FAD), redox centers of iron (heme and iron-sulfur clusters), molybdenum, or copper-containing proteins. The standard electrical potentials, E_o', of these redox centers are controlled by the ligands in the protein that coordinate the metal ion. Refer to Figure 1.2 for examples of standard potentials found in the respiratory chain of both *G. sulfurreducens* and higher eukaryotes.

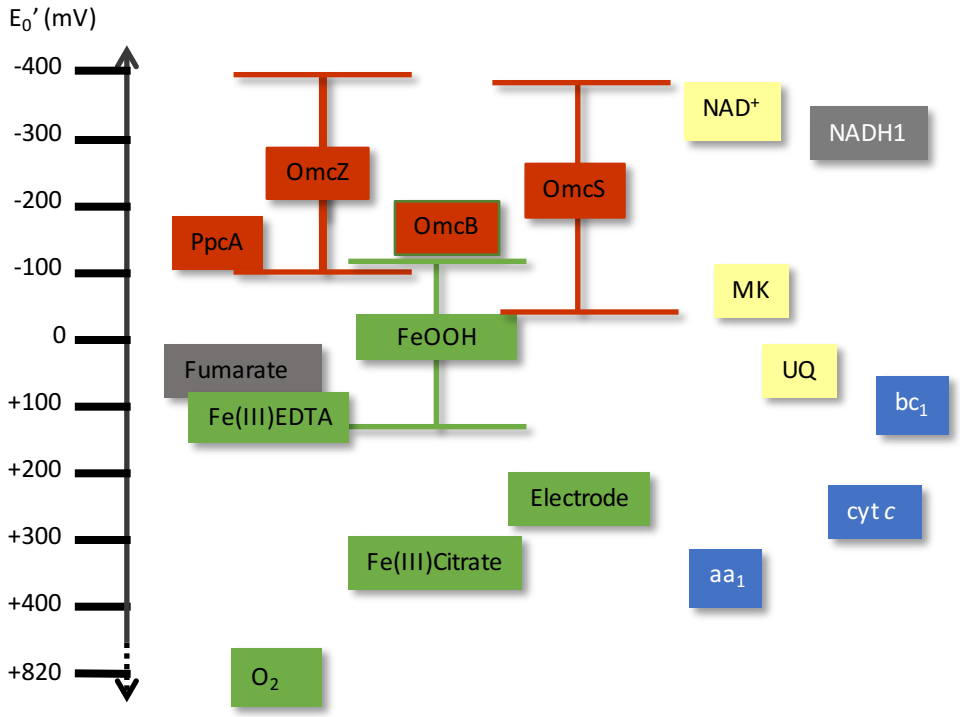

Figure 1.2 *A redox tower illustrating the differences in standard electrical potentials of redox mediators in iron and oxygen respiration.* Green= electron acceptors, red= examples of *G. sulfurreducens* cytochromes, yellow= physiological electron carriers, blue= small selection of redox centers in aerobic respiration

There are three categories of proteins that are known to generate *pmf*. 1) Redox-driven "pumps", that physically translocate protons or sodium during enzyme turnover, 2) pairs of redox proteins that cycle quinones or membrane-soluble carriers known as 'redox loops', and 3) light-driven rhodopsin-based pumps. Of these strategies, the first two are common in metal-reducing bacteria.

While there are only a few examples of the first category of *pmf* generation complexes, they are ubiquitous in eukaryotes and prokaryotes. For example, the proton-pumping NADH dehydrogenase complex otherwise known as Complex I is widespread in bacteria, where it is often denoted "*nuo*" for NADH ubiquinone oxidreductase. It couples reduction of quinones to large-scale protein domain movements in antiporter-like domains to translocate protons. The terminal

cytochrome *c* oxidase in aerobic bacteria and mitochondria is also a proton pump, but differs from Complex I in that it uses metal centers to directly move protons during electron transfer (Simon, van Spanning, and Richardson 2008). The second category of *pmf* generating enzymes is much more diverse, as these enzymes only need to interact with the quinone pool on opposite sides of the membrane, or catalyze reactions on opposite sides of the membrane to contribute to electrogenic proton movement. A specialized subset of quinone oxioreductases, known as bc_1 (or Complex III in mitochondria) generate additional *pmf* by what Mitchell named the "Q-cycle". In this case, quinol oxidation releases two protons on the P side of the membrane, but one electron is diverted to a high potential FeS cluster while the other flows to a low-potential cytochrome *b*. After a second quinol oxidation, the heme *b* can catalyze quinone reduction on the N side of the membrane allowing two additional protons to be transported out of the cell.

The activity of bc_1 – like quinone oxioreductases, and their involvement in redox loops and Q-cycles is of direct relevance to this dissertation. The popularity of this system in anaerobic bacteria is likely due to the relatively small available free energy (compared to aerobes). Proteins with both *b*-type and *c*-type hemes (referred to here as Cbc-type proteins) can act as both quinone reductases and quinol oxidases, passing electrons from the quinone pool to an electron acceptor that is either P facing or N facing, and the protons released from the quinone can be deposited on the P or N face. These quinone oxioreductases can be paired with other enzymes in highly modular fashion, and could allow for unique or variable proton/electron stoichiometries (for a discussion of every possible permutation the reader is referred to Simon, van Spanning, and Richardson 2008).

Figure 1.3 illustrates the effect of quinone interaction sites at opposite faces of the membrane. In this instance, the electron donors and acceptors are oxidized and reduced on the P membrane face. This pair of reactions results in a proton motive force, and represents a known respiratory strategy of *S. oneidensis*. For example,

the quinone reductase could be a periplasmic formate dehydrogenase, and the quinol oxidase could be CymA, which can then transfer electrons to a terminal acceptor such as periplasmic fumarate reductase (Simon, van Spanning, and Richardson 2008). In the case of the illustration in Figure 1.3, two protons are translocated per two-electron reaction, and the H^+/e^- ratio is 1.

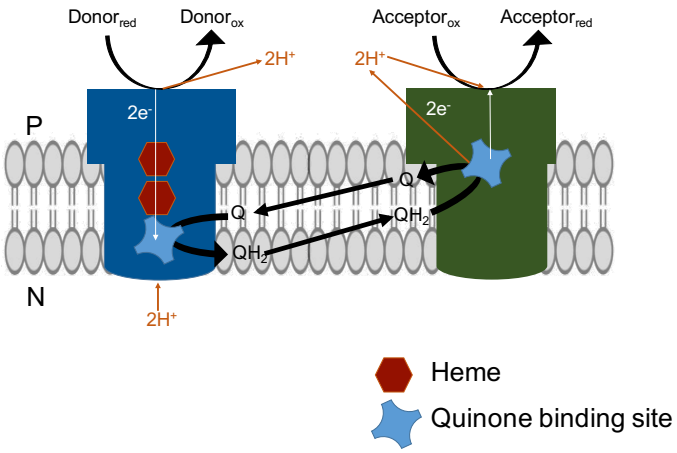

Figure 1.3 *An example of a proton motive quinone cycle.* The quinol oxidase is green and the quinone reductase is blue. Adapted from Simon, van Spanning, and Richardson 2008.

The energy available to an organism is dependent on the change in the Gibbs free energy (ΔG) of the entire respiratory process. Insoluble iron oxides range in potential from -0.3 V to 0.3 V versus standard hydrogen electrode (SHE). Soluble ferric citrate at 0.37 V as well as other relatively higher potential chelated metals are also available (Majzlan 2012).

1.1.6 The inner membrane of *Geobacter sulfurreducens* has many putative quinone oxidoreductases

The quinone oxidoreductase used by *G. sulfurreducens* during metal respiration has been sought after for many years (Butler 2009; Ding 2008; Aklujkar 2013). While Butler (2009) first proposed a role for different inner membrane complexes based on their conservation across *Geobacter* genomes, Aklujkar (2013) made the

first attempt at systematically identifying inner membrane proteins important for respiration to metals in *G. sulfurreducens*. Transcriptomic profiles of *Geobacter sulfurreducens* during growth with insoluble iron oxides and manganese oxides were compared to transcriptomic profiles during soluble ferric citrate reduction. This paper laid out a nomenclature for five operons that encode proteins containing hallmarks of quinone interactions (summarized in Table 1.1 and depicted in Figure 1.3). These operons vary in the number of genes encoded and range from the monocistronic Cbc1 operon to the five-gene Cbc5 operon. All but one operon contains a multiheme *c*-type cytochrome with a periplasmic domain protein. Other common occurrences include iron sulfur clusters, b/b_6 domains and hypothetical proteins with no known functional domains.

Table 1.1 lays out a more detailed description of these putative quinone oxioreductases, as well as what has been reported in expression and gene disruption experiments (Aklujkar et al. 2013). For example, more *cbcV* transcripts were found when *G. sulfurreducens* respired ferrihydrite than when respiring soluble ferric citrate, but when this *cbcV* gene was deleted, no metal reducing phenotype was detected. Interestingly, the subject of this dissertation, *cbcL,* was reported to <u>not</u> be important for metal respiration, because proteomic and transcriptional data did not target it for further study. Because of differences in metal preparation and the difficulties involved in obtaining RNA or protein from cells grown in the presence of insoluble metal oxides, it is not clear that these pioneer studies are reliable indicators of the function of these ‘Cbc’ complexes.

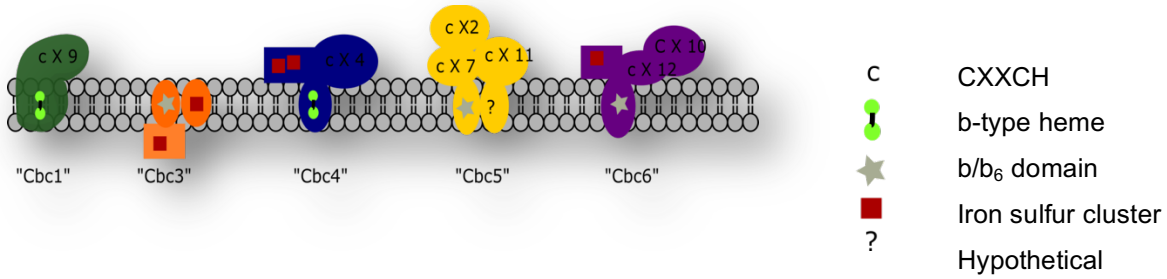

Figure 1.4 *Pictorial representation of proteins predicted by the cbc gene operons.* CXXCH is the canonical heme binding motif.

Table 1.1 *Summary of predicted properties of proteins encoded by* cbc *genes*. Transcriptomic and gene disruption strain phenotypes. Transcriptomic data is reported relative to expression from growth with ferric citrate. N/A means no data have been published.

Predicted Properties			Aklujkar (2013)		
Gene name	**Locus tag**	**Predicted domains**	**Ferrihydrite**	**Birnessite**	**Deletion strain phenotype**
Cbc1					
cbcL	GSU0274	*b*,*c*-type hemes	down	down	N/A
Cbc3					
cbcW	GSU1649	cytochrome b/b_6	No change	no change	N/A
cbcV	GSU1650	hypothetical	up	no change	no phenotype identified
cbcX	GSU1648	cytochrome b/b_6 complex, iron-sulfur subunit	N/A	N/A	
Cbc4					
cbcU	GSU0070	nrfD pfam domain (polysulfide reductase) *b*-type, oxidoreductase	up	up	N/A
cbcT	GSU0069	4Fe-4S, cytochrome b/b_6 complex	up	up	N/A
cbcS	GSU0068	*c*-type, 4 heme binding sites	up	down	no phenotype identified
Cbc5					
cbcD	GSU0591	HAMP domain, *c*-type, 1-2 heme binding sites	up	up	N/A
cbcB	GSU0593	hypothetical	up	N/A	N/A
cbcE	GSU0590	thiosulfate reductase cytochrome B subunit, cytochrome b(N-terminal)/b_6/petB	N/A	N/A	N/A
cbcA	GSU0594	*c*-type, 7-heme binding sites, Calcium binding site (EF hand)	up	no change	N/A
cbcC (*omcQ*)	GSU0592	c7-type trihaem cytochrome domains	N/A	N/A	essential for Mn(IV)
Cbc6					
cbcP	GSU2931	*b*-type	N/A	N/A	N/A
cbcQ	GSU2932	cytochrome b/b_6 complex, membrane protein subunit	N/A	N/A	N/A
cbcO	GSU2933	Reiske (2Fe-2S) iron-sulfur	N/A	N/A	N/A
cbcM	GSU2935	*c*-type (12 heme binding sites)	N/A	N/A	N/A
cbcN	GSU2934	*c*-type (10 heme binding sites)	up	no change	N/A
cbcR	GSU2930	*c*-type, 4 heme binding sites	up	no change	N/A

1.2 Cytochromes: A “Normal” Heme Containing Protein

1.2.1 Introduction

This section provides an introduction to heme and multiheme proteins. First, I will make the case that cytochromes are going to be an important part of respiration *Geobacter sulfurreducens*. A discussion of the techniques used to study multiheme proteins will be used illustrate the difficulty in assigning functions to multiheme proteins of *Geobacter sulfurreducens*. Some of the basic properties of the heme group itself and how these properties pertain to persisting questions of *G. sulfurreducens* respiration is also presented here.

1.2.2 An over-abundance of predicted cytochromes in *Geobacter sulfurreducens*

Multiheme cytochromes appear to be an important component of metal respiration which is immediately apparent in the genomes of the *Geobacteraceae* family of metal respiring bacteria. Here, it is assumed that in order to qualify as multiheme, a protein must have three or more predicted heme binding sequences, such as CXXCH (cysteine, any amino acid, any amino acid, cysteine, histidine). More rarely, CXXXCH (Glockner and Zumft 1996; Levar et al. 2014) and CXXCK (Einsle et al. 2000) have also been found in proteins, and these motifs are also counted when appropriate.

To date, there are 24 sequenced bacteria of the family *Geobacteraceae* (which includes 14 *Geobacter spp., 6 Desulfuromonas spp*., 3 *Pelobacter spp.*, and 2 *Geoalkalibacter spp*). 72 multiheme *c*-type cytochromes are encoded in the genome of *G. sulfurreducens*. Of these multiheme cytochromes there are ~30 cytochromes predicted to exist in the extracellular space, ~8 heme containing transmembrane complexes in the outer membrane, ~30 in the periplasm, and eight Cbc complexes built from 5 *b*-type heme proteins and 7 *c*-type multiheme proteins in the inner membrane (as shown in Table 1.1 above). Making functional

predictions for any of these proteins has yet to be accomplished since there is little homology to cytochromes with known function.

Pelobacter species are in the same lineage as freshwater *Geobacter* and marine *Desulfuromonas*, yet do not respire insoluble metals and instead ferment compounds such as benzene conjugated ring systems (D R Lovley et al. 1995; Brune and Schink 1990). The *Pelobacter carbinolicus* genome has only 6 mulitheme cytochromes (Aklujkar and Lovley 2010). While, Sharma et al. (2010) noted that multiheme *c*-type cytochromes are more abundant in Gram negative bacteria (Sharma, Cavallaro, and Rosato 2010) genomes of recently sequenced Gram positive metal reducing bacteria are also enriched in multiheme cytochromes. For example, the Gram positive metal-reducer *Thermincola ferriacetica* contains 35 multiheme proteins (Lusk et al. 2015). (Genome statistics of multiheme cytochromes listed here were generously provided by Jon Badalamenti. The Python script used to generate these statistics is available in Badalamenti et al. 2016).

1.2.3 The study of heme proteins

Heme consists of a macrocyclic tetrapyrrole backbone (Figure 1.4). The eight outward-facing carbons are known to be modified in nature and synthetically by different sidechains, while the four inward facing nitrogen atoms commonly coordinate metal ions such as iron (heme), magnesium (bacterio-chlorophyll) or cobalt (vitamin B_{12}). Synthetically, many other metals have been added such as cadmium, copper, nickel and zinc (Falk 1964). The minimal porphyrin structure is 8.5 Å in diameter and 4.7 Å in thickness. Planarity of the porphyrin is not necessarily maintained. Heme groups are ring systems that are fully substituted (at each carbon position,1 – 8) and coordinate an iron molecule. This molecule is sometimes referred to as protoporphyrin IX before iron addition and protoheme IX when the iron is coordinated (Munro et al 2009).

Type *c* heme prosthetic groups are covalently attached to the protein backbone via thioether linkages formed between two cysteines (in the CXXCH motif) and the 2 and 4 carbons of the porphyrin. Perpendicular to the plane of the porphyrin ring is the axial or z- axis of the iron. Amino acid sidechains from within the protein can provide axial coordination of the iron. The iron atom can become pentacoordinate, with one axial ligand, or hexacoordinate with two axial ligands (Figure 1.4C and D). Bis-histidine and histidine-methionine are common endogenous axial ligands in naturally occurring multiheme proteins (Kleingardner and Bren 2015; Falk, 1964).

The coordination of a heme can only be determined experimentally and in some cases, heme ligation can be altered during the course a reaction cycle. There are however, two broad rules that serve as starting points to determining the function of a multiheme cytochrome. First, bis-histidine coordinated heme groups are often thought to be used primarily for electron transfer. This kind of coordination has been prominent in those multiheme cytochromes that have been purified and characterized from metal reducing organisms. Secondly, pentacoordinate heme groups can more readily acquire exogenous axially ligands such as gases and ions. CymA for example, contains one pentacoordinate heme, two bis-histidine coordinated hemes and a histidine-lysine coordinated heme. While the specifics of the reaction mechanism are still being studied, it is assumed that the pentacoodinated heme (with the fifth ligation provided by a methionine, rather than a histidine from the CXXCH) serves as a reaction site and the other three heme groups function as an electron relay (Marritt et al. 2012).

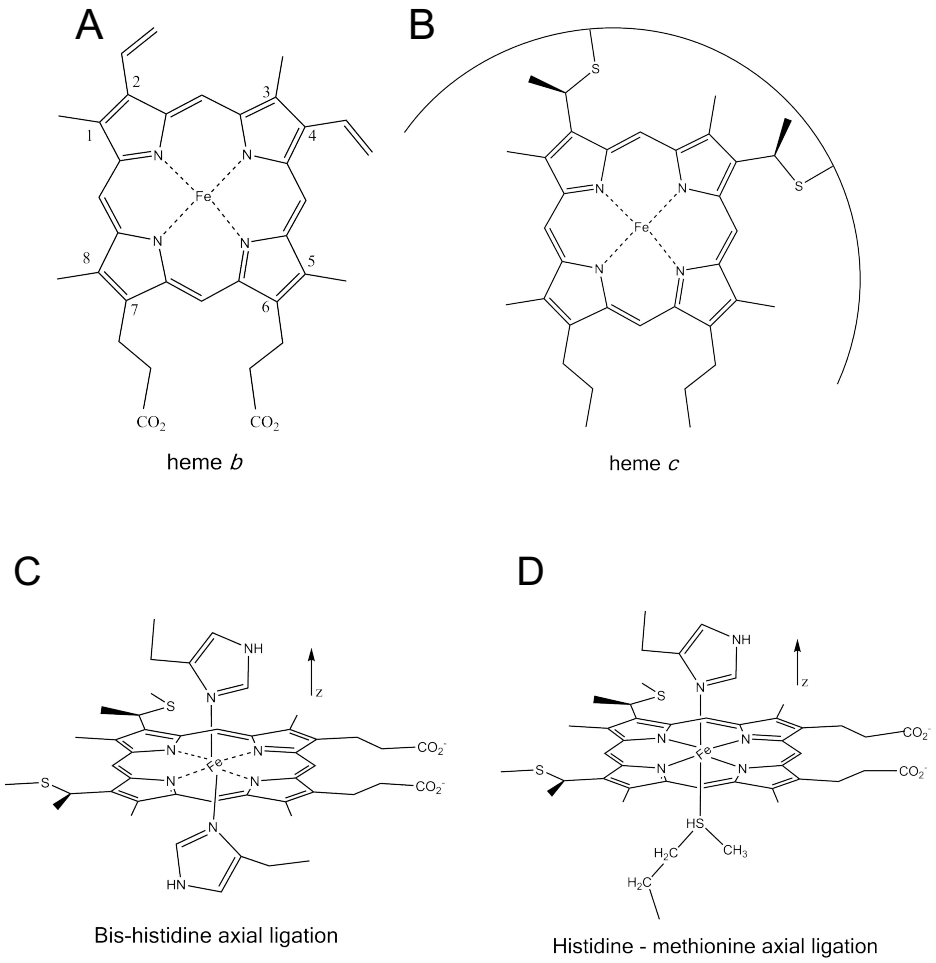

Figure 1.5 *Iron coordination by the porphyrin ring and common axial ligands in metal reducing organisms.* A. *b* – type heme. B. *c* – type heme. C. Bis-histidine axial ligands D. Histidine-methionine axial ligands. Figures were generated using ChemDraw Professional.

1.2.4 Heme function is hard to predict

Axial ligands and sidechain modification exist in a large array of combinations some found in nature and some synthetic. Despite this abundance, there are no rules that precisely predict the behavior of these redox active centers (Kleingardner and Bren 2015; Fufezan, Christian and Zhan 2008). Heme ligands have been called a “multi-purpose” tool because of the wide range of enzymatic reactions known to be catalyzed by an iron containing porphyrin (Munro 2009), such as

interaction with gases (hemoglobin), electron transfer (cytochrome *c*), and gene regulation (PAS domain; Londer et al. 2006). Redox-active heme groups are a common feature of respiratory chains. This one prosthetic group has the ability to perform so many functions in a regulated fashion because of the wide range of redox potentials achievable (Figure 1.6) and solvent accessibility/inaccessibility of the heme in the protein. *b*-type hemes have oxidation reduction potentials in a higher range compared to *c*-type hemes. The range in midpoint potentials of *c*-type hemes spans an entire volt (Kleingardner 2015)!

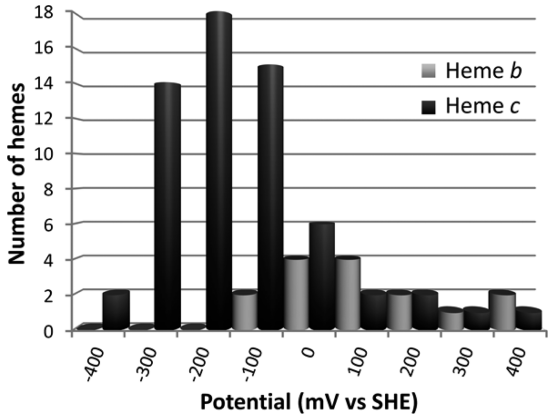

Figure 1.6 *Distribution of oxidation/reduction potentials of heme groups in proteins.* From Kleingardner, 2015.

1.2.5 Heme iron spin states, ligations and electron transfer capabilities

A main consideration when predicting the function of heme has been a particular heme's ability to achieve a high spin state or not. The *d* shell can contain up to ten electrons. Iron, in its elemental state, has six electrons in the *d* orbital and 2 electrons in the highest energy *s* orbital. In the case of the ionic states of the iron atom, Fe(II) still contains 6 electrons in the *d* orbitals and Fe(III) has five. When Fe(III) has five unpaired *d* electrons, the spin state is "high." When Fe(III) has one unpaired electron the spin is "low." An intermediate spin state is also possible with 3 unpaired *d* electrons. Similarly, Fe(II) has high, intermediate, and low spin states with 4, 2, and 0 unpaired *d* electrons, respectively. The axial ligands of the iron atom in a heme complex can influence the spin state of the electrons in iron. When

the ligand electron field is weak, the high spin state will be preferred because the energy required for an electron to invert its spin and become paired with an electron in a different *d* orbital is more than the energy needed for the same electron to remain unpaired. In general: high spin= maximum number of unpaired electrons, which occurs in the presence of weak field ligands. Additionally, there are no free *d* orbitals for high spin Fe(III) or Fe(II) (Silberberg 2003). For heme proteins, the bis-histidine axial ligation is common and a low spin state is favored. Generally, pentacoordinated heme iron will favor a high spin and hexacoordinate will favor a low spin. Thus far, prediction of heme potential based on axial ligation is not possible (as reviewed by J. Liu et al. 2014).

A number of exogenous effects can influence the spin state and oxidation potential. For instance, the heme group in hemoglobin changes affinity for the bound gas (oxygen or carbon dioxide) at different pH, a phenomenon known as the redox Bohr affect (Voet and Voet 2011). The *G. sulfurreducens* triheme cytochrome PpcA has a catalytic cycle that responds in redox Bohr manner. The three hemes are all bis-histidine coordinated but one of the hemes changes its affinity for a H^+ based on the redox status and conformation of the entire protein. The result is a protein that can bind and release a H^+ on demand. The authors of this study postulate that PpcA could act in concert with another, not yet identified, protein to act as a proton pump (Morgado et al. 2012). While the consequence of this protein's ability to bind and release protons at the level of the cell has yet to be determined, in general, the redox Bohr affect is highly relevant to *G. sulfurreducens* cells coexisting in a biofilm where the byproducts of metabolism include CO_2 and H^+. The existence of CO_2 and H^+ gradients in a biofilm are discussed further below (section 1.3.2).

The strength of the ligand fields for common ligands is: $I^- < Br^- < Cl^- < SCN^- < F^- < OH^- <$ oxalate $< H_2O < NH_3$ and pyridine < ethylenediamine < dipyridyl < o-phenanthroline $< NO_2^- <$ CN and CO (adapted from Campbell and Dwek, 1984).

Consideration of axial field ligand affects are also important for laboratory techniques such as the pyridine hemochrome assay discussed in Supplemental method 5.6 of this dissertation.

1.2.6 Spectroscopy is a powerful tool for monitoring and characterizing cytochromes

The porphyrin ring is a highly conjugated electronic environment created by many unsaturated bonds (Figure 1.4). The delocalization of electrons in the heme lowers the energy required for electronic transitions to occur. Electron delocalization causes longer wavelengths of light to be absorbed. When the iron atom is added the absorption peak in the Soret region, around 400 nm (sometimes referred to as γ), has a high extinction coefficient, sometimes exceeding 100,000 $M^{-1}cm^{-1}$ (Monro, 2009). When the heme iron is reduced, absorbance maxima are also formed at approximately 530 nm (β) and 552 nm (α) but these can shift depending on the type of heme and the heme environment. Figure 1.6 shows an oxidized and reduced spectrum of a triheme protein (PgcA) that exhibits classic heme features. Absorption of light in the Soret region cause electrons in the heme system to undergo $\pi \rightarrow \pi^*$ transitions, from bonding to antibonding π molecular orbitals (Campbell and Dwek 1984, Chapter 4). This makes the UV-visible spectrum a sensitive tool for monitoring the oxidation/reduction state of the heme. Illuminating a heme molecule with infrared radiation creates a charge transfer from the porphyrin to the iron atom. Generally, such charge-transfers occur in the ultraviolet and visible regions but the heme molecule is an exception. Charge-transfer spectra are highly sensitive to the effects of ligand field splitting. The near infrared region (900 nm to 1090 nm) has been useful in determining axial ligations of heme groups (Simpkin et al. 1989). The sensitivity to the absorbance spectra in the infrared region to molecular vibrations complicates characterization. Using the technique magnetic circular dichroism (MCD) enhances the signal to noise ratio. (Munro 2009 has examples of MCD spectra of heme groups with different axial ligations).

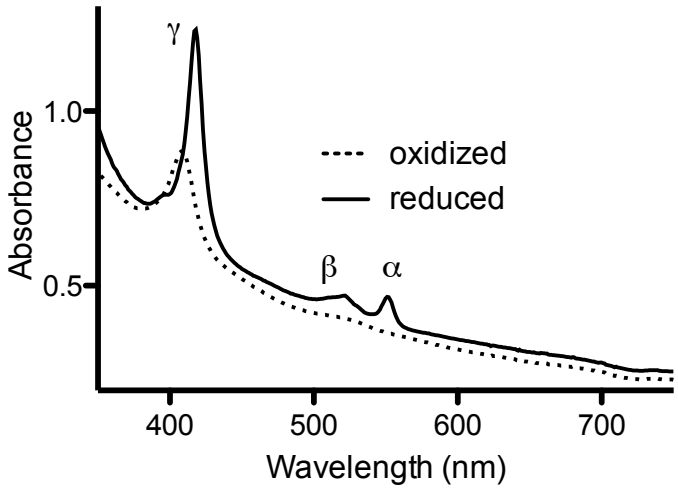

Figure 1.7 *Electronic absorbance spectra in the visible light region of* Geobacter sulfurreducens *cytochrome PgcA*.

1.3 Modeling the electrochemistry of extracellular electron transfer in *G. sulfurreducens* biofilms

1.3.1 Electrochemistry as a tool for investigating the respiratory pathway of *G. sulfurreducens*

While bioreactor design has varied greatly throughout the years and between labs, the design of the reactor for microbiological studies has recently converged. Figure 1.7A shows a photograph of the most recent generation of electrode bioreactors. The conical chamber holds 15 mL of fluid, contains a stir bar, and is kept at a constant 30 °C with a circulating water bath. All three electrodes (working, reference and counter) are placed in close proximity in the same chamber. The working electrode is a polished graphite flag with a surface area of 3 cm^2. The graphite flag is attached to a loop of platinum with a Teflon screw. The counter electrode is a piece of platinum wire. The reference electrode communicates with the solution across a Vycor frit. Calomel and Ag/AgCl are common reference electrodes. These electrodes are connected to a potentiostat. This system allows bacterial respiration to be continuously monitored in the form of electrical current.

An example of current production by a wild type *G. sulfurreducens* biofilm is shown in Figure 1.8B. At any time during growth different electrochemical techniques can be performed on the biofilm, such as cyclic voltammetry (CV). This procedure scans current production at different electrical potentials. The rate at which the working electrode sweeps across different redox potentials can be varied. An example of a cyclic voltamogram is shown in Figure 1.8C. A further discussion of the interpretation of cyclic voltamograms is covered below.

The work in this dissertation is reliant on results produced from *Geobacter sulfurreducens* biofilms that use poised electrodes as an endless source of terminal electron acceptor. When research began on *G. sulfurreducens* bioreactors in 2003, there were a lot of unresolved questions about what was actually being measured at the potentiostat. For instance, what is governing the electron transfer properties? In order to trust phenotypic measurements, it is necessary to discuss other possible reasons why electron transfer rates could be changing during growth and during a cyclic voltamogram.

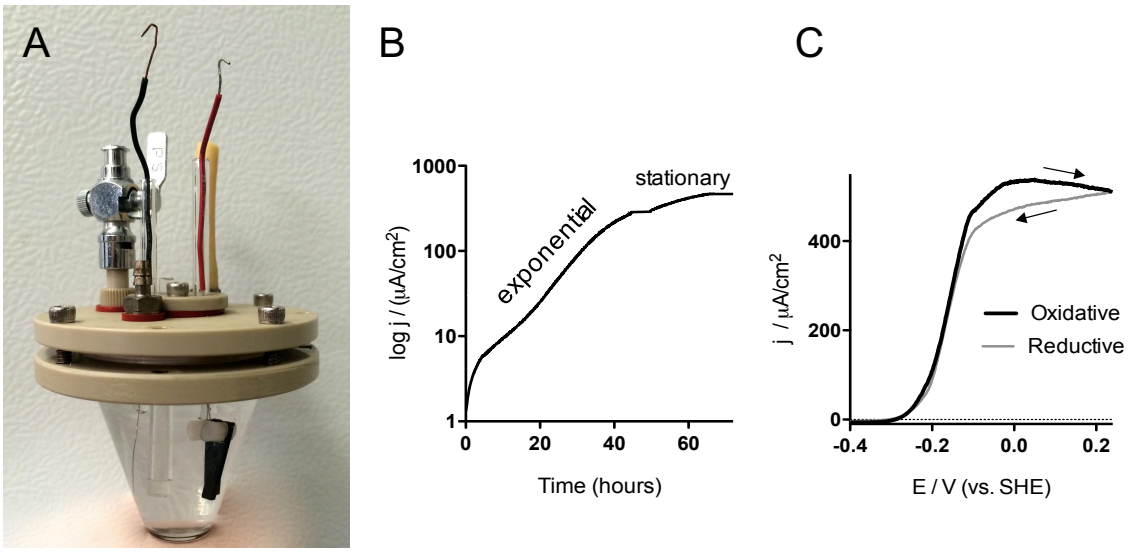

Figure 1.8 *Electrode bioreactor design used in the Bond lab.* A. The latest design of the bioreactor that features a PEEK top secured with stainless steel screws. B. Current production by wild type *Geobacter sulfurreducens*. Working electrode is

poised 0.24 V vs standard hydrogen electrode. C. Cyclic voltamogram performed on a stationary phase biofilm. Scan rate of 1 mV/s.

1.3.2 Cyclic voltammetry models

G. sulfurreducens biofilm growth can be studied quantitatively using standard electrochemical techniques, which apply a fixed electron-accepting potential, and monitors the rate of electron transfer by bacteria to the poised electrode over time (referred to as chronoamperometry). By also measuring the amount of attached biomass, or the thickness of the attached biofilm, the rate of electrons transferred per cell, and how this specific rate changes as biofilms mature, can be measured. As the electrode potential can be swept from low to high potentials at any time during the experiment (cyclic voltammetry) it is possible to also determine the relationship between applied potential and electron transfer rate, revealing insights into the redox potentials of proteins involved in electron transfer. If cells are starved for electron donors, then proteins can be reversibly oxidized and reduced, producing information regarding formal potentials of these proteins. By altering the rate that the electrode potential is changed, one can also deduce rate constants of some of these redox reactions, and test hypotheses related to how these reactions are interfaced with the electrode. In general, reactions directly in communication with an electrode can be accelerated by increased driving force (applied potential), while reactions requiring collisions or diffusional steps do not respond directly to driving force. This information can be used to describe the nature of the mediator(s) carrying electrons out of the cell.

Voltammetric analysis has been used to examine purified enzymes bound to electrodes, and those systems appear to identify the redox potential of rate-controlling electron transfer steps (Armstrong 1999). Researchers hope to extract similar midpoint data from *Geobacter sulfurreducens* biofilms. The additional complexities presented by biofilms has made interpretation of electrochemical

data less straightforward. With this in mind, a series of papers by Dr. Leonard Tender's group attempt to break down electron transfer into major steps that need to happen in order for a biofilm to function as an electrode respiring unit, and derive mathematical expressions for each of these steps (Strycharz-Glaven et al. 2011). These five steps are depicted in Figure 1.9. Simulated data sets representing instances that assume one each of the five steps was rate-limiting were produced, and compared to data from known *Geobacter* cultures.

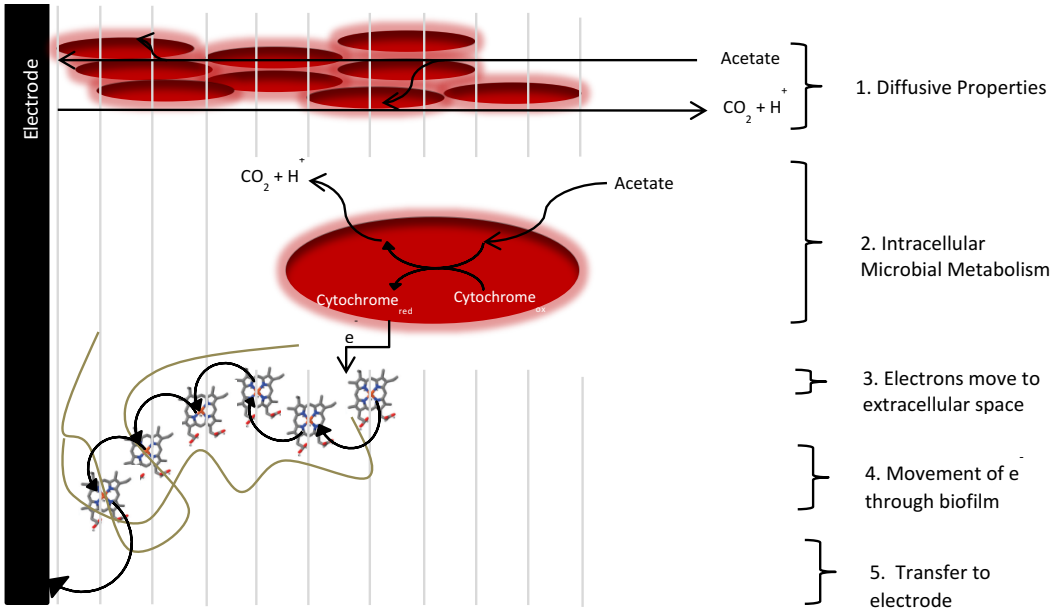

Figure 1.9 *Modeling a complicated respiratory mechanism.* A. The Tender 5 step mechanism of biofilm metabolism (Strycharz et al. 2011).

The first step that needs to occur is that the energy source, in the case of *G. sulfurreducens,* acetate, needs to permeate the biofilm. Fick's laws of diffusion can be used to describe the change in concentrations of a molecule at specific points over time based on diffusion gradients. To model the possible effects, the authors varied the diffusion coefficient from a high value, representing free diffusion within the film, to a low value, representing restricted motion. The modeling predicts changes to slow scan rate cyclic voltammetry and scan rate analysis. It is important to note that the byproducts of acetate metabolism, H^+ and

CO_2 also have to diffuse out of the biofilm. For the sake of simplicity this model assumes that buffering is not diffusion limited and is able to mitigate these byproducts before potentially interacting with redox mediators, a case which will be true in thin films but has been shown to be a factor in thicker (>20 μm) films (Torres, Kato, and Rittmann 2008; Torres et al. 2010; Torres 2014). When diffusion became a limitation in the biofilm, the midpoint potential of the response did not change, but the sigmoid shape of a voltamogram would be altered (Figure 1.8C). The ability of CVs obtained from wild type biofilms to be fit to Butler-Volmer derived equations under all conditions indicates that the diffusion limitations do not explain the electrical behavior of biofilms (Rollefson et al. 2009). Other evidence has also confirmed that acetate freely diffuses in the biofilm. For example, if the biofilm is purged of electron donor, and acetate is added in small increments, there is a linear increase in metabolic activity and absence of significant midpoint potential shifts (Liu et al. 2011, 2012). In addition, transcriptome analysis and live-dead staining of cells consistently shows that cells at different depths of the biofilm have sufficient access to acetate and are metabolically active (Rollefson et al. 2009).

Simulations involving steps 2 and 3 are most informative when examining the balance between the rate of internal electron production, and transfer of these electrons to the outer surface. Step 2 is modeled as Michaelis-Menten based uptake and turnover of acetate, while Step 3 is controlled by Nernstian behavior. These modeling experiments predict significant changes could occur to the midpoint potential at which biofilms respond most strongly to applied potential. A key conclusion of these simulations is that, while the interplay of steps 2 and 3 can in theory alter the cyclic voltammetry response of *Geobacter* biofilms, the data produced by wild type cultures agrees with cases where the rate of step 3 appears to be significantly faster than step 2. Thus, small changes in external potential largely control the rate that electrons exit cells, regardless of local acetate concentrations. As this shows that Step 3 is sensitive to potential in a way that

predicts the sigmoidal shape of slow scan CV, this step also becomes a candidate for being a bottleneck in electron flow in a biofilm.

Once the electrons are out of the cell, the electrons must flow through every layer in the biofilm before reaching the electrode. Step 4 assumes that the mediators responsible for this electron transfer are in fixed positions within the biofilm, i.e. they do not freely diffuse. Also assumed in this model is that the movement of electrons between these mediators occurs through collisions or exchange reactions, causing long-distance movement through a field of these mediators to obey simple laws of diffusion. This stage of the transfer is thought to be a freely reversible second order reaction process driven only by the availability of oxidized mediators. As it responds to applied potential in a Nernstian fashion, Step 4 also emerges as a likely candidate for being the electron flow-limiting step because of the ability to fit to observed data.

Finally, step 5, representing the transfer from a redox protein to the actual electrode, was considered. Since the formal potential of the mediator directly in contact with the electrode is equal to the anode potential, than the rate of the transfer of electrons to the surface can be predicted by the Butler-Volmer equation. As electron transfer increases exponentially with applied potential, any limitation should be easily overcome by simply increasing the driving force. As no such relationship between potential and electron transfer rate has been observed in *Geobacter* biofilms, even as multiple layers grow and require this interfacial transfer to 'carry the weight' of multiple bacteria, there is no evidence that Step 5 is an electrical bottleneck (Strycharz-Glaven 2012).

One of the limitations of this paper, that the authors acknowledge, is the dismissal of the proton gradient that could be forming in the biofilm. Since *c*-type cytochromes are thought to have a significant role, a proton and carbon dioxide gradient should not be involved. Both of these byproducts have been known to

change the binding properties of heme groups. These papers would be strengthened if there was a more consistent picture of when in biofilm development CV analysis was performed. There is also no indication of the thickness of the biofilms. However, even at this early stage of modeling, the authors are able to conclude that step 4 is likely to be the source of the electrical bottleneck. The reasoning for favoring this view over the possibility of step 3 is less based on data than on the fact that step 4 can easily be conceptualized as the cause of this bottleneck. The authors suggest that cells embedded in a network of immobilized mediator could create a gradient with fewer and fewer oxidized mediators available the further away from the electrode surface the bacterium is located. This means that in the outermost layers there are fewer acceptors to move electrons from step three to step four. It is then step 4 that is predicted to be the factor that limits biofilm thickness and the ultimate limiting factor in the production of current. This in turn would limit how quickly electrons could escape the cell.

There are three types of experiments that are going to be revisited here in the context of the Tender model. Measuring the redox state of biofilm cytochromes supports the Tender conclusion. Microelectrode experiments have provided interesting results that are largely in support of the Tender model, but in light of some of the other experiments these need to be reexamined. Experiments that treat the biofilm as a capacitor have been used as evidence against the Tender conclusions.

1.3.3 Biofilm spectroscopy - in support of Tender

In order to study spectral characteristics of extracellular cytochromes during biofilm development a spectroelectrochemical cell made from optically transparent indium tin oxide as the electrode was designed to allow for the simultaneous observation/manipulation of biofilm potential and redox state of the cytochromes

(Y. Liu et al. 2011, 2012). The researchers performed CV analysis on both thick (stationary phase, ~450 μA/cm^2) and thin (log phase, ~100 μA/cm^2) biofilms which showed that in a thick biofilm, a smaller percentage of cytochromes in the biofilm are in an oxidized state, and that the rate that cytochromes changed redox status in response to applied potential was slower. This indicated that a pool of electrons in the extremities of the biofilm do not communicate with the electrode as rapidly as those located close to the electrode surface. For each of these biofilm thicknesses, they also starved the system of acetate and then titrated in acetate, performing CV after each addition. The starvation experiment was able to demonstrate the link between step 3 (electron production) and steps 4 and 5, extracellular electron transfer. Here, as the rate of acetate metabolism increased, so did the current production. But above a threshold thickness, the cytochrome pool became relatively more reduced. These results led to the conclusion that within a biofilm a pool of *c*-type cytochromes exists in a redox gradient, and this gradient is responding to an electrical bottleneck that is not overcome by higher electrode potentials, supporting the limitations of step 4. Similar conclusions have been reached with studies leveraging resonance Raman based spectroscopies (Lebedev, Strycharz-Glaven, and Tender 2014; Virdis et al. 2012; Millo 2012).

1.3.4 Microelectrodes - a suggestion that we should look beyond Tender

When an electrode has at least one dimension in the micron scale, higher current densities can be achieved because of an increased diffusion layer. Electrodes that create these conditions are known as microelectrodes or ultramicroelectrodes (UME)(Compton 2007). *G. sulfurreducens* has been grown on smaller electrodes in order to not only gain overall power output (as seen in biomedical devices) but also to understand limiting factors in biofilm electron transfer. The latter is greatly aided by the fact that UMEs have rapid response times and a decreased current contribution due static charge accumulation at the electrode surface. Gold line array electrodes (5 μm wide) used by Liu et al. (2012) demonstrated three

properties that indicate that even on smaller scales, the limiting factor in current density is still related to the distance cells are from the electrode surface, suggesting that diffusion plays a minor role. In these experiments; 1) Current density did not increase linearly with potential scan rate, which would be expected with MEs where diffusion issues were lessened, 2) Acetate depletion and addition of incremental amounts of acetate did not change the midpoint potentials, which would again be influenced by diffusion, and 3) Biofilms formed on electrodes of differing geometries slowed growth at similar thicknesses. Pocaznoi et al. (2012) used similar approaches with thin wires to create UME-like conditions, with bacterial compost isolates that behaved similar to *G. sulfurreducens*. Contradicting results from flat electrodes, many of these biofilms appeared to extend much further from the electrode surface, and suggest that further work with UMEs could address this hypothesis in new ways. However, voltammetry under these conditions was identical to flat electrodes, showing that dominant biofilm electron transfer characteristics are not controlled by diffusion of acetate or escape of products (Pocaznoi et al. 2012).

1.3.5 The biofilm as a capacitor - disagrees with Tender but it is unclear why

Bonnani et al. (2012) created essentially the same model as Tender and coworkers. However, Bonnani et al. did not interrogate the system with CV analysis, but instead, treated the biofilm as a capacitor and used discharge patterns to infer properties of the metabolic steps of electron flow. Current flow was halted for 10, 20 and 45 minutes by changing to an open circuit potential (OCP) and then reconnecting the electrode.

The rate of initial discharge, within the first second, was very high compared to current density normally achieved. For example, while active biofilms may produce as much as ~1 mA/cm^2, initial discharge rates were 10- to 40-fold higher. If nothing else, this shows that the interfacial transfer reaction is capable of much higher

rates, consistent with the Tender model. However, the sheer number of electrons discharged during this first burst exceeds the number which could be stored in a monolayer of proteins in direct contact with the electrode. The charge collected during this step remained almost constant after disconnection for 20 minutes or less, which implies the existence of a pool of proteins, extending beyond the realm of 'direct contact', which are capable of rates of electron transfer faster than seen in active films. In other words, if between-cell electron transfer is rate limiting (Step 4 in the Tender model), then why is this pool of proteins between cells able to discharge so fast?

Bonnani et. al. made a number of additional conclusions from this model about the capacitance and rate limiting steps of biofilm electron transfer. However, it seems that these conclusions are based on assumptions that may or may not be true. First, these observations were collected from biofilms that were both discharging stored electrons, and restarting metabolism in the presence of acetate, producing very complex discharge events. If Bonnani et al. had washed the acetate from the biofilms it would have been more clear what the size of the cytochrome/mediator pool was, as there would be no way to regenerate it. Without this control, it cannot be said that acetate metabolism is a limiting step in electron transfer, as Bonnani interpreted their results. The authors also make assumptions about the location of electrons in the biofilm (in the inside of cells or extracellular space, for instance). The authors also do not consider the possibility that there are more electrons built up on the exterior of the cell, as compared to the inside of the cell. While this technique is valuable, more experiments are needed to isolate the limiting step, and more data regarding the location of electrons in these biofilms is crucial.

1.3.6 Conclusion

Taking these four approaches of studying electron transfer and comparing the similarities provides a direction for future research. The authors of these papers all

agree on two points. First, diffusion of acetate and uptake of acetate are not rate limiting steps. Secondly, there is a final step that happens when an electron makes its final move onto a poised electrode. This event is not rate limiting in itself but can reflect bottlenecks of electron movement upstream from this event. It is suggested by Bonani et al. and Liu et al. that this bottleneck step could be a different step in thin biofilms versus thick biofilms. This is similar to the prediction made by the Tender group that the movement of electrons to the electrode, step four, is the ultimate factor that limits biofilm growth. Taken in light of data from Liu, step four is likely happening amongst the many *c* type cytochromes. Also, these papers agree that there are different redox species that are involved in the final movement of electrons from the electrode and that these species behave differently during the growth of the biofilm.

It is these observations that have stimulated further research into step 4, the movement of electrons through the biofilm. There are two broad ways to study this problem. Many researchers seek to discover individual proteins thought to be involved in this step through characterization of deletion mutants and isolated proteins. Others study the electrochemical and quantum mechanical mechanisms that could make such electron transfer between proteins possible (Pirbadian and El-Naggar 2012; Polizzi, Skourtis, and Beratan 2012). Ultimately, it will be necessary to understand how this complex network of redox proteins is able to interact in three dimensions to support this unique mode of extracellular respiration to surfaces. This dissertation supports the conclusion that step four is the rate limiting. It is further shown that this step occurs at the inner membrane and is determined by the multiheme cytochrome CbcL. The function of this protein is dependent on the electrical potential of the terminal electron acceptor. This, together with the observation that biofilms of Δ*cbcL* mutants are significantly smaller, gives intriguing support for the existence of a redox gradient within the biofilm.

1.4 Dissertation Rationale and Goals

This dissertation presents a comparison between two multiheme proteins, CbcL and PgcA. Previous work on the molecular mechanisms for extracellular electron transfer by *Geobacter sulfurreducens* has focused on the extracellular matrix and extracellular cytochromes. This dissertation seeks to build on the understanding of extracellular respiration by focusing on an inner membrane protein, CbcL. Of the inner membrane proteins identified as possible menaquinone oxidoreductases, CbcL has been suggested by a proteomic study (Bond lab, unpublished) and a comparative genomics study (Butler et al. 2010). Since energy conservation must occur at the inner membrane, there must be proteins in the inner membrane that can cycle menaquinones. The ability of CbcL to function as an inner membrane respiratory conduit was assessed using electrochemical, microbiological and biochemical techniques.

In comparison to the inner membrane cytochrome, CbcL, the extracellular protein PgcA was characterized. This protein has been implicated as an important component in extracellular respiration in literature discussing adapted *G. sulfurreducens* strains (Tremblay et al. 2011; Smith et al. 2014; Yi et al. 2009). More importantly, previous students in the Bond lab identified phenotypes created by transposon insertions that disrupted the gene encoding PgcA (Bond lab, unpublished). While recent research has described the function of the regulatory mechanism of this protein, nothing is known about the function of the protein itself. The amino acid sequence of PgcA contains unique repetitive sequences as well as three heme binding sites.

1.5 Summary of dissertation

Chapter 2 is the beginning of the characterization of *G. sulfurreducens* strains lacking *cbcL* and presents strong evidence that the rate limiting step of electron transfer is at the level of the inner membrane. These mutants were created using a scarless genome editing technique (Chan et al. 2015). In Chapter 2, I show that

cyclic voltammetry measurements are reflective of the mutants deficit in respiring to terminal electron acceptors with relatively low potentials. This ability of CbcL to alter growth and electron transfer properties is followed up in Chapter 3. Mutations in CbcL can recover respiration using high potential electron acceptors in a strain otherwise lacking the capacity to respire to high potential acceptors. Supporting data for Chapters 2 and 3 are included in Chapter 4.

This work has increased our understanding of the three mysteries of *G. sulfurreducens* respiration. First, the energy that is available to provide a driving force for respiration is relatively small. In other words, the available free energy is based on the electron acceptor (iron oxides range from -0.3 V to 0.3). Energy conservation at the inner membrane must be highly efficient. This dissertation demonstrates that the inner membrane protein CbcL is the favored respiratory pathway when the acceptor potential is relatively low. When relatively high potential metals are available, *G. sulfurreducens* uses an ImcH dependent pathway (Levar et al. 2015). The rate limiting step of extracellular respiration is the step that couples electron transfer to energy harvesting. This work also explains *G. sulfurreducens* approach to respiring complicated metal oxides.

Finally, chapter 5 contains experimental data characterizing a *Geobacter sulfurreducens* mutant lacking *pgcA.* I show that PgcA is involved in the respiration of insoluble metals. This protein has the ability to work in the extracellular space. Some of the characteristics of this protein are similar to those of known redox active shuttles. The terminal electron acceptors themselves are highly complex. Insoluble metals exist in complexes with each other and with other molecules. These metals change potential and forms while being reduced (Nealson and Saffarini 1994).

Chapter 2: Reduction of Low Potential Electron Acceptors Requires the CbcL Inner Membrane Cytochrome of *Geobacter sulfurreducens*

Adapted from Zacharoff, L., Chan, C., Bond, D. (2016) Bioelectrochemistry

2.1 Abstract

The respiration of metals by the bacterium *Geobacter sulfurreducens* requires electrons generated from metabolism to pass from the interior of the cell to electron acceptors beyond the cell membranes. The *G. sulfurreducens* inner membrane multiheme *c*-type cytochrome ImcH is required for respiration to extracellular electron acceptors with redox potentials greater than -0.1 V vs. SHE, but ImcH is not essential for electron transfer to lower potential acceptors. In contrast, deletion of *cbcL,* encoding an inner membrane protein consisting of *b*-type and multiheme *c*-type cytochrome domains, severely affected reduction of low potential electron acceptors such as ferrihydrite and electrodes poised at -0.1 V vs. SHE. Catalytic cyclic voltammetry of a Δ*cbcL* strain growing on poised electrodes revealed a 50 mV positive shift in driving force required for electron transfer out of the cell. In non-catalytic conditions, low-potential peaks present in wild type biofilms were absent in ∆*cbcL* mutants. Expression of *cbcL in trans* increased growth at low redox potential and restored features to cyclic voltammetry. This evidence supports a model where CbcL is a component of a second electron transfer pathway out of the *G. sulfurreducens* inner membrane that dominates when redox potential is at or below -0.1 V vs. SHE.

2.2 Introduction

Microorganisms thrive in anoxic environments by coupling oxidation of compounds to the reduction of terminal electron acceptors (K. A. Weber et al. 2005; Blöthe and Roden 2009; Simon, van Spanning, and Richardson 2008). Due to differences in the redox potential of each electron source and sink, variable amounts of energy are available to bacteria catalyzing this electron flow. For example, every 0.3 V of potential drop between a donor and acceptor releases -58 kJ/2 e-, essentially enough to generate an ATP. In the environment, insoluble metal oxide acceptors span a large range of reduction potentials, from values as low as -0.2 V to as high as +0.5 V vs. standard hydrogen electrode (SHE) (Salas et al. 2011; Majzlan 2012). This represents an array of thermodynamic opportunities for metal-reducing bacteria, but only if molecular mechanisms evolved to couple these different metal forms with different respiratory pathways.

In microbial electrochemical devices, anode surfaces act as electron acceptors, offering a unique opportunity to test if electron transport chains in different organisms are optimized for growth at particular redox potentials (Zhu et al. 2014; Commault et al. 2013; Ishii et al. 1841). One consistent finding from environmental enrichment experiments is the predominance of *Geobacter* spp. in electrode-reducing biofilms, even though anode potentials are dynamic in fuel cell-like devices, and poised anode potentials vary over a range greater than 0.5 V. These results suggest that members of the *Geobacter* genus, originally described as organisms able to reduce a wide variety of Fe(III) and Mn(IV) oxides, could be redox potential generalists able to compete across a wide range of electrode potentials.

Further evidence of redox potential generalization comes from observations of the *Geobacter* j-V cyclic voltammetry response, or rate of electron transfer at different redox potentials. The highly repeatable voltammetric response does not follow a simple Nernstian relationship for a single one-electron process (Strycharz et al. 2011; Richter et al. 2009). Based on impedance measurements by Yoho et. al. (Yoho, Popat, and Torres 2014), the broad window of electron transfer out of *Geobacter* is best described by the presence of least two different pathways, with midpoint potentials of -0.15 V and -0.09 V vs. SHE. Consistent with this prediction, deletion of the inner membrane cytochrome gene *imcH* eliminates growth of *G. sulfurreducens* at redox potentials above -0.1 V vs. SHE, but Δ*imcH* mutants remain able to grow at potentials below this value (Levar et al. 2014). These observations lead to the hypothesis that the ImcH-dependent pathway has the capacity to generate additional ATP compared to the lower potential route. This gives a mechanistic explanation for slower growth rates of *G. sulfurreducens* at low redox potentials (Yoho, Popat, and Torres 2014) even when *imcH* is deleted (Levar et al. 2014).

The *G. sulfurreducens* genome encodes at least five putative quinone oxidoreductase protein complexes that contain a transmembrane *b*-type diheme domain fused to, or adjacent to, a multiheme *c*-type cytochrome (Cbc)(Butler, Young, and Lovley 2010; M Aklujkar et al. 2013). Transcriptomic and proteomic data indicate that Cbc gene clusters are differentially expressed by *G. sulfurreducens* in response to changes in electron acceptor availability or growth in syntrophic coculture with other strains (Ding et al. 2008a; Shrestha et al. 2013). Transcript abundance of genes encoding Cbc-family proteins is also affected when electrode-reducing communities containing *Geobacteraceae* are exposed to changes in anode potential (Ishii et al. 2013). Even though Cbc complexes share characteristics with other electron transfer proteins; show a high degree of conservation across *Geobacter* genomes; and display dynamic responses in

environments where electron acceptor potential is a variable, they have not been investigated.

This work describes a redox potential-dependent respiratory role for the inner membrane cytochrome CbcL. Deletion of *cbcL* primarily impaired growth with low-potential extracellular electron acceptors, and eliminated an electron transfer process with a midpoint potential of -0.15 V vs. SHE. Electron transfer with a higher midpoint potential, near -0.1 V vs. SHE, remained intact in Δ*cbcL* mutants. These results indicate that voltammetry of *G. sulfurreducens* under catalytic conditions is mainly influenced by reactions at the inner membrane rather than the outer surface, consistent with these being the rate-limiting or least-reversible steps. Both CbcL- and ImcH-dependent pathways are present in wild type cells, regardless of growth conditions. However, electron flow appears to switch from the low- to high-potential pathway as external redox potential is raised during a 1 mV/s cyclic voltamogram. Identification of CbcL supports the emerging model of multiple electron transfer pathways in *Geobacter*, where these bacteria can rapidly move electrons to take advantage of different amounts of energy in extracellular electron acceptors.

2.3 Materials and Methods

2.3.1 Strains and growth conditions

For routine culturing, *Geobacter sulfurreducens* PCA (ATCC 51573) or mutants (described below) were revived from frozen lab stocks by directly plating at 30°C on 1.5% agar solid medium containing 20 mM acetate donor and 40 mM fumarate acceptor (NBFA medium) containing defined salts (Marsili, Rollefson, et al. 2008). All anaerobic medium was prepared using 80:20 N_2:CO_2 passed over a heated copper column to remove oxygen. Colonies were propagated in liquid medium with acetate as the electron donor and fumarate (40 mM) as the electron acceptor, then transferred to medium containing 55 mM Fe(III) oxide, 50 mM Fe(III) citrate or 20 mM Mn(IV) oxide as the electron acceptor. Independent cultures were revived from

freezer stocks for all experiments to avoid repeated transfers in soluble electron acceptors that could select for variants.

To determine Fe(III) reduction, 100 μL samples were dissolved in 900 μL 0.5 N HCl, and a FerroZine assay adapted from (Derek R Lovley and Phillips 1986) for use in 96 well plates was performed. 300 μL of FerroZine solution (2 grams FerroZine reagent/liter in 100 mM HEPES, pH 7) was added to 50 μL of sample and absorbance at 625 nm was measured. This protocol was adapted for Mn reduction by first dissolving samples in 0.5 N HCl with 4 mM $FeSO_4$, allowing the Fe(II) to reduce remaining Mn(IV), and then proceeding with the steps described above. The extent of Mn reduction could then be calculated by difference.

2.3.2 Deletion and complementation of cbcL

Strains used for this study are summarized in Table 1. One kilobase up and downstream of *cbcL* (GSU0274) was amplified and purified. Overlapping PCR was performed, and the resulting product was digested and ligated into the pK18*mobsacB* vector (Schafer et al. 1994), leaving the flanking regions in tandem. This cloned product was sequence verified (BMGC, University of Minnesota) then transformed into a S17-1 *E. coli* donor strain (Simon, R., Priefer, U., Puhler 1983). Wild type *G. sulfurreducens* and *E. coli* mating strains in late exponential phase of growth were applied to filter paper on NBFA agar media in an anaerobic chamber. Twelve hours later a sample was streaked for isolation on NBFA + kanamycin plates to select for plasmid integration. Counter selection on 10% sucrose NBFA selected for recombination events, and colonies were patched on both NBFA and NBFA kanamycin plates. Cells sensitive to kanamycin (indicating plasmid excision) were further screened for complete gene deletion using up and downstream flanking primers (see supplemental Table 1) For complementation, a *G. sulfurreducens* expression vector was generated by cloning the *acpP* (GSU1604) promoter and ribosome binding site to the 5' region of *cbcL* (GSU0274). Vectors

were maintained with 200 µg/mL kanamycin. Before inoculation of reactors, cultures were transferred once into kanamycin-free NBFA to limit the amount of kanamycin carryover into electrochemical reactors, which can reduce final current density.

Table 2.1 *Plasmids and strains*

Strain or Plasmid	Description	Source/Reference
Strains		
G. sulfurreducens PCA	Wild Type (ATCC 51573)	Lab collection
ΔcbcL G. sulfurreducens	Markerless deletion of *cbcL* gene in Wild Type *G. sulfurreducens background*	This study
E. coli S17-1	Donor strain for conjugation	Simon, 1983
Plasmids		
pK18mobsacB	Markerless deletion vector	Schafer, 1994
pRK2geo2	Vector control and backbone for complementation vector	Lab Collection
pcbcL	Complementation vector with constitutive expression of *cbcL. cbcL* was cloned into pRK2Geo2.	This study

2.3.3 Electrochemical analysis

Bioreactors consisted of a polished 3 cm^2 graphite electrode (1500 grit), platinum counter electrode and calomel reference electrode connected to the reactor through a Vycor frit. Bioreactors were constantly stirred, maintained at 30°C and kept under a constant stream of oxygen-free 80% N_2:20% CO_2 throughout the course of experimentation. Reactors were controlled via potentiostat (VMP, Bio-Logic, Knoxville, TN) running EC-lab software. Bioreactors were poised at either +0.24 V or -0.1 V versus SHE. Experiments were initiated with a 50% (v/v) inoculum of 0.52 OD_{600} cultures entering stationary phase due to electron acceptor limitation.

2.3.4 Electrochemistry

Cyclic voltammetry and single turnover experiments were performed by poising the electrode at -0.55 V versus SHE and scanning to a reversal potential of +0.245 V versus SHE at a rate of 1 mV/s, for at least three sweeps. Twenty-four hours before non-turnover voltammetry was performed, electrode medium was replaced with acetate free medium, and the electrode was poised as an acceptor to deplete available donors. Cells were washed again in acetate-free buffer immediately before scanning. Cyclic voltammetry was initiated once current was less than 10 $\mu A/cm^2$.

2.3.5 q-RT-PCR

Biofilms were grown on electrodes for 60 hours and harvested at 4°C. Cells were removed by scraping with a sterile, RNase-free pipette tip and collected via centrifugation. RNA was extracted from electrode grown cells with PureLink system (Life Technologies, Calsbad, CA). cDNA was synthesized using iScript from Bio-Rad (Bio-Rad, Hercules, CA) with random primers as provided. Amplification was observed using SsoAdvanced Universal SYBR green from Bio-Rad per manufacturer's instructions on a Bio-Rad iCycler (supplemental Table 2). Primer efficiencies were calculated from genomic DNA extracted from wild type *G. sulfurreducens* using Wizard Genomic DNA purification Kit (Promega, Madison, WI). Samples were normalized to starting RNA levels. The Pfaffl (Fleige and Pfaffl 2006) method was used to compare gene expression levels to housekeeping gene levels. Control genes *rpoD* and *proC* did not change relative to each other when compared to high and low potential grown biofilms. The C_T values used to calculate expression ratios were: *cbcL* high potential = 26.1$\pm$ 2.7, low potential = 24.96 $\pm$ 0.69; *rpoD* high potential 27.18 $\pm$ 2.4, low potential 26.39 $\pm$ 0.32.

2.4 Results and Discussion

2.4.1 Deletion of cbcL primarily affects Fe(III)-oxide reduction

In previous work, deletion of *imcH,* encoding an inner membrane multiheme *c*-type cytochrome, eliminated the ability of *G. sulfurreducens* to reduce acceptors with potentials higher than -0.1 V vs. SHE (Levar et al. 2014), despite the fact that acetate oxidation linked to reduction of these compounds is energetically favorable. However, the Δ*imcH* strain still reduced acceptors with potentials at or lower than -0.1 V at near wild type rates. These observations led to the hypothesis that *G. sulfurreducens* utilizes different electron transfer pathways, depending upon the redox potential of the terminal electron acceptor.

Inner membrane respiratory proteins such as hydrogenases and formate dehydrogenases often contain membrane-embedded HydC/FdnI domains that act as menaquinone oxioreductases (Jormakka 2002). In the *G. sulfurreducens* genome, a monocistronic gene (Qiu et al. 2010) referred to here as *cbcL* (c- *and b-type cytochrome for Low potential,* GSU0274, sometimes annotated in databases as *cbc*1 [14]), is predicted to encode an inner membrane HydC/FdnI diheme *b*-type cytochrome linked to a 9-heme periplasmic *c*-type cytochrome (Figure 2.1). Homologs are present in genomes of most *Geobacteraceae*, *Acidobacteria, Caldithrix* and *Campylobacter,* but this family of putative quinone oxioreductases lacks an identified function in any of these microorganisms.

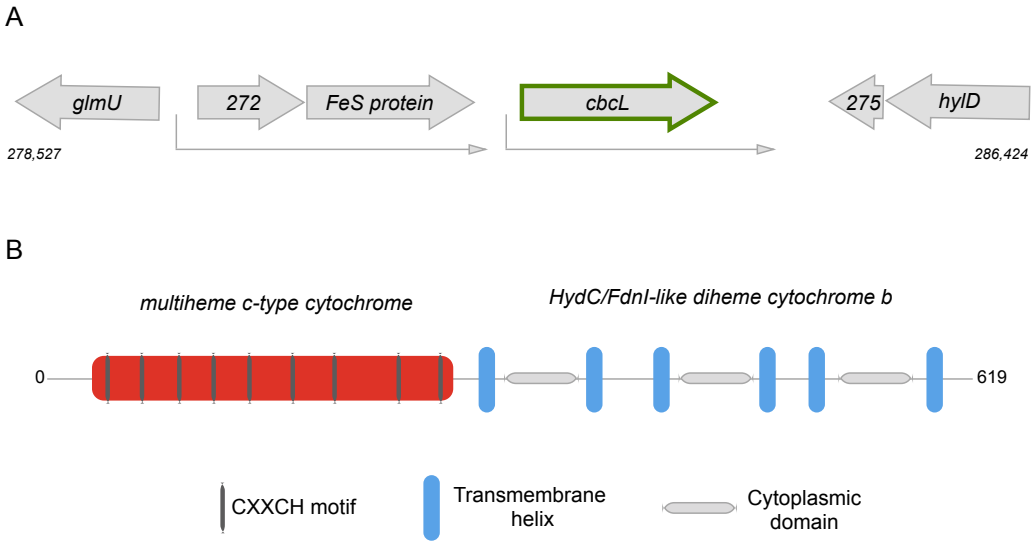

Figure 2.1 *Genome context and domain structure of CbcL.* (A) *G. sulfurreducens cbcL* (GSU0274) is monocistronic. In all *Geobacteraceae* genomes, *cbcL* is encoded adjacent to an Fe-S protein, while in *Campylobacter* genomes, the N-terminus includes an Fe-S domain. (B) Predicted features of CbcL include a 9 CXXCH-motif multiheme periplasmic *c*-type cytochrome, anchored by six inner membrane transmembrane helices. The transmembrane domains are highly similar to diheme *b*-type cytochromes found in menaquinone-dependent formate dehydrogenases.

To test if CbcL was utilized for respiration by *Geobacter sulfurreducens*, *cbcL* was removed using a markerless deletion protocol. The Δ*cbcL* mutant had no apparent growth defect when fumarate was the electron acceptor, and an only 10% slower doubling time when grown with soluble Fe(III)-citrate as the electron acceptor (Figure 2A). Reduction of the insoluble electron acceptor Mn(VI)-oxide (birnessite) was also similar to wild type (Figure 2.2B). In contrast, when ferrihydrite was the electron acceptor, growth of the Δ*cbcL* mutant was severely impaired. Both the overall rate of Fe(III) reduction and extent after 200 hours was less than 30% of wild type cultures (Figure 2.2C).

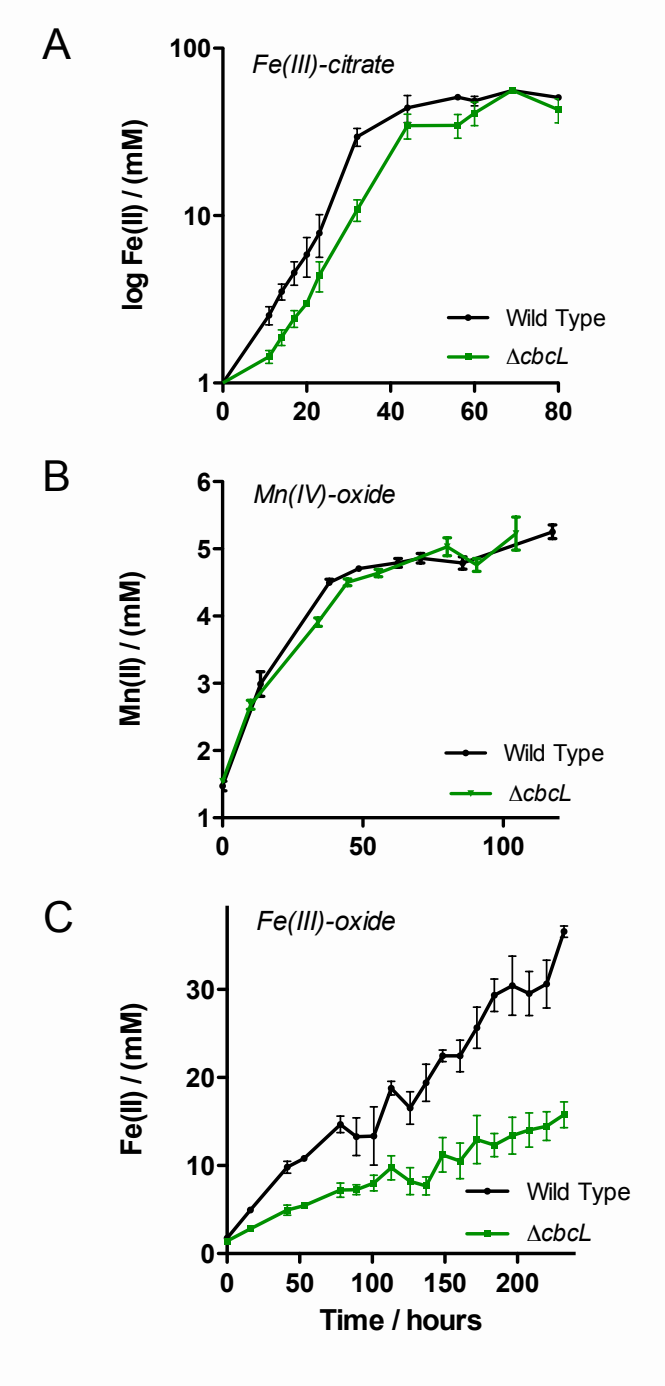

Figure 2.2 *Metal reduction phenotypes.* Growth of wild type and Δ*cbcL* mutants with acetate as the electron donor and different metals as electron acceptors. (A) Soluble Fe(III) citrate reduction to Fe(II), (B) Insoluble Mn(IV)-oxide reduction to Mn(II), and (C) Fe(III)-oxide reduction to Fe(II). Data points are mean +/- SD of three replicates.

The growth phenotype of the Δ*cbcL* strain was the opposite reported for the Δ*imcH* mutant, which could not reduce Fe(III)-citrate and Mn(IV), yet reduced Fe(III)-oxides at wild type rates. Fe(III)-citrate and Mn(IV)-oxide have relatively high redox potentials (> +0.3 V vs. SHE (Straub, Hanzlik, and Buchholz-Cleven 1998; Straub and Schink 2004), while the Fe(III)-oxides in these experiments have redox potentials below 0 V. These data suggested the Δ*cbcL* mutant could be specifically impaired in reduction of lower redox potential acceptors. To further test this hypothesis, the Δ*cbcL* mutant was grown on anodes held at different electron accepting potentials.

2.4.2 Deletion of cbcL impairs reduction of electrodes poised at lower potential

When electrodes were poised at +0.24 V vs. SHE, the wild type and Δ*cbcL* mutant grew exponentially without lag, with average doubling times of 6.5 +/- 0.5 hours for wild type and 8.0 +/- 0.9 hours for the Δ*cbcL* mutant (Figure 3A, average of 6 experiments, growth rates measured between 12 and 24 h). The Δ*cbcL* mutant achieved 74% of wild type final current density (Figure 2.3A, inset). This decrease in final current density was coupled to a decrease in total protein in the Δ*cbcL* biofilm, indicating that this was primarily due to thinner biofilms layering on electrodes in the final growth stages. This hints at the possibility that CbcL is more important at the biofilms extremities because of the existence of a redox potential gradient existing in biofilms formed on electrodes poised at +0.24 V.

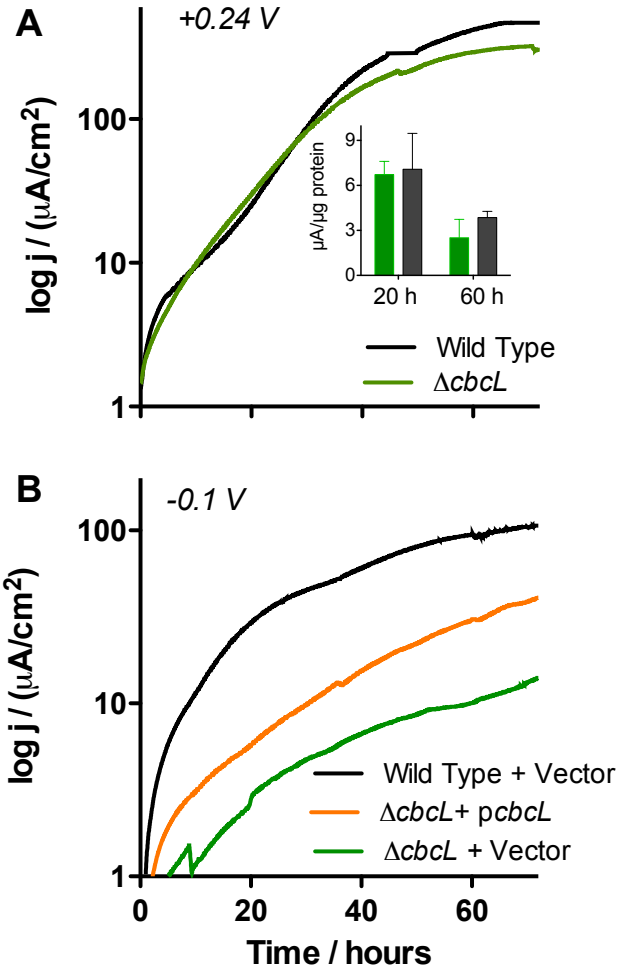

Figure 2.3 *Growth on electrodes poised at high vs. low redox potentials.* Total current density, j, as a function of time on polished graphite electrodes with acetate as the electron donor. (A) High potential growth of wild type and Δ*cbcL* mutant on a working electrode poised at +0.24 V vs. SHE. Inset: current per unit attached protein at 30 hours and 100 hours, (values are different at 100 h, $p < 0.05$) (B) Low potential growth of wild type + vector, Δ*cbcL* + vector, and Δ*cbcL* + p*cbcL* on a working electrode poised at -0.1 V vs. SHE. All experiments were performed in triplicate, representative traces shown.

In contrast, the Δ*cbcL* mutant had a significant growth defect when redox potential was -0.1 V vs. SHE (Figure 2.3B). Wild type cells doubled in 8 +/- 0.8 hours at this redox potential, but the Δ*cbcL* mutant grew poorly, rarely demonstrating doubling

times faster than 20 hours, and reaching only 14% of the final current density of wild type (Figure 2.3B, average of 4 observations). When *cbcL* was expressed from a constitutive promoter in the Δ*cbcL* strain, the complemented Δ*cbcL* mutant grew faster, with a doubling time of 12 hours, and reached a final current density 2.8-fold higher than the mutant carrying the empty vector alone. This complemented strain was used to further investigate the electrochemical effects of removing and re-expressing *cbcL* in *G. sulfurreducens.*

2.4.3 Voltammetry of the ΔcbcL mutant reveals a missing response at low redox potential

Wild type and mutant biofilms grown at +0.24 V were subjected to catalytic cyclic voltammetry (CV) at 1 mV/s in the presence of acetate as the electron donor (Figure 2.4). Wild type biofilms produced a characteristically broad sigmoidal response, with an onset potential of approximately -0.25 V, a midpoint potential of -0.15 V, and a limiting current plateau stabilizing by 0 V. In contrast, the onset of current production by Δ*cbcL* mutants was more positive than wild type. Once initiated, the catalytic wave was steeper, with a midpoint potential of -0.1 V. This indicated that mechanism(s) typically used for electron transfer at lower redox potentials were absent in the Δ*cbcL* mutant.

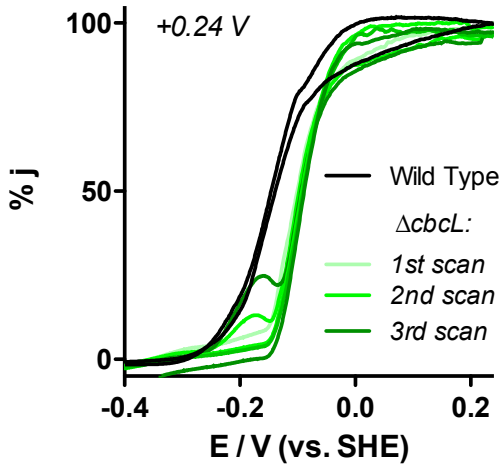

Figure 2.4 *Shifts in voltammetry due to* cbcL *deletion.* After 60 hours of growth on working electrodes poised at +0.24 V vs. SHE, 3 cycles at a scan rate of 1 mV/s were performed in the presence of acetate as an electron donor. Data is normalized to the limiting current at +0.2 V. Wild type data was similar regardless of scan number, only third scan is shown.

Repeated voltammetry scans of Δ*cbcL* mutants grown at high potential (+0.24 V) revealed a previously unreported feature. While the first scan contained only the single steep rise at the more positive midpoint potential, later cycles produced a small peak at approximately -0.2 V. After three full cycles, this peak did not increase in magnitude. This was not observed in wild type biofilms, although it could have easily been obscured by the major processes already present in wild type voltamograms. These results suggested that some electron transfer mechanisms could be activated by exposure to lower redox potentials, such those occurring during voltammetry scans.

When wild type and Δ*cbcL* biofilms were pre-grown at the lower redox potential of -0.1 V, CV data was similar to 'third scan' data shown in Figure 4. For example, Δ*cbcL* biofilms already demonstrated the small feature at -0.2 V, and still had positively shifted voltammetry with a midpoint at -0.1 V. The major electron transfer

process centered at -0.15 V was always absent in the Δ*cbcL* mutant, regardless of growth conditions or redox potential exposure.

When *cbcL* was expressed in the Δ*cbcL* background, voltammetry of the biofilm shifted back towards the lower potential wave characteristic of wild type, and electron transfer at a midpoint potential of -0.15 V could again be detected (Figure 2.5A). By plotting the derivative of these voltamograms, three separate midpoint potentials could be identified, with the process at -0.15 V being dependent upon the presence of *cbcL* (Figure 2.5B). Notably, the plasmid used to express *cbcL* only restored 80% of the wild type growth rate, and also only partially restored the voltammetry phenotype. This allowed the peak near -0.15 V to be more easily resolved than in wild type cultures, where the three processes appear as one feature.

Voltammetry of biofilms incubated in the absence of acetate (single-turnover conditions, or non-catalytic) revealed further differences between wild type and Δ*cbcL* mutants (Figure 2.5C). Both cultures produced a high-potential reversible peak centered at approximately -0.07 V vs. SHE. However, the Δ*cbcL* mutant biofilm failed to produce many peaks commonly observed at potentials below -0.1 V. In the partially complemented strain, peaks in this lower potential domain were restored, particularly cathodic peaks that are characteristic of wild type *G. sulfurreducens*.

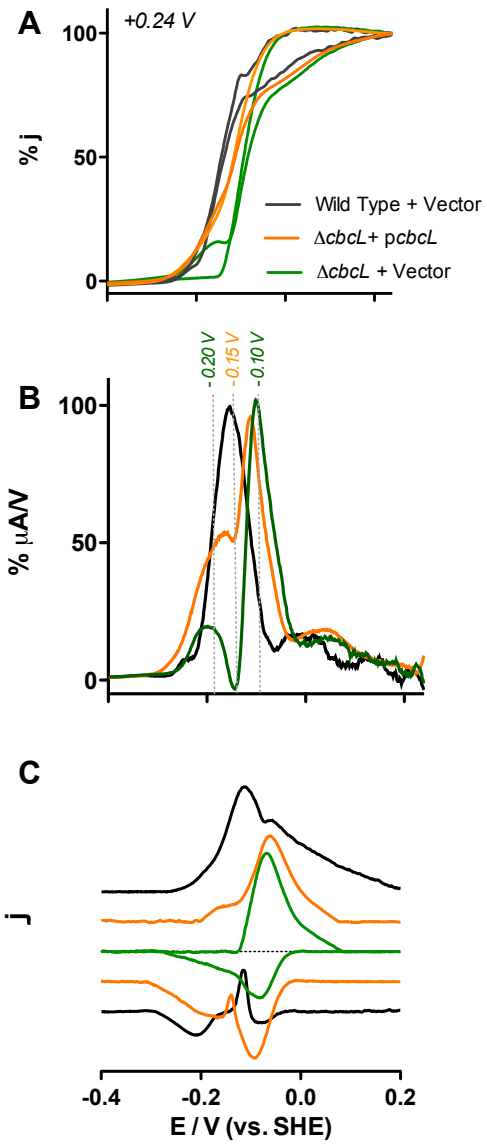

Figure 2.5 *Cyclic voltammetry of complemented mutants.* After 60 hours of growth on working electrodes poised at +0.24 V vs. SHE, 3 cycles at a scan rate of 1 mV/s were performed in the presence of acetate as an electron donor, third scan is shown normalized to the limiting current at +0.2 V. (A) Wild type with empty vector, Δ*cbcL* expressing *cbcL* and Δ*cbcL* with empty vector control cyclic voltammetry, (B) First derivative of data in (A), showing the presence of a process in the complemented strain that is absent in the Δ*cbcL* mutant, (C) Non-catalytic cyclic voltammetry of wild type, complemented and Δ*cbcL* biofilms in the absence of acetate. Each data set is normalized to the highest peak and baseline subtracted.

2.4.4 CbcL also contributes to electron transfer at higher potentials

The broad response seen in wild type voltammetry, regardless of the growth conditions, and minor phenotypes with high potential acceptors, suggested that *cbcL* was present at both high and low redox potential in wild type cells. According to this hypothesis, *cbcL* is constitutive, but only catalyzes a minor amount of electron transfer when cells encounter high potential acceptors. When quantitative RT-PCR of the *cbcL* mRNA was performed on biofilms grown at +0.24 V and -0.1 V, *cbcL* mRNA was detected under both conditions, and the ratio of *cbcL* mRNA (normalized to *rpoD* levels) at low potential compared to high potential was 1.22 (mean of 3 independent biofilms for each condition). These results were also consistent with the slight growth defect observed when Δ*cbcL* mutants utilized high potential metals (Figures 2 and 3), and the low-potential peaks in single-turnover voltammetry (Figure 2.5C) even when cells were grown at high potential.

Experiments with electrode-grown biofilms repeatedly show that *G. sulfurreducens* catalytic voltammetry fails to conform to a simple Nernstian model in which one redox enzyme is rate-limiting (Torres, Marcus, and Rittmann 2008; Strycharz et al. 2011; Hamelers et al. 2011). Evidence for multiple electron transfer pathways in *G. sulfurreducens* was also described by Yoho et. al. (Yoho, Popat, and Torres 2014), based on the improved fit of electrochemical impedance spectroscopy data to a 2-mediator model. The availability of voltammetry from the Δ*cbcL* strain made it possible to observe as many as three rate-limiting steps in *G. sulfurreducens* electron transfer, and provided support for the observations of Yoho et. al. (Yoho, Popat, and Torres 2014).

A variation on the limiting current approach described by Richter et. al. (Richter et al. 2009), was expanded to use the three midpoint potentials (E_o, -0.23, -0.15, and -0.07 V) observed in Δ*cbcL* mutant and complemented strain data, to produce a simulation of *G. sulfurreducens* catalytic voltammetry (Eq 2. 1).

$$\frac{i_{max} - i}{i} = exp\left(\frac{E - E_o'}{\left(\frac{nF}{RT}\right)}\right) \quad \text{(Eq.2. 1)}$$

In this model, plotted in Figure 6, i_{max} is the maximum current that can flow through a given pathway, E_o' is the midpoint potential in V, and n = 1 for each pathway. (Here Figure 2.6). The limiting current values for each pathway were chosen by fitting to wild type biofilm voltamograms. Shown in Figure 6 is a derivative plot of a simulation overlaid on a cathodic scan from a wild type *G. sulfurreducens* biofilm, which was grown for 120 h at +0.24 V to obtain an example of the most complex, or heterogeneous voltamograms typically studied in these cells. According to this model, the wild type catalytic wave can be described as a result of three pathways with redox potentials spaced roughly 50 mV apart, causing their output to merge into one broad response.

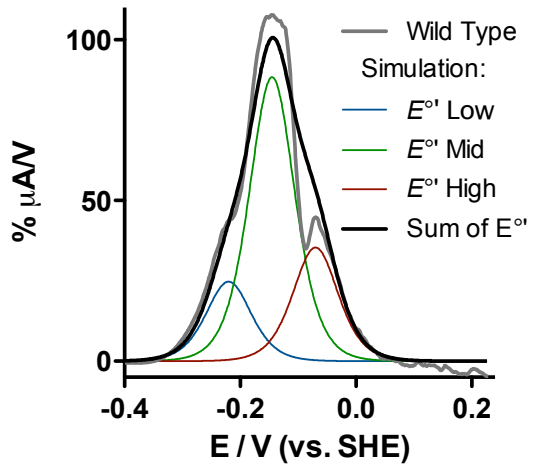

Figure 2.6 *Comparison of wild type voltammetry to 3-site model.* Grey line is the derivative from the cathodic sweep of a fully grown, 120-h old biofilm. Using the equation generated by Richter et. al. [10], derivatives of three different catalytic waves are indicated, with the "Low" midpoint at -0.23 V vs. SHE, "Mid" at -0.15 V and "High" at -0.07 V. The sum of these three catalytic waves is shown by the bold line for comparison to the wild type biofilm scanned at 1 mV/s.

2.4.5 Evidence for redox-dependent regulation of electron flux

Interpreted in the simplest way, this model predicts the CbcL-dependent pathway is responsible for nearly 80% of the flux out of *G. sulfurreducens* cells when an electrode is poised at -0.1 V, which is in agreement with the severe growth inhibition observed when *cbcL* was deleted. However, this model also predicts the CbcL-dependent pathway could contribute over 60% of electron flux out of cells even when redox potentials rise to +0.24 V. This second prediction is at odds with the fact that mutants containing CbcL, but lacking the ImcH inner membrane cytochrome, are unable to grow at higher potentials. CbcL appears not to function when cells are inoculated into a condition where redox potential is above -0.1 V. One explanation could be that the CbcL-dependent pathway is significantly restricted from operating when redox potential rises above -0.1 V, allowing the ImcH-dependent pathway to take over, generate more ATP, and support faster

growth. In Δ*imcH* mutants, the CbcL pathway shuts down as designed, and Δ*imcH* cells fail to respire.

A switching of respiratory pathways above -0.1 V is further indicated by Figure 2.6. Rather than a smooth handoff from the process centered at -0.15 V to those at higher potential, voltamograms reflect a sharp drop and recovery that deviates from any model prediction. A similar event occurs in the same region of single-turnover voltamograms; a sharp cathodic peak near -0.1 V disappears when *cbcL* is deleted (Figure 2.5C). The fact that both *imcH* and *cbcL* have constitutive expression, and are possibly post-transcriptionally regulated via unknown redox potential-dependent interactions, may also explain why earlier 'omic' studies did not draw attention to these proteins (Merkley et al. 2014; Ding et al. 2008a).

2.4.6 Implications for anode growth and analysis of microbial voltammetry

While electrochemical techniques yield useful response curves from bacteria undergoing extracellular respiration, an explanation for the nonstandard sigmoidal voltamogram has remained elusive. Midpoint potentials of outer membrane redox proteins, or electron transfer rate constants at the electrode surface, could govern these features, as extracellular proteins do interface with the electrode. Similarly, based on analogy to redox polymers, many conceptual models of microbial electron transfer invoke a rate-limiting 'mediator' step on the cell exterior with a single diagnostic midpoint potential. However, most analyses of anode bacteria conclude that voltammetry is inconsistent with interfacial electron transfer reactions being slow (Strycharz et al. 2011), and that the midpoint potentials of mediators catalyzing between-cell electron transfer are lower than the midpoint potentials in catalytic voltammetry (Snider et al. 2012). These conclusions point to something other than outer membrane cytochromes being rate-limiting, and show voltammetry does not reflect the mechanism of interfacial electron transfer *per se*. Analogous to protein film voltammetry, electron flow between surfaces and within

redox networks is easily reversible in *Geobacter*. It is instead the reaction with a significant ΔG that controls the kinetics of microbial respiration.

These results provide a warning that subtle redox potential differences can affect pure cultures or communities enriched from the environment. Changes in acceptor potential, such as from 0 V to -0.1 V vs. SHE, are enough to switch *G. sulfurreducens* between two modes of growth. This leads to longer doubling times and smaller biofilms on electrodes. Studies demonstrating similar redox potential effects at this resolution are emerging, such as by Commault et. al. (Commault et al. 2013), Yoho et. al. (Yoho, Popat, and Torres 2014), and Rose et. al. (Rose and Regan 2015).

2.5 Conclusion

There is mounting evidence for at least two electron transfer pathways out of the *G. sulfurreducens* inner membrane that are used in reduction of distant acceptors with distinct redox potentials. These results have implications in energy-generating devices such as microbial fuel cells, because the most valuable pathways are those that operate at the lowest anode potentials, such as those revealed by CbcL. The existence of multiple pathways also suggests that electron transfer to freshly precipitated high potential FeOOH requires different proteins than low potential Goethite or $UO_2(CO_3)_2^{=}$. Syntrophic interspecies electron transfer may also require the donor organism to utilize a low potential strategy (Shrestha et al. 2013). Thus, redox potential must be carefully controlled in the study of extracellular respiration, as regardless of where the electrons ultimately travel, a respiratory bacterium first confronts the reality of thermodynamics at the inner membrane.

2.6 Summary

This study of *cbcL* demonstrates how well controlled respiration is at the inner membrane. It is also now clear how over-looked the role of the inner membrane in

extracellular respiration has been. Future work will have to determine the mechanism of CbcL. The list of protein biochemistry that needs to be done include: determining the involvement of CbcL in menaquinone cycling; determining why CbcL does not function in respiration to high potential acceptors; determining if CbcL interacts with cytosolic and periplasmic proteins, and of course, being able to draw a line of electrons entering CbcL and leaving CbcL in a specific sequence of steps.

Chapter 3: Alterations in CbcL Lead to Phenotypic Changes

Manuscript in preparation. Zacharoff, L., Levar, C., Chan, C., Bond, D.

3.1 Abstract

Recent studies have shown that *Geobacter sulfurreducens* uses two different inner membrane cytochromes for extracellular respiration. The usage of one cytochrome over the other depends on the electrical potential of the terminal electron acceptor. CbcL is used when low potential acceptors are present and ImcH is used when high potential electron acceptors are present. It is unknown why CbcL is incapable of functioning when high potential acceptors are present. Two approaches are used to address the hypothesis that *G. sulfurreducens* protein CbcL can contribute to redox potential selectivity during electrode and metal reduction. First, a *G. sulfurreducens* strain deficient in high potential respiration, Δ*imcH,* was used to create suppressor strains capable of reducing high potential extracellular electron acceptors. Mutations in *cbcL* were identified and recreated. Cells expressing mutants of *cbcL* had different electrochemical profiles and growth properties. CbcL has been shown to function primarily in respiration to low potential electron acceptors but can be mutated to function as an ersatz high potential pathway.

3.2 Introduction

The differences between metal reduction by *Shewanella oneidensis* and *Geobacter sulfurreducens* should not be underestimated, particularly at the inner membrane. The dissimilatory metal reduction of *S. oneidensis* begins at the inner membrane with one menaquinone oxidoreductase, CymA. Electrons are transferred from CymA, through the periplasm and then to the Mtr complex. The Mtr complex uses secreted flavins to shuttle electrons from the Mtr complex to the insoluble terminal electron acceptors (Marsili, Baron, et al. 2008; Kotloski and Gralnick 2013; Hartshorne et al. 2009). Parallels can be draw between metal respiration by *S. oneidensis* and delta proteobacteria such as *Geobacter sulfurreducens*. Comparisons have been made between CymA and the *G. sulfurreducens* protein ImcH (Levar et al. 2015). But, it also important to highlight the differences between inner membrane respiratory systems of these two organisms. Based on the organization of the respiratory chain of *S. oneidensis*, it can be postulated that the organism obtains as much energy from the reduction of manganese oxide (0.5 V versus the standard hydrogen electrode (SHE)) as it does poorly crystalline ferrihydrite (potentials as low as -0.1 V versus SHE)(Majzlan 2012). In other words, the energy yield for these terminal electron acceptors is the same. For example, the number of protons pumped at the inner membrane for every electron moved is the same regardless of the potential of the metal being reduced. One can image that an increase in terminal electron acceptors and/or an increase in shuttle concentration would be able to increase respiration rate *S. oneidensis* extracellular respiration but would not affect the yield. This creates the assumption that insoluble terminal electron acceptors (metals, poised electrodes) are all treated the same by a bacterium and that there was no need of niche differentiation in insoluble metal reduction. In other metal reducing organisms this does not seem to be applicable.

One example of a bacterium broadening electrical niches comes from another phylum. *Geothrix fermentans,* an Acidobacterium, uses two secreted shuttles of

different potentials (-0.2 V and 0.3 V) which allows for access to a wider range of terminal electron acceptors (Mehta-Kolte and Bond 2012). Currently, it is unclear whether *G. fermentans* can optimize respiration using the two shuttle strategy. One mechanism for niche differentiation to occur would require the organism to optimize respiratory pathways at the inner membrane. There is mounting evidence that this is the case for *G. sulfurreducens*. *G. sulfurreducens* has at least two mechanisms for extracellular electron transfer that are terminal electron acceptor potential dependent and that begin at the inner membrane (Levar et al. 2014; Zacharoff, Chan, and Bond 2015). It is possible that these mechanisms exist because of the diversity of iron species and other organisms *G. sulfurreducens* interacts with in its native habitat.

Bosch (2014) predicted that a flexible adjustment of metabolism would be necessary to fully utilize different redox potentials. To that end, the authors calculated the metabolic efficiency of biofilms grown at six different accepting potentials, ranging from -0.105 V to 0.645 V (versus SHE). A general pattern emerged that more protein can be made from a smaller amount of available energy, particularly when the potential of the working electrode was -0.105V. The Bosch 2014 data are consistent with the model in which *G. sulfurreducens* utilizes multiple energy conserving pathways depending on the energy available in the extracellular electron acceptor (Zacharoff, Chan, and Bond 2015). Based on cyclic voltammetry we would not expect any different, metal respiration strategy above ~0.24 V (Zacharoff, Chan, and Bond 2015). Further, unlike *G. fermentans*, the pH neutral environments of *Geobacter* species would not have much need to respire to higher potential metals. There are at least two reasons why *G. sulfurreducens* could benefit from different inner membrane pathways in this potential range. The potential energy differences of these two systems could be enough to generate an additional mole of ATP for every mole of acetate. The other possible reason is that *G. sulfurreducens* utilizes inner membrane respiratory “gears”. For example, one pathway might have a higher rate of turnover. This would not generate more ATP

per electron but one pathway would be more efficient when a lower amount of driving force is available.

Thus far, two potential dependent pathways located at the inner membrane have been characterized in *G. sulfurreducens*. The *b* and *c* type cytochrome CbcL was found to be used primarily to respire low potential acceptors (< -0.1 V) and ImcH (Levar et al. 2014), a cytochrome was found to be essential for the respiration to high potential acceptors (> 0 V) (Zacharoff, Chan, and Bond 2015). Two different approaches are used here to test if insoluble terminal electron acceptor potential niche differentiation could be driven by changes in the electron carriers present at the inner membrane. The first strategy was to isolate suppressors of Δ*imcH* (GSU3359) to respire high potential electron acceptors. This resulted in three instances of single base pair changes to *cbcL* (GSU0274) which resulted in single amino acid changes. Reconstruction of point mutations in *cbcL* in Δ*imcH* backgrounds restored high potential respiration. Expression of CbcL homologs demonstrated that *cbcL* could have different electrical ecological niches in *Geobacter* species closely related to *G. sulfurreducens*. These data further strengthen the hypothesis that CbcL is used specifically for respiration to low potential electron acceptors.

3.3 Materials and Methods

3.3.1 Media, culturing conditions

The basis for all experiments and genetic manipulations was *G. sulfurreducens* MN-1 (Chan et al. 2015). All experiments were conducted using a simple salts media (NB) with donor (20 mM acetate) and a variety of acceptors (40 mM fumarate, 55 mM ferric citrate, poised electrodes required sodium chloride for salt balance (in lieu of sodium fumarate) at 30 °C, under 80% N_2, 20% CO_2. Cultures and experiments were performed in an anaerobic glovebag that had a 5% H_2 in

the atmosphere. Iron reduction was monitored by FerroZine assay as described previously (Zacharoff, Chan, and Bond 2015).

3.3.2 Bioreactors, growth and electrochemistry

Three electrode bioreactors were used for all potentiostatic experiments. Similar to previous studies, a polished (1500 grit sandpaper) 3 cm^2 graphite flag was used as working electrode surface. The counter electrode was a piece of platinum wire and a calomel reference electrode completed the reactor. Conical liquid chambers were anaerobically sealed with a PEEK top. The reactor top further comprised gaskets to keep seals tight around openings that housed electrodes. Eight stainless steel screws are tightened around the top perimeter. Computer aided drafting (CAD) files for this design are provided online by the Angenant lab (Komal Joshii, unpublished data). Potentiostatic control was performed using a VMP, Biologic (Knoxville, TN) potentiostat operated through EC-lab software. A 15 mL total volume of medium was maintained during experimentation. Inoculation was 33% V/V using a 0.5 OD_{600} *G. sulfurreducens* culture. Electrodes were poised at either -0.1 V ("low") versus SHE or 0.24 V ("high").

Cyclic voltammetry was performed on biofilms by poising the electrode at -0.55 V and sweeping at 1 mV/s to a vertex potential of 0.25 V (anodic scan) and then reversing scan direction (cathodic scan). This program was repeated for four cycles. The same program was used to generate nonturnover cyclic voltamograms. To achieve nonturnover conditions, potentiostat programs were paused and bioreactor media was swapped with acetate free medium. Biofilms were allowed to starve overnight. Media was swapped once more with acetate free media. This created current generation of less than 10 $\mu A/cm^2$. Then cyclic voltammetry was performed.

3.3.3 Engineering of *Geobacter sulfurreducens* strains

Ferric citrate and 0.24 V electrode suppressor strain generation.

Both ΔimcH::kan^R and Δ*imcH* cells were inoculated into ferric citrate growth media to a calculated OD_{600} of 0.05. Cells were allowed to fully reduce ferric citrate (as monitored by ferric citrate clearing and FerroZine assay) and were then transferred into fresh ferric citrate medium. This reduction and transfer process was repeated for five cycles. The resulting cultures were streaked for isolation on NBFA agar plates. Isolates were selected, saved and DNA was extracted for sequencing. Two isolates were further pursued, named 5A5 and 5B2.

50/50 Δ*imcH* cells/ electrode medium (OD_{600} 0.52) were used to inoculate three reactors poised at 0.24 V vs. SHE. Electrodes were harvested from bioreactors in an anaerobic chamber when biofilms were producing at least 50 μA/cm^2. Electrodes were rinsed with nongrowth medium and then placed in NB medium with 20 mM acetate, 40 mM fumarate (NBFA). When this electrode outgrowth reach OD_{600} 0.5 reactor inoculation process was repeated. This cycle was completed three times in succession. Three isolates resulting from this process were inoculated into bioreactors. This created strains A, B and C (Figure 3.1B). Strain C was further pursued.

Scarless genomic modification of cbcL to generate single amino acid changes.

The 750 bp flanking regions to the T614C and T614G, encoding the V205A and V205G change in CbcL were amplified using primers GACTTCTAGA TGGCTGTCAATAATGCGCCCTGA and GACTACAAGCTT GGAACAGGAACCAGCGGACCAT from genomic DNA extracted from the Δ*imcH::kan* suppressor mutants that can reduce Fe(III) citrate, strains 5B2 and 5A5. The 1.5 kb DNA fragments were digested with XbaI and HindIII and ligated into the same sites in pK18mobsacB. The 750 bp flanking regions to T1574A, encoding the F525Y change in CbcL was amplified using primers GACT TCTAGA TGGCTGTCAATAATGCGCCCTGA and GACTACAAGCTT

GGAACAGGAACCAGCGGACCAT from genomic DNA extracted from a scarless Δ*imcH* suppressor mutant able to reduce electrodes poised at + 0.24 V vs SHE. The 1.5 kb DNA fragment was digested with XbaI and HindIII and ligated into the same sites in pK18mobsacB.

To generate the single nucleotide mutations in *cbcL* in the chromosome, the pK18mobsacB plasmid with the nucleotide change (T614C, T614G and T1574A) was conjugated into wild type or Δ*imcH* strains using S17-1 *E. coli* donor strain. Genomic plasmid integration encouraged in the presence of kanamycin. A counter-selection using 10% sucrose selected for excision of the pK18mobsacB plasmid. This looping out event generated either the wild type or the mutated allele of *cbcL*. The desired mutants were screened by PCR sequencing of *cbcL*.

cbcL complementation.

cbcL and homologs of *cbcL* were cloned from DNA extracted from *G. sulfurreducens*, *G. metallireducens*, *G. pickeringii* and *G. uraniireducens.* Amplification products were ligated into both prkGeo2 and prkGeo5 plasmid multi-cloning sites using restriction enzyme digestion. Plasmid backbones used in this study are described in detailed in Chan, 2015. Complementation plasmids were mated into *G. sulfurreducens* strains using *E. coli* strain S17-1. Plasmids were maintained in cells in the presence of 200 μg/mL kanamycin. Summary of plasmids and strains are listed in Table 3.1.

Table 3.1 *Plasmids and strains used in this study*

Strain or Plasmid	Description	Source/Reference
Strains		
G. sulfurreducens PCA	Wild Type (ATCC 51573)	Lab collection
ΔcbcL G. sulfurreducens	Markerless deletion of *cbcL* gene in Wild Type *G. sulfurreducens* background	Zacharoff, 2016
Δ*imcH G. sulfurreducens*	Markerless deletion of *imcH* gene in Wild Type *G. sulfurreducens* background	Chan, 2015
ΔimcH::kan^{R}	Kanamycin replacement of *imcH* (GSU3259)	Levar, 2014
5A5	Ferric citrate suppressor strain, from Δ*imcH*::kan^{R}. Contains: *cbcL*^{V205G}, Δ*omcB*, ΔGSU0279	This study.
5B2	Ferric citrate suppressor strain, from Δ*imcH*. Contains: *cbcL*^{V205A}, GSU0758 R133W.	This study.
Electrode C	Electrode suppressor strain, from Δ*imcH*::kan^{R}. Contains *cbcL*^{F525Y}	This study.
cbcL^{V205G} *G. sulfurreducens*	Markerless cbcL point mutation, changing amino acid 205 to a glycine in Wild Type *G. sulfurreducens* background	This study.
cbcL^{V205A} *G. sulfurreducens*	Markerless cbcL point mutation, changing amino acid 205 to an alanine in Wild Type *G. sulfurreducens* background	This study.
Δ*imcH, cbcL*^{F525Y} *G. sulfurreducens*	Markerless cbcL point mutation, changing amino acid 525 to a tyrosine in Wild Type *G. sulfurreducens* background	This study.
Δ*imcH, cbcL*^{V205G} *G. sulfurreducens*	Markerless cbcL point mutation, changing amino acid 205 to a glycine in the Δ*imcH G. sulfurreducens* background	This study.
Δ*imcH, cbcL*^{V205A} *G. sulfurreducens*	Markerless cbcL point mutation, changing amino acid 205 to an alanine in the Δ*imcH G. sulfurreducens* background	This study.
Δ*imcH, cbcL*^{F525Y} *G. sulfurreducens*	Markerless cbcL point mutation, changing amino acid 525 to a tyrosine in the Δ*imcH G. sulfurreducens* background	This study.
E. coli S17-1	Donor strain for conjugation	Simon, 1983
Plasmids		
pK18mobsacB	Markerless deletion vector	Schafer, 1994

pRK2geo2	Vector control and backbone for complementation vector. P_{acpP}.	Chan, 2015
pRK2geo5	Vector control and backbone for complementation vector. P_{TacLac}.	Chan, 2015
P2GS*cbcL*	Complementation vector with constitutive expression of *cbcL*. *cbcL* was cloned into pRK2Geo2.	Zacharoff, 2016
p5GS*cbcL*	Complementation vector with constitutive expression of *cbcL*. *cbcL* was cloned into pRK2Geo5.	This study.
pGM*cbcL*	*Geobacter metallireducens* homolog of *cbcL* in pRK2Geo5	This study.
pGP*cbcL*	*Geobacter pickeringii* homolog of *cbcL* in pRK2Geo5	This study.
pGU*cbcL*	*Geobacter uraniireducens* homolog of *cbcL* in pRK2Geo5	This study.
pDS*cbcL*	*Desulformonas soudanensis* WTL homolog of *cbcL* in pRK2Geo5	This study.

3.3.4 Sequencing

Genomic DNA was extracted from suppressor strains using the Wizard genomic DNA purification kit (Madison, WI). Illumina sequencing of genomic DNA using 50-bp or 250-bp paired end reads were mapped onto the genome of *G. sulfurreducens* strain MN-1 (Chan et al. 2015). Breseq was used to interpret alteration in suppressor strain DNA (version 0.24rc6; Barrick Lab, University of Texas at Austin, TX).

3.4 Results

3.4.1 Δ*imcH* suppressors reveal mutations in *cbcL*.

One main question arose from the potential dependency observation: why are the low potential pathways nonfunctional at higher potentials (when more driving force is available driving force is present). *G. sulfurreducens* cells lacking *imcH* will eventually (after one hundred hours) begin to respire high potential electron acceptors such as ferric citrate and electrodes poised at 0.24 V. Using this phenotype, cells were transferred repeatedly (5 times) onto ferric citrate (+370 mV vs SHE) (Majzlan 2012) until suppressor strains resulted in a wild type levels of

total ferric citrate reduced. Two isolates, 5B2 and 5A5 exhibited reduction rates similar to wild type (Figure 3.1A).

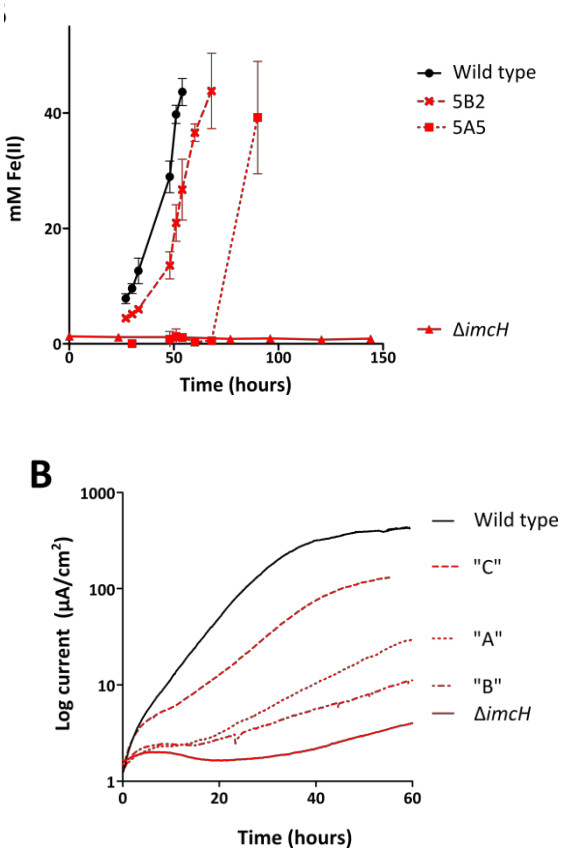

Figure 3.1 *Phenotypes of Δ*imcH *suppressor strains.* A. Ferric citrate reduction during growth permissive conditions. B. Electrode growth phenotypes of resulting suppressor strains.

Genomic DNA from 5A5, 5B2, and "C" Δ*imcH* suppressor strains were sequenced and compared to the sequence of the Δ*imcH* parent strain. (Supplemental Table 1). To ensure the least number of false positives, DNA sequences were compared to a fully sequenced genome of the Bond lab stock *G. sulfurreducens* strain, MN-1. Of interest, were three point mutations occurring in *cbcL* (GSU0274). Ferric citrate suppressor strains sequenced both had a mutation in the DNA sequence encoding for the valine residue at position 205. In 5A5, a single base pair changed the residue valine to a glycine and in 5B2 valine became an alanine. The mutations

in residue 205 are located in the periplasmic domain between hemes 7 and 8 (Figure 3.2A). Both of these amino acid changes are nonpolar neutral replacements of a nonpolar neutral amino acid. In CbcL homologs sharing greater than 64% amino acid identity to *G. sulfurreducens* CbcL this residue is most commonly a valine but has also been changed to a histidine (*G. lovleyi*) and an isoleucine (*Pelobacter selenigenes*) (Figure 3.2B). In the suppressor strain "C", selected by transfer on electrodes poised 0.24 V, the residue 525 was converted from a phenylalanine to tyrosine. This is in a cytoplasmic facing loop of the transmembrane portion of the protein (Figure 3.2A). Phenylalanine 525 is highly conserved. In homologs with over 64% identity, this residue is always a phenylalanine (Figure 3.2B).

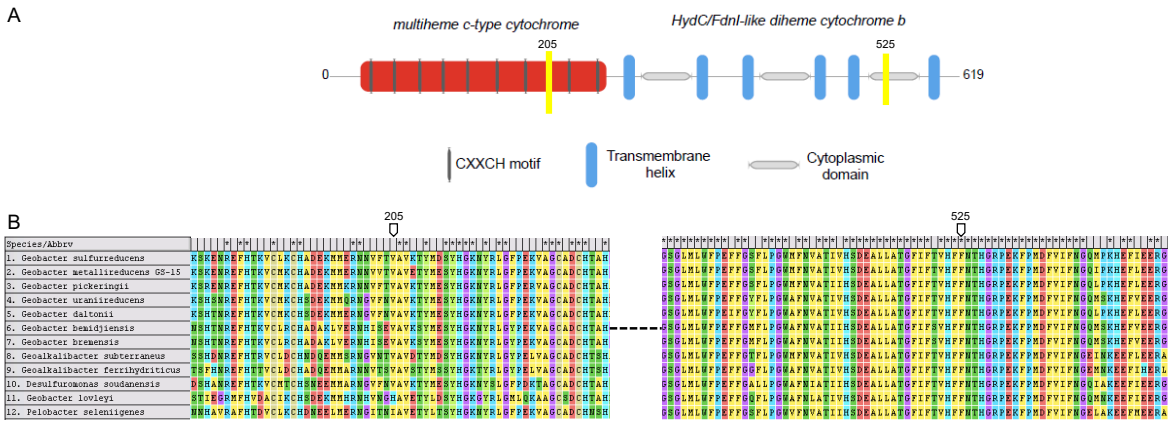

Figure 3.2 *Mutated amino acid residue context and comparison to homologs.* A. Schematic of the domains of CbcL highlighting locations of mutated amino acids. B. Residues in homologs of CbcL. Generated in Mega 7.

Originally, a double mutant containing Δ*imcH*, Δ*cbcL* was created and plasmids containing *cbcL* wild type or one of the *cbcL* variants (containing one of the point mutations) were conjugated into these strains. While cultivation was unimpaired on fumarate, these strains were not able to reduce any terminal electron acceptor (ferric citrate, high and low poised electrodes)(Not shown). This could likely be due to the poor ability of these plasmids to complement the single deletion mutant Δ*cbcL*.

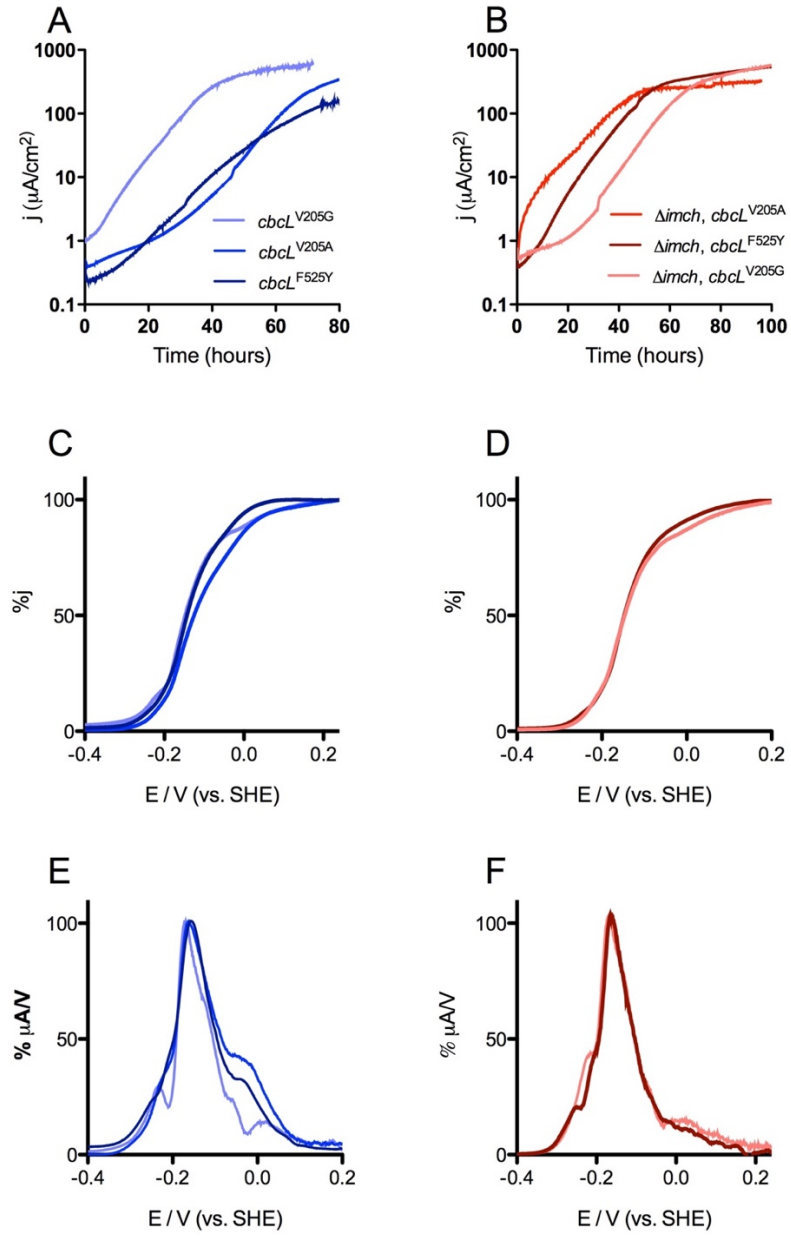

Figure 3.3 *Electrochemical assessment of point mutations in CbcL in wild type (A,C,E) and ΔimcH (B, D, F) backgrounds.* A. Chronoamperometry of *cbcL* variants in wild type background B. Chronoamperometry of *cbcL* variants in Δ*imcH* background. Current production, j, of cells growing on polished graphite electrodes poised at 0.24 V versus SHE. C. Cyclic voltamograms of *cbcL* variants in wild type background during stationary phase biofilms cultivated at 0.24 V. Only the third reducing scan is shown. D. Cyclic voltamograms of *cbcL* variants in Δ*imcH*

background. Cyclic voltamograms are normalized to the maximum current in an individual data set. E., F., Normalized first derivatives of the data in C., D.

3.4.2 Partial recapitulation of suppressor phenotype in Δ*imcH, cbcL* variants

Genomic mutations in *cbcL* (GSU0274) were created so that mutations in *cbcL* could be studied free of variables that come with expression from plasmids. These mutations in *cbcL* were created in both wild type *G. sulfurreducens* and Δ*imcH* backgrounds (summarized in Table 3.1). The resulting strains were tested for reduction phenotypes. The three point mutants had differing abilities to reduced ferric citrate (Figure 3.3A). This ability to reduce ferric citrate was improved from the Δ*imcH* strain which had a lag of over 100 hours before ferric citrate reduction occurred, likely accumulating suppressor mutations. Similarly, when point mutants were presented with a graphite electrode poised at 0.24 V, phenotypes were greatly improved from the Δ*imcH* only strain. Δ*imcH*, *cbcL*^{V205G} exponential reduction did not occur until 20 hours after inoculation in ferric citrate growth medium. The original suppressor strain that contained the V205G mutation had a 55 hour lag in ferric citrate reduction and the final total amount of iron compared to wild type was the same. Δ*imcH*, *cbcL*^{V205A} also had comparable ferric citrate reduction phenotype when compared to the suppressor strain that carried the originally identified mutation. Phenotypes are summarized in Table 3.2. Δ*imcH*, *cbcL*^{V205A} and Δ*imcH*, *cbcL*^{V205G} respired and formed biofilms comparable to wild type in bioreactors with working electrodes poised to 0.24 V. Δ*imcH*, *cbcL*^{V205G} did have a slight lag before exponential growth (Figure 3.3B).

Δ*imcH*, *cbcL*^{F525Y} was created to recapitulate suppressor strain “C” cultivated by selective pressure using a poised electrode (0.24 V). The electrode respiration phenotype of this mutant was not significantly different than that of wild type (Figure 3.3B). If potential was the only variable governing respiration, it predicts that this mutant would be able to respire ferric citrate with wild type rates and

extents. This was not the case. This mutant had more than a 70 hour lag phase before beginning exponential reduction of ferric citrate.

In these strains, the respiration rate and total final current was not significantly different than found for wild type. Since absence of the *cbcL* gene in *G. sulfurreducens* creates strains with near normal growth at high potential but also has 0.05 V positive shift midpoint potential, cyclic voltammetry (CV) was used to assess whether or not the CbcL variants were still functional when these point mutants were present. When potential scans were performed on fully grown biofilms both Δ*imcH*, *cbcL*^{F525Y} and Δ*imcH*, *cbcL*^{V205G} strains had wild type CVs. This was highly reproducible. Δ*imcH*, *cbcL*^{V205A} showed instability. 50% of biofilms had a wildtype character and the other 50% had a Δ*cbcL* character even though growth of these biofilms was not significantly different (Supplemental figure 3.1).

Table 3.2 Phenotypic summary of point mutations in *cbcL*.

	cbcL^{V205G}	*cbcL*^{V205A}	*cbcL*^{F525Y}	Δ*imcH*, *cbcL*^{V205G}	Δ*imcH*, *cbcL*^{V205A}	Δ*imcH*, *cbcL*^{F525Y}	Δ*imcH**	Δ*cbcL***	Wild Type
Doubling time, ferric citrate (hours)	7.1	6.1	N/A	10.0	N/A	3.9	N/A	8.3	5.7
Lag time ferric citrate (hours)	0	0	0	50	70	90	>100	0	0
Doubling time 0.24 V electrode (hours)	5.5	5.7	6.9	5.9	6.7	6.1	N/A	8.0	5.6
Lag time, 0.24 V (hours)	0	0	0	30	0	0	>100	0	0
Current density 0.24 V ($\mu A/cm^2$)	470	615	487	600	452	454	N/A	338	459
μA/V at 0.15 V	638	705	714	703	N/A	710	N/A	N/A	719

*from Levar, 2015, **from Zacharoff, 2016

3.4.3 Expression of *cbcL* homologs alters cyclic voltammetry

If single point mutations were causing detectable phenotypes, it could be questioned if any point mutations, or any combination of point mutations, could

cause phenotypes. To narrow down candidates, the top three homologs were cloned into expression vectors. *G. metallireducens cbcL* (GMET_0100) homolog has an 89% amino acid identity with *G. sulfurreducens cbcL* (in prkGeo5 plasmid backbone, pGM*cbcL)*; *G. uraniireducens,* 83% identity (pGU*cbcL,* GURA_0125); *G. pickeringii* 90% identity (pGP*cbcL*, Gpick_14345). To see how CbcL homologs affect the CV of *G. sulfurreducens* grown on electrodes, plasmids encoding them were conjugated into wild type and Δ*cbcL* strains and grown on electrodes poised at + 0.24 V.

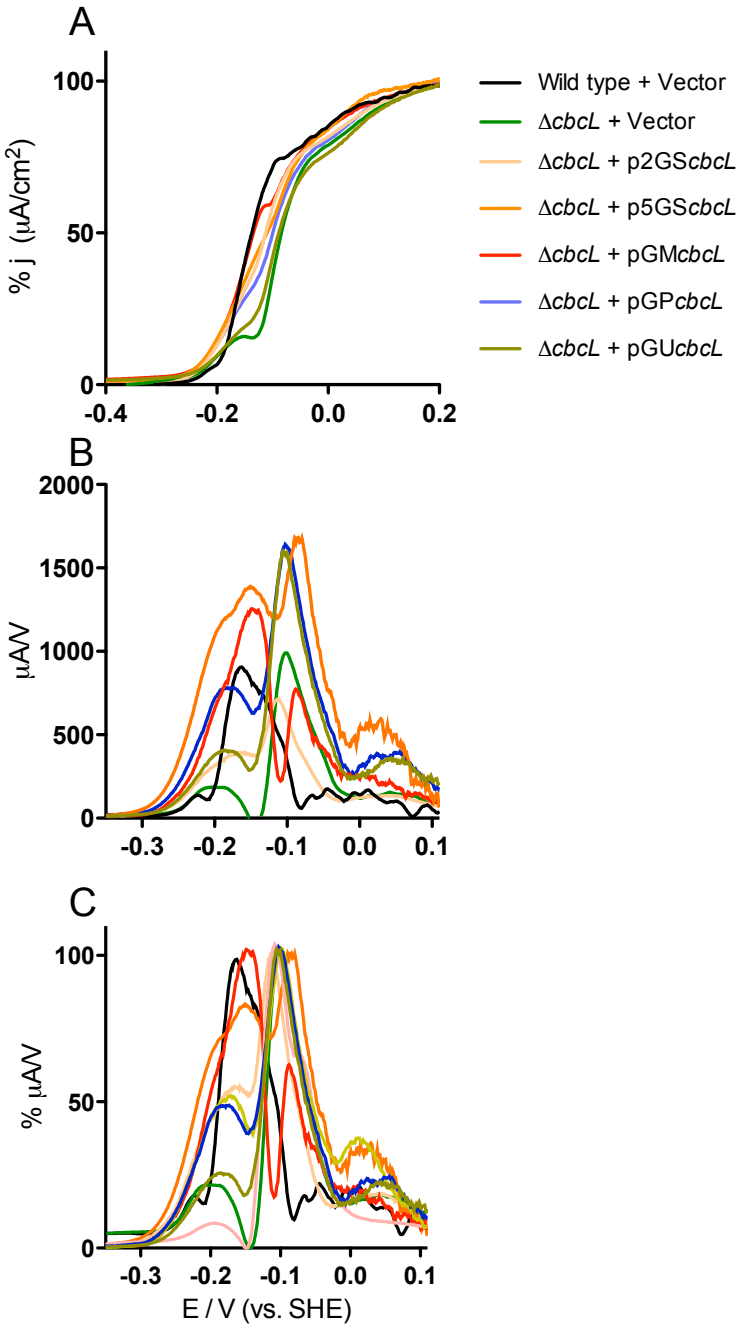

Figure 3.4 *Cyclic voltammetry (CV) of ΔcbcL strains complemented with cbcL homologs*. All biofilms used to generate CV were poised at 0.24 V. A. Current production over different potentials scanned at a rate of 1 mV/s. Just the third oxidizing (anodic) scan in shown. B. First derivatives of CVs from figure A. C. First derivatives normalized to a particular scans highest peak height.

Table 3.3 *Cyclic voltammetry summary of cbcL homologs.*

	p5GS*cbcL*	P5GM*cbcL*	pGP*cbcL*	pGU*cbcL*	pDS*cbcL*
Doubling time 0.24 V electrode (hours)	6.23 (0.917)	8.56	7.8	6.1	19.6
Current density 0.24 V ($\mu A/cm^2$)	311	208	213	292	127
μA/V at 0.15 V	310	671	724	300	591
μA/V at 0.10 V	726	400	527	591	586

All complemented strains grew biofilms at high potential. As listed in Table 3.3, doubling time and total current density was less than that of wild type *cbcL*. Under these conditions, cyclic voltamograms were performed (Figure 3.4). It is clear that different homologs can augment the properties of the redox mediator attributed to the CbcL potential at -0.15 V. Properties to the CV that were changed in the 0.15 V region include the rate of current production ($\mu A/cm^2$) (Figure 3.4C). It is interesting that the catalytic voltamograms cannot predict ability to grow on a low potential electrode. This would mean that is likely that CbcL is affecting electron transfer in a way that is more indirect to growth, for instance, changing the proton balance across the inner membrane. Non-turnover CV measurements of these biofilms support of this idea. In the absence of acetate, the predominant non-turnover peak seen in wild type is not complemented to any extent. This is compared to Δ*cbcL* that are complemented with the native version of *cbcL* which have partially complemented non-turnover CVs (Figure 3.5). Since complementation is not complete, even with the wild type version of this gene on any plasmid tested, it is hard to say anything conclusively about the lack of complementation at low potentials.

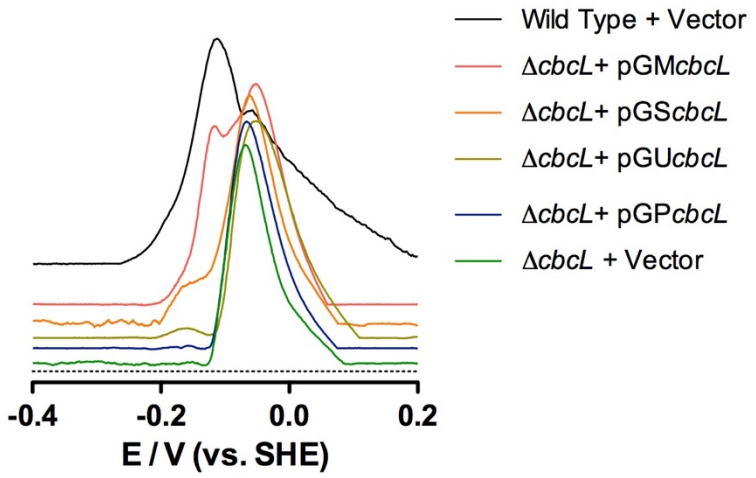

Figure 3.5 *Noncatalytic cyclic voltammetry* of Δ*cbcL complemented with homologs*. Acetate deplete biofilms were rinsed in acetate free medium and further starved. The third oxidizing scan for different complemented strains is displayed. All sweeps are normalized to highest peak height within a given data set. Scans displayed are offset in the y-axis to aid in clarity.

3.5 Discussion

The results of this experiment allude to CbcL as being specifically used when the driving force for respiration is low, i. e. not abundant. ImcH on the other hand is used when there is an excessive amount of driving force available. *E. coli* use an analogous system for oxygen respiration. The *E. coli* genome encodes two terminal oxidases. One terminal oxidase, cytochrome *o* has a K_m of 1.4 to 2.9 μM (oxygen concentration). The other terminal oxidase, cytochrome, *d*, has a K_m of 0.23 to 0.38 μM. Under low oxygen conditions *E. coli* expresses the high affinity oxidase, cytochrome *d* (White 2007). Thus, *E. coli* makes a tradeoff for a slower reaction rate, higher affinity oxidase when the concentration of the terminal electron acceptor is low.

In order for this to be true about *cbcL* and *imcH,* there needs to be a regulatory mechanism. *G. sulfurreducens* transcribes *cbcL* and *imcH* to similar levels when electrodes are poised to high potential or low potential (Zacharoff, Chan, and Bond

2015). This rules out regulation at the level of transcription. Additionally, during the course of cyclic voltammetry, there is evidence that *G. sulfurreducens* switches between CbcL and ImcH dependent pathways. During the course of cyclic voltammetry the potential is changed at a rate of 1 mV/ s. This would not give the organism enough time to translate new proteins. This rules out a regulatory mechanism at the level of protein translation. Together, this means there would need to be a built in ability for CbcL and ImcH to undergo reversible inactivation. Further work will need be done on the isolated protein to determine this mechanism. There is also precedence for this behavior in respiratory chains. For instance, [Fe-Fe] or [Fe-Ni] hydrogenases exhibit reversible inactivation at high potentials (Vincent et al. 2005). Redox dependent conformational changes in heme proteins are not unprecedented and are an intriguing explanation for the potential dependent responses of CbcL and ImcH (Morgado et al. 2007; Smith and Rosso 2014).

3.6 Summary and future directions

Two intriguing questions need to be answered. First, is there a difference in the amount of energy produce between CbcL and ImcH dependent pathways? Second, are the point mutations identified in CbcL preventing reversible inactivation of CbcL?

The first question can be answered in a few different ways. Membrane potential sensitive dyes can detect differences in the inner membrane of bacteria. These difference in membrane charge can be detected either by microscopy or by flow cytometry. The balance of ATP/ADP in cells lacking *cbcL* and *imcH* would also be informative of the efficiencies of these pathways. This could be compared to the amount of protein that these mutants are capable of making under different respiratory conditions.

The second question would be affectively addressed using protein biochemistry of CbcL and CbcL variants. Cyclic voltammetry of purified CbcL could be performed to detect differences in responses to electrical potential. This technique has been used to successfully characterized the kinetics of CymA (McMillan et al. 2012).

Additionally, other dissimilatory metal reducing bacteria contain copies of *cbcL* and *imcH*. In the genome of *Desulfuromonas soudanensis*, for instance, *cbcL* and *imcH* are only separated by one gene (Badalamenti et al. 2016). Like *G. sulfurreducens*, *D. soudanensis* can respire electrodes. Cyclic voltammetry performed on this organism identified a midpoint potential that is 100 mV more positive than the dominant midpoint potential of *G. sulfurreducens.* Deletion mutants of *cbcL* should be created in *D.* soudanensis to see if CbcL is similarly involved in *D. soudanensis* respiration. Additionally, growth and respiration studies should be conducted on

Δ*imcH* and Δ*cbcL* strains to see if these genes have the same specificity to high and low potentials of terminal electron acceptors.

Chapter 4: Supporting data for CbcL studies including gene deletions ΔGSU0273 and ΔGSU0070

4.1 Localization of CbcL in wild type *Geobacter sulfurreducens*

4.1.1Introduction

In this section the cellular location of CbcL is confirmed. For this protein to function as a menaquinone oxidoreductase the transmembrane helices must be in the inner membrane. The gene sequence of *cbcL* (GSU0274) predicts this inner membrane localization for the transmembrane region of this protein. Protein localization prediction algorithms, such as PSORTb, concur with an inner membrane localization. Additionally, there would be no reason to suspect that the transmembrane helices of CbcL would be located anywhere but the inner membrane. Nonetheless, wild type *Geobacter sulfurreducens* cells were subjected to a membrane fractionation procedure. Succinate dehydrogenase of *G. sulfurreducens* is located in the inner membrane and the enzymatic activity of this enzyme was used to confirm the fraction associated with the inner membrane. An antibody generated against a small peptide fragment of CbcL was used to demonstrate CbcL enrichment in the inner membrane.

4.1.2 Materials and Methods

Geobacter sulfurreducens growth and membrane fractionation.

Stationary phase *G. sulfurreducens* cells grown in 20 mM acetate, 40 mM fumarate were pelleted at 4,000 X *g* for 10 minutes. The cell pellet was then washed with a 50 mM Tris-HCl buffer (pH 8, 1 mM $MgSO_4$, 0.2 mM $CaCl_2$, 1 mM EDTA). After a second pelleting cells were resuspended in 50 mM Tris-HCl (pH 7.5 1 mM $MgSO_4$, 0.2 mM $CaCl_2$). Cell lysis was accomplished by three passes through a French pressure cell (1500 pounds per square inch). Lysate was moved through the following centrifugation sequence: 12,000 X *g* for 20 minutes (debris removal, pellet discarded), 100,000 X *g* for 1 hour (this pelleted membranes, supernatant discarded). The Membrane pellet was resuspended in same buffer. The tris-HCl, divalent cation buffer was used to make 30%/50%/70% sucrose gradient layers. The resuspended membrane sample was layered on top of the sucrose gradient

and centrifuged in a swinging bucket rotor for 20 hours at 113,000 X *g*. This created two distinct red bands. The sample was carefully removed from the top. The first red band designated “top,” the medium between red bands designated “middle,” and the last red band removed from the gradient tube labeled “bottom.” Samples were dialyzed (10 kDa molecular weight cut off, Thermo Scientific, Rockford, IL) against 1 L 50 mM Tris-HCl for 1 hour and then repeated for 24 hours. Resulting samples were concentrated using Amicon centrifuge tubes (30 KDa molecular weight cut off, Merck Millipore, CO). Resulting samples were tested for the presence of succinate dehydrogenase (Levar et al. 2014) activity to determine inner versus outer membrane fractions and were also used for western blotting.

Succinate dehydrogenase assay

PMS (40 μM) and DCPIP (50 μM) were added to protein fractions (13 mg/ml). This sample was then made anaerobic. The sample was monitored for absorbance at 600 nm. Succinate was then spike into the sample, the sample was mixed and monitoring at 600 nm continued.

Western blotting

Protein samples were resolved on 12% polyacrylamide gels in SDS-Tris gels run at 200 V for 60 minutes. Proteins were transferred onto a PVDF membrane at a constant 0.4 amps for 80 minutes. The membrane was then blocked in 5% dry milk solution in blotting buffer for one hour. Polyclonal primary antibody was generated in a goat against a synthetically generated peptide fragment of CbcL (GenScript, Piscataway, NJ). The primary antibody was applied to the membrane in 1% milk and blotting buffer solution and incubated at 4°C overnight. The membrane was then washed using five ten minute rinses in blotting buffer. 1:10,000 secondary antibody (Alexa Fluor 633 mouse anti goat Thermo Fisher) in 1% milk in blotting buffer was applied and the membrane was incubated for one hour. Protein labeling was visualized by the Storm 860 western blot imaging system (University of Minnesota Imaging Center).

4.1.3 Results and Discussion

As expected, antibodies detected CbcL to be most enriched in the “bottom” red fraction (Figure 4.1B). There is some slight labeling by this antibody in the other fractions. This could be improved upon by centrifuging the fractionation tube for a longer amount of time. The predicted weight of CbcL (including all nine heme groups, 685 Da per heme) is 76.7 kDa and this is the weight of the antibody labeled band as judged by the protein ladder. Likewise, the same membrane fraction having the highest amount of CbcL also had the highest level of succinate dehydrogenase activity (Figure 4.2B). This is also consistent with similar experiments that localized *Geobacter sulfurreducens* protein ImcH to the inner membrane (Levar, 2015).

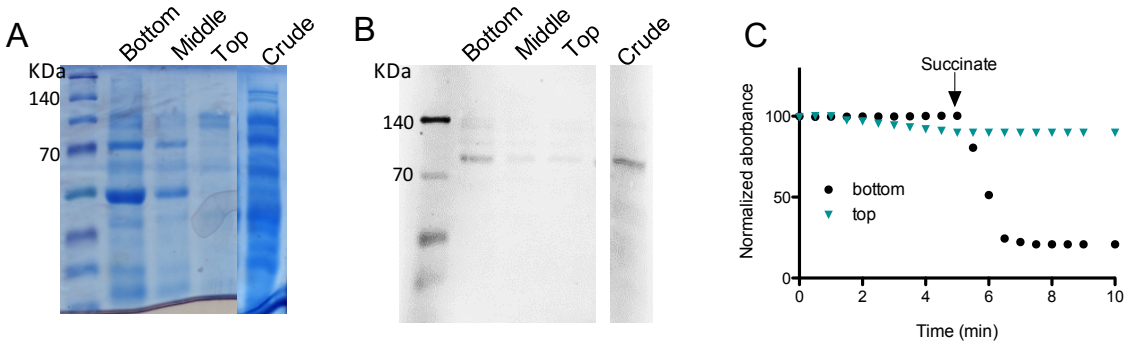

Figure 4.1 *Antibody based localization of of CbcL in sucrose gradient* A. Total protein stain of an SDS-PAGE gel. B. Western blot analysis. C. Succinate dehydrogenase activity assay.

4.2 Determination of nitrogen utilization phenotype in *Geobacter sulfurreducens* cells lacking *cbcL*

4.2.1 Introduction

Other functions for putative quinone oxidoreductases involve utilization of other sources of nitrogen. In routine growth and experimentation *Geobacter sulfurreducens* media contain ammonia as a nitrogen source. In the environment other sources of nitrogen might have to be utilized and these nitrogen sources probably would require *Geobacter* species to divert respiratory electrons to nitrogen assimilation. It was necessary to test whether or not the phenotypes observed in *cbcL* deletion strains were due to an underlying nitrogen utilization impairment.

4.2.2 Results and Discussion

Transcriptome data of *Geobacter sulfurreducens* while using different nitrogen sources is available for access through the data base Microbes online. Figure 4.2 was generated with this website which is based on Qi, 2013 data. (Source, Microbesonline.org. on data from Qi, Y, 2013 (http://www.ncbi.nlm.nih.gov/geo/query/acc.cgi?acc=GSE17834).

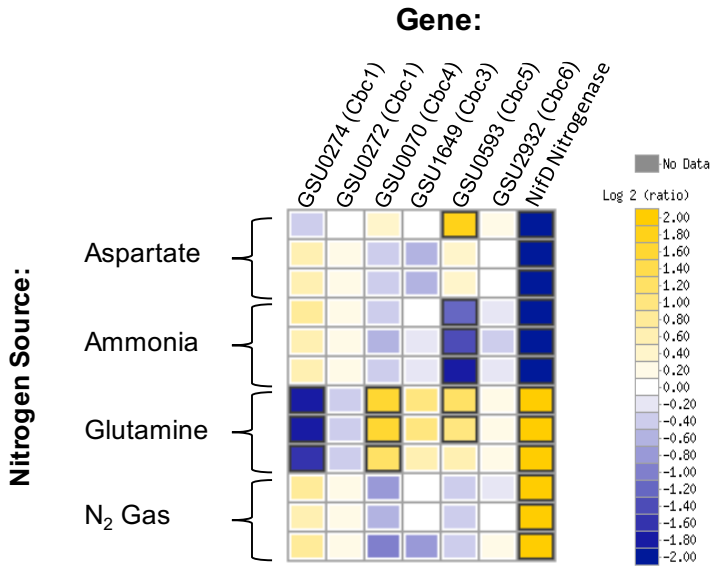

Figure 4.2 *Transcriptome data from microbes online*. One representative from each of the *cbc* operons is included. Yellow is increased transcription and blue is decreased transcription. Source, Microbesonline.org on data from Qi, Y, 2013 (http://www.ncbi.nlm.nih.gov/geo/query/acc.cgi?acc=GSE17834).

The transcriptome data suggests that *cbcL* gene is downregulated when glutamine is the nitrogen source provided. Which makes it possible that *cbcL* is used when cells are grown with other nitrogen sources but not with glutamine. Since Δ*cbcL* has the most prominent phenotype on low potential terminal electron acceptors, different nitrogen sources were supplemented in the electrode growth media. Nitrogen sources made no difference on growth ability.

4.4 Removal of GSU0273 does not create same phenotypes as removal of GSU0274 (*cbcL*)

4.4.1 Introduction

The genomic region just upstream of *cbcL* (GSU0274) encodes an iron sulfur cluster containing protein, GSU0273. As respiratory systems often make use of iron sulfur cluster proteins, and these proteins are often low potential, it was hypothesized that a deletion of this protein might affect the same low potential respiratory pathway that invokes *cbcL*. Here it is shown that a scarless deletion of the iron sulfur cluster protein has no detectable electrode respiration phenotype.

4.4.2 Materials and Methods

Markerless deletion of GSU0273 was created as previously described (Chapter 2 of this thesis)(Chan et al, 2015). Cells were inoculated into three electrode bioreactor systems and cyclic voltamograms were performed on stationary phase biofilms.

4.4.3 Results and Discussion

No difference in growth rates or extents were seen when the electrode was poised to +0.24 V or when the electrode was poised to -0.1. Figure 4.3 shows the results of potential sweeping in a cyclic voltamogram. No phenotype was detected in all conditions tested.

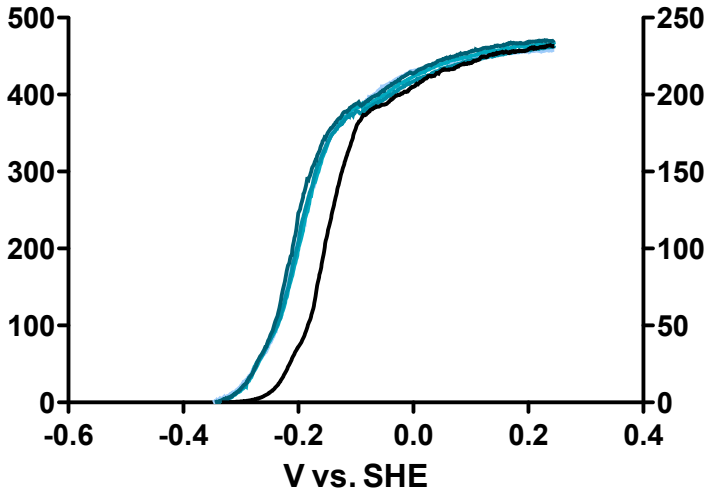

Figure 4.3 *Cyclic voltamograms of ΔGSU0273* mutants in teal, compared to Δ*cbcL* mutants in black. Y- axes are in current densities, j, μA/cm^2.

4.5 Removal of GSU0070 creates a nitrogen source utilization phenotype during high potential respiration

Cbc3 is an operon containing *cbcU* (gsu0070) which encodes a predicted cytochrome *b*/b_6 domain (Table 1.1). To test for other respiratory pathways, a scarless deletion of *cbcU* was created and tested for respiration deficits. Like all *cbc* operons, there is also transcriptome data suggesting that nitrogen assimilation is dependent on different inner membrane systems. To that end, the Δ*cbcU* was also tested for respiratory deficits when nitrogen sources other than ammonia were used.

Under growth conditions typically used in the Bond lab, there was no detectable phenotype of Δ*cbcU.* However, when either glutamine or aspartate was used instead of ammonia a growth impairment was noticed when biofilms were cultivated at high potential only (Figure 4.5A). Since Δ*cbcL* had an altered cyclic voltamogram, Δ*cbcU* was also tested for altered cyclic voltamograms. Under normal conditions (high potential, ammonia as a nitrogen source) there was no alteration in the cyclic voltamogram (figure 4.5B).

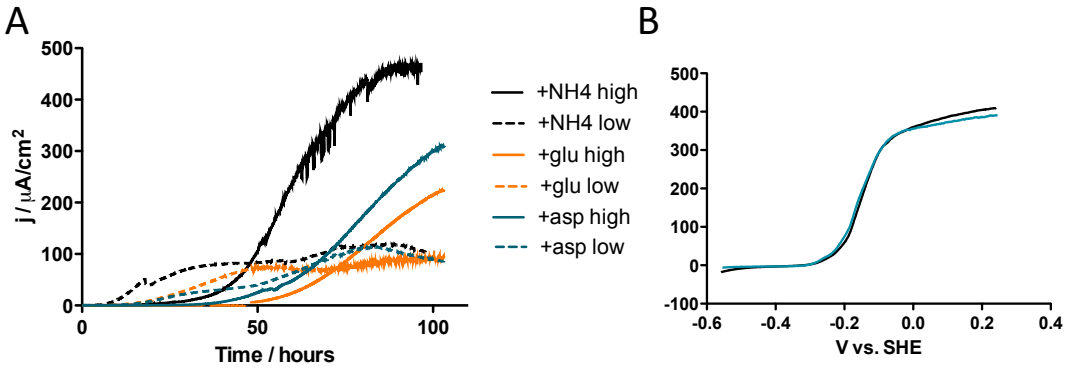

Figure 4.5 *Electrochemical phenotype of Δ*cbcU*.* A. Chronoamperometry of Δ*cbcU*. Growth at low potential under different nitrogen sources was unaffected. Diminished growth at high potential when glutamine (glu) or aspartate (asp) were provided instead of ammonia (NH_4). B. Cyclic voltamograms of Δ*cbcU* (teal) and wild type *G. sulfurreducens* (black).

4.6 Summary

The inner membrane, like the rest of the genome of *G. sulfurreducens*, cannot be analyzed with proteomic and transcriptomic approaches because of the number of hypothetical proteins. One of the most promising approaches is the method of transposon sequencing and transposon screening. Testing nitrogen sources during such transposon experiments would be useful. In the end, mutants will need to be constructed in combination to prevent pathway overlap

Chapter 5: PgcA facilitates respiration to insoluble iron oxides but not to electrodes in *Geobacter sulfurreducens*

Lori Zacharoff, Dana Morrone, Daniel Bond
Manuscript in preparation

5.1 Abstract

Metal reduction and electrode reduction by *Geobacter sulfurreducens* had long been assumed to use similar processes. Recent studies make this assumption seem less and less likely to be the case. Here a triheme *c*-type cytochrome is characterized in terms of phenotypic significance and biochemical properties. Data presented here supports a function for PgcA during reduction of insoluble metals, not for reduction of electrodes. Cells lacking the *pgcA* gene cannot reduce ferrihydrite or birnessite. Contrarily, these cells have no impairment respiring ferric citrate or poised electrodes. PgcA protein was expressed and purified from a host organism, *Shewanella oneidensis*. The purified protein has an unusually high oxidation-reduction potential and a secondary structure composed mostly of alpha helices. Further, PgcA is demonstrated to act extracellularly in a manner that is synergistic to a known electron shuttle, flavin mononucleotide.

Importance

Biogeochemical cycling of metals is performed by bacteria dwelling in the anaerobic subsurface of the Earth. Some anaerobic bacteria are capable of using insoluble metals and poised electrodes as terminal electron acceptors during respiration. These same organisms, such as the bacterium, *Geobacter sulfurreducens*, are now being exploited in wastewater treatment and environmental remediation. Little is known about the mechanisms these bacteria use to interact with metals. Here, *Geobacter sulfurreducens* is used as a model organism for metal and electrode respiration. PgcA is a protein from *Geobacter sulfurreducens* that is identified here as having a powerful impact on metal reduction.

5.2 Introduction

Dissimilatory metal reducing bacteria, such as *Geobacter sulfurreducens*, have to transfer terminal respiratory electrons to the extracellular space and then to insoluble metals such as iron oxides and manganese oxides. Iron oxides exist as a heterogenous mixture of insoluble particles in nature. These particles have a range of redox potentials and also have a tendency to change redox potentials as they are being reduced by bacteria (Majzlan 2012; Nealson and Saffarini 1994). Respiration of recalcitrant iron oxides in anaerobic soil and sediment requires *G. sulfurreducens* to respond and overcome these challenges by modifying the extracellular space. The composition of the extracellular matrix is complex and regulated. *G. sulfurreducens* secretes polysaccharides (Rollefson et al. 2011), pili (Klimes et al. 2010) and multiheme *c*-type cytochromes (Ding et al. 2006; Ding et al. 2008b) depending on the respiratory conditions.

Researchers have wondered if a protein could serve as a shuttling compound for *G. sulfurreducens*, in a way that is similar to small redox active molecules that are used by *Shewanella oneidensis* (Marsili, Rollefson, et al. 2008; Coursolle and Gralnick 2012; Lies, 2005; von Canstein, 2008) and *Geothrix fermentans* (Mehta-Kolte and Bond 2012). In 1999, Lloyd and Lovley noted a 41 kDa protein that was secreted by *G. sulfurreducens* into the supernatant that absorbed strongly to iron oxides. The properties of PgcA, as identified in the study presented here, bears striking similarity to this unidentified protein. PgcA (periplasmic GEMM regulated cytochrome A) is amongst the extracellular multiheme *c*-type cytochromes. Transcription of *pgcA* is controlled by an upstream riboswitch known as the GEMM (genes for the environment, motility and membranes) motif. In response to an increase in cyclic AMP-GMP dinucleotide levels, *pgcA* mRNA transcript is derepressed and translation increases (Kellenberger et al. 2015; Winkler and Breaker, 2005; Nelson, Breaker 2014). Proteomic studies of *G. sulfurreducens* all concur that PgcA is more abundant when insoluble iron oxide is the terminal

electron acceptor, when compared to soluble ferric citrate (Ding et al. 2008b), and when compared to manganese oxides (Aklujkar et al. 2013). Despite this knowledge of the regulatory mechanisms and importance for reduction of metals, little is known about the function and biochemistry of the protein itself.

PgcA contains three CXXCH motifs, which predicts that three *c*-type hemes are present. Given the putative extracellular localization of PgcA it is implicated in electron transfer from other heme proteins to a final terminal electron acceptor, such as insoluble iron oxides. PgcA and its corresponding gene have not previously been studied in a system free of factors complicated by laboratory evolution studies (Tremblay et al. 2011; Smith et al. 2014; Yi et al. 2009a). Here, an investigation into the function of PgcA itself is progressed by using a markerless *pgcA* (Δ*pgcA*) deletion strain to characterize phenotypic deficits. The prediction that *pgcA* is important in insoluble iron oxide respiration was validated. However, it seems that the role of *pgcA* is exclusive to insoluble metals. It has been assumed in the past that poised electrodes and insoluble metal substrates required the same to similar processes. This is not the case with *pgcA*. What can be said definitively is that the role of PgcA is specific to insoluble metals and not to extracellular electron transport in general.

5.3 Materials and Methods

5.3.1. Cell culture and growth assays

Bond laboratory stocks of *G. sulfurreducens* PCA and mutants (described below) were resuscitated by streaking on to 1.5% agar containing minimal salts medium (NB) (Chan et al. 2015; Marsili, Rollefson, et al. 2008) with 20mM acetate and 40mM fumarate (NBFA). All *Geobacter sulfurreducens* cultures and media were prepared anaerobically under 80% N_2, 20% CO_2 atmosphere.

Bioreactor experiments contained salt balanced NB medium with 20 mM acetate. Overnight cultures of *Geobacter* strains, OD (600) of 0.5, were used as an inoculum. Polished graphite flags, with a surface area of 3 cm^2, were used as working electrodes. A small piece of platinum wire was used as a counter electrode and a calomel electrode was used as a reference electrode. Bioreactors were maintained at a constant 30 °C. Electrodes were harvested after uninterrupted growth at a potential of 240 mV versus standard hydrogen electrode (SHE) for use in determining current to protein ratio. Bacterial proteins were stripped from electrodes using 0.2 N sodium hydroxide, boiling and vortexing. Total protein of resulting supernatant was determined using bicinchoninic assay (Thermo Scientific). Similarly, reduction of insoluble iron oxide (55 mM), ferric citrate (55 mM) and manganese (30 mM) during growth conditions was performed in NB, 20 mM acetate.

Progress of Fe(III) reduction was measured by monitoring accumulation of Fe(II) by means of a FerroZine assay. As previously described (Rollefson, Levar, and Bond 2009; Levar et al. 2014) 100 μL samples were extracted from 10 mL Balch culture tubes and digested in 1N hydrochloric acid until experiment conclusion when the FerroZine assay was performed in 96 well plate format.

5.3.2 Biofilm formation

Cell attachment phenotype to surfaces was characterized using a crystal violet, 96 well plate assay as described in detail previously (Rollefson, Levar, and Bond 2009; Rollefson et al. 2011) Growth media contained 30 mM acetate, 40 mM fumarate. Incubation occurred for 72 hours. Optical density at 600 nm was measured, cells were stained with 0.006% crystal violet and incubated for 15 minutes at room temperature. Excess dye was carefully rinsed away with distilled water. 300 μL of 100% DMSO was used to solubilize the dye that remained

attached to cells that had been adhered to the well surfaces. Microwell plates with Nunclon were used in this study (Thermo Fisher Scientific).

5.3.3 Strain construction

G. sulfurreducens Δ*pgcA* was created using the markerless deletion method described in Chan et al., 2015 and Zacharoff et al., 2016. 1 kB up and downstream regions of GSU1761 (*pgcA*) were cloned into pk18mobsacB vector. This plasmid was mated into *G. sulfurreducens* via *E. coli* strain S17-1. First round of selection was performed on (200 μg/mL) kanamycin NBFA plates. Kanamycin resistant colonies were restreaked and plated on 10% sucrose for a second round of selection. Bacterial colonies capable of growth on sucrose plates underwent recombination events that resulted in reversion to wild type or to gene deletion. Colonies from this round of selection were then patched onto NBFA plates and kanamycin NBFA plates. Colonies that remained sensitive to kanamycin were then screened for loss of GSU1761 using PCR. GSU1761 was cloned into prkGeo3 (Chan et al., 2015) backbone for growth complementation testing. GSU1761 was also cloned in pBAD202/D-TOPO® (Thermo Fisher Scientific) plasmid backbone which resulted in an arabinose inducible expression vector containing PgcA fused to a 6X – histidine tag on the carboxy terminus (pBAD202PgcA).

S. oneidensis was electroporated in the presence of pBAD202PgcA plasmid. Prior to this transformation the expression plasmid was passaged through a methylation minus *E. coli* K12 ER2925 strain (New England Biolabs, Ipswich, MA). Transformants were selected on 50 μg/mL kanamycin infused LB plate. *S. oneidensis* strains were obtained from the Gralnick laboratory stock. See Table 5.1 for strain designations. *S. oneidensis* was routinely cultured in lysogeny broth (LB)

(Becton, Dickinson & co, Franklin Lakes, NJ). Plasmids and deletion strains were sequence confirmed at UMGC, University of Minnesota.

5.3.4 Protein purification

10 mL cultures of the PgcA expressing strain of *S. oneidensis* were used to inoculate 1 liter of LB medium containing 50 μg/mL kanamycin. Cells were incubated at room temperature (25 °C) at slow rotation speed to achieve microaerobic conditions. The use of non-baffled shake flasks also decreased the amount of oxygen in the medium. The optical densities at 600 nm of the cultures were monitored until an optical density of 0.5 was achieved. At this time 3 mM (final concentration) of arabinose was added to induce PgcA expression. 100 μM $FeCl_3$ was also added at this time to increase the amount of bioavailable iron in the medium. Cells were pelleted 18 hours after induction at 4,000 × *g*. The pellet was washed with 100 mM Tris-HCl, 200 mM NaCl, pH 7.5 buffer. Resuspension and lysis via sonication (50% duty cycle, amplitude of 20%, 2 cm horn, for 30 minutes) was performed in the same buffer with lysozyme and DNase. Lysate was centrifuged at 30,000 × *g* for thirty minutes. The soluble fraction was loaded on to a nickel affinity column. Protein was eluted with 300 mM imidazole. Concentrated eluent was further purified with gel filtration or anion exchange chromatography. Gel filtration was done using a 45 cm length, 1 cm diameter column filled with Sepharose 6B (Sigma-Aldrich, St. Louis, MO). A flow rate of 1 mL/min was used during column equilibration and sample separation. Anion exchange separation was performed using HiTrap Q HP, 5 mL columns (GE Health Care, Uppsala, Sweden). A flow rate of 5 mL/min was used. Sample was loaded onto column in no salt 100 mM Tris-HCl. Then a gradient program was initiated using a mixture of 0.5 M NaCl, 100 mM Tris-HCl and no salt 100 mM Tris-HCl. Protein sample was monitored throughout purification using SDS-PAGE gel stained for total protein and for peroxidase activity based heme stain 3,3',5,5' tetramethylbenzidine (TMBZ) (Smith et al. 2015; Thomas 1976).

5.3.5 Nongrowth ferrihydrite reduction

Deep well plates were prepared with 20 mM ferrihydrite media lacking acetate. Wells had any one, or a combination of flavin mononucleotide (FMN), bovine serum albumin (BSA), horse heart cytochrome *c*, or purified PgcA. 100 μL of 0.6 OD (600nm cells), either wild type *G. sulfurreducens*, or Δ*pgcA* strain, were added to the wells. No cell controls were also included. Cells were allowed to reduce ferrihydrite overnight in an anaerobic chamber with an atmosphere of 20% CO_2, 75% N_2, 5% H_2. FerroZine assay was used for Fe(II) quantification, as described above.

5.3.6 Mass spectrometry

Protein samples that resulted from nickel affinity purification were run on a BisTris, SDS, polyacrylamide gel. Bands at 41 kDA and 57 kDa were excised from the gel. Trypsin digest and LCMS mass spectrometry using Thermo LTQ were performed on each of the band sizes (Center for Mass Spectrometry and Proteomics, University of Minnesota). PEAKS Studio software was used to analyze fragments (BSI Informatics Solutions).

5.3.7 Redox titrations

An anaerobic cuvette was assembled containing two platinum electrodes (one for working, one for counter) and a silver/ silver chloride reference (MF-2052, BasI, West Layfette, Indiana). A mediator cocktail was made such that the final reaction contained 10 μM of each: diaminodurene, phenazine methosulfate, phenazine ethosulfate, anthraquinone 2,6-sulfonate, anthraquinone 2-sulfonate, benzyl viologen and methyl viologen (Marritt et al. 2012). Throughout the course of the redox titration the sample was kept under a stream of argon gas and at 25 °C. 2 mM sodium dithionite (Sigma-Aldrich, St. Louis, Missouri) was added 2 μL at a time until the absorbance spectrum indicated that the absorbance was maximized

at 552 nm (the fully reduced state). Similarly, 2 mM ferricyanide (Sigma-Aldrich, St. Louis, Missouri) was added 2 μL at a time until absorbance spectra indicated no further oxidation could be achieved. Instrumentation composition: Cary 50 dual beam spectrometer, Varian Peltier temperature controller, CH Instruments electrochemical analyzer.

5.3.8 Circular dichroism

Protein sample was dialyzed with 50 mM phosphate with 100 mM sodium fluoride to decrease background signal in ultraviolet region (Greenfield 2007). A JASCO-J815 spectropolarimeter was used to acquire circular dichroism spectra in the range of 185 nm to 600 nm. Samples were maintained at room temperature for the entirety of experimentation. Spectra were analyzed using K2D3 program (Pellegrini, 2015).

Table 5.1Strains used in this study

Strain or Plasmid	**Description**	**Source/Reference**
Strains		
G. sulfurreducens PCA	Wild Type (ATCC 51573)	Lab collection
Δ*pgcA G. sulfurreducens*	Markerless deletion of *pgcA* gene in Wild Type *G. sulfurreducens background*	This study
E. coli S17-1	Donor strain for conjugation	Simon, 1983
Shewanella oneidensis	Wild Type	Myers and Nealson, 1988
Plasmids		
pK18mobsacB	Markerless deletion vector	Schafer, 1994
pRK2-Geo2	Vector control and backbone for complementation vector	Chan et al., 2015
p*pgcA*	Complementation vector with constitutive expression of *pgcA*. *pgcA* was cloned into pRK2Geo2.	This study
pBAD202/D-TOPO®	Arabinose inducible expression vector backbone	Thermo Fisher Scientific
pBAD202PgcA	Arabinose inducible expression vector containing PgcA	This study

5.4 Results

5.4.1 Predicted features and properties of the PgcA protein

The amino acid sequence of the PgcA protein predicts three *c* –type heme binding (CXXCH) motifs and proline rich repetitive elements (Figure 5.1). Tandem repeats are common between PgcA and its known homologs. These were identified using PTRStalker which detects fuzzy tandem repeats (Pellegrini, Renda, and Vecchio 2012; Pellegrini 2015). Fuzzy tandem repeats are computed by a BLOSUM algorithm with a means to weight amino acids by distance and similarity. This results in a theoretical origin string of amino acids from which the tandem repeats diverge (Pellegrini 2015). Within these tandem repeats are simple repeats. For instance, in PgcA, the amino acids threonine (T) and proline (P) are alternated. The *G. sulfurreducens* version of PgcA is unique in the 29 PT_X repetitions inside a fuzzy tandem repeat (Figure 5.1) that it encodes. Homologs from even the most closely related organisms (that have sequences available) have the tandem repeat but also have other paired repeats. For instance, PA_x repeats are found in *G. uranireducens* and *Desulfuromonas soudanensis*. These paired repeats vary in length and level of fuzziness, for instance the *G. metallireducens* homolog does not contain any simple repeats.

A

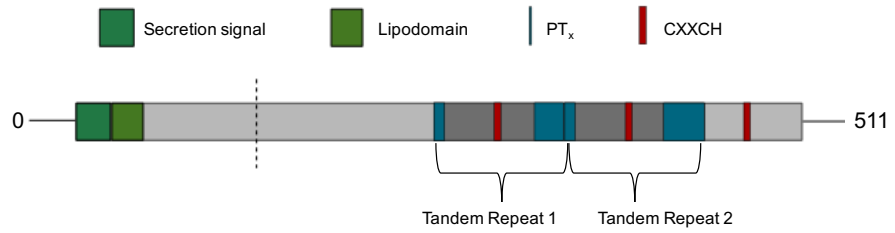

B

Organism	Locus Identifier	Tandem Repeat 1 Sequence
Geobacter sulfurreducens	GSU1761	PTPTPTNTPTPPTPATDGSGLYANNCQACHGAIATNSEIKTRTVARLQSAISANAGGM GFLSSLTSAEIQAIVTSLAVAPTPTPTPTPTPT
Geobacter pickeringii	Ga0069007_11150	TVGTTPAPTPTPAPTATPAPAPTPSPTPAIDGAALYASNCAGCHGALATSSKKGATLT RLQNAISGNVGGMGFLSTLTAAQLQAIANALNGTTTT
Geobacter uraniireducens	GURA_0706	ISKTGVYTSDGTGLSGAMSDAVQATLANGVTIYYAKTAVISAGKSDPNVWNAATDVN PTPAPPAVPAAPAGLTATGGAKQVTLSWNAVSNATSYNVYYSTTSGVTAANGTRIAG ATSPYVQSGLTAGTTYYYIVTAVNSAGESAASTQATATTNATPTPAPPAAPTGVMAT GGANQVTLSWSAVSGATSYNIYST
Geobacter metallireducens	GMET_2185	VGESAPSAQVSATPSAVATVPAAPVATAAAGAGQVTITWPAVTGATSYNLYWSTTTG VTPANGTLIANVTSPYTQTGLTNGTTYFYVVTAVNA
Geobacter bemidijiensis	GBEM_4028	TPPPATTPLDGQALYTQYCNGCHGSAKLGKTALAIQGAINANTGGMGSLSTLTAAQV AAIATTTAPVV
Desulfuromonas sudanensis WTL	Ga0081808_112930	DDHSDEKTRWKRYLNSQTAPDDTPAPAPTPTPTPIPTPTPTPTPTPIDVNGQAVFNSC AGCHTLSGTSKMNLAGDGSKVSSAHNTGSLS

Figure 5.1 *Defining characteristics of PgcA amino acid sequence to scale.* A. Red boxes indicate location of CXXCH *c*-type cytochrome binding motifs. Blue boxes show positions of PT_x dense stretches. Emphasized is the repeating arrangement of PT_x stretches and CXXCH motifs as identified by PTRStalker program. B. Conservation of repetitive pattern and heme motifs in relatives of *G. sulfurreducens*.

PT_X repeats of equal or greater length can be found in putative chitin binding, carbohydrate binding, and cellulose binding proteins. PT_X rich proteins have been reported twice in archaeal viruses. The viral studies strengthen the allusion to a function of viral life outside the host and to a life in extreme environments. *Thermoproteus tenax* virus (TTV) was isolated from a “sulfotaric mud hole” (Katti et al. 2000; Horst Neumann and Zillig 1990; H. Neumann and Zillig 1990) and the ATV hyperthermophilic archaeon virus isolated from the organism *Acidianus convivator*, which is another hyperthermophilic archaeon, was isolated from and Italian hot spring (Prangishvili et al. 2006) To date, there is no known function for these viral proteins. The number of hemes within this set of PgcA homologs varies. Only one CXXCH motif is observable in *G. metallireducens* and six in *G. bemidjiensis*. *G. sulfurreducens* is in the middle with three CXXCH motifs located within the tandem repeat region.

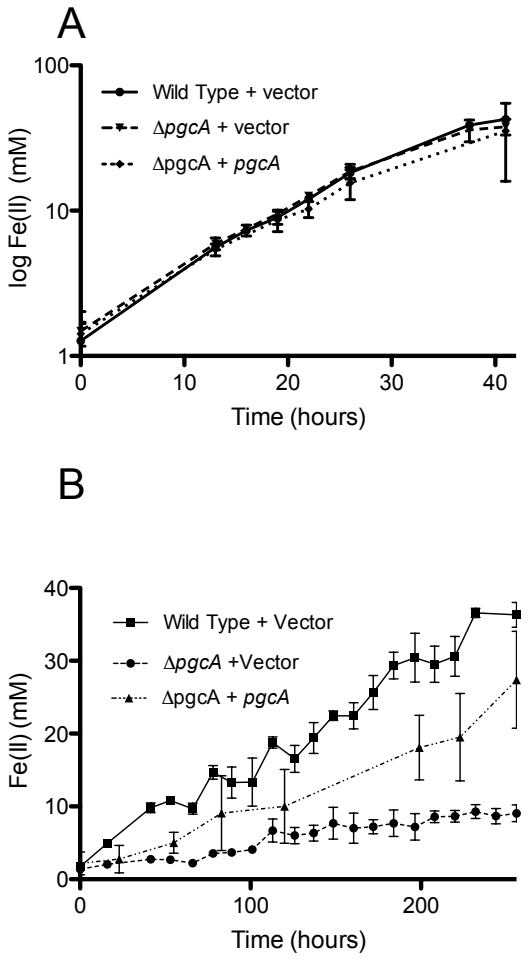

Figure 5.2 *Active respiration phenotypes of Δ*pgcA *and wild type* G. sulfurreducens *using various terminal electron acceptors*. A. Ferric citrate reduction as detected by the presence of Fe(II). B. Ferrihydrite respiration monitored by presence of Fe(II). Fe(II) was detected using FerroZine assay. Error bars are +/- standard deviation of four replicates.

5.4.2 *Geobacter sulfurreducens* cells lacking *pgcA* are metal respiration deficient but capable of electrode respiration

A battery of cell growth dependent tests were used to determine phenotypic differences between *G. sulfurreducens* cells lacking *pgcA* (Δ*pgcA*) and wild type cells. When presented with insoluble electron acceptors such as manganese (birnessite, 350 mV vs. SHE) and iron oxide (ferrihydrite, -100 to +100 mV vs. SHE)(Caccavo et al. 1994; Majzlan 2012) reduction was impaired in the Δ*pgcA* strain (Figure 5.2A)(manganese data not shown). Ferric citrate reduction rate and

final reduction level were no different than in wild type (Figure 5.2B). The doubling time of cells cultured on a graphite electrode was 5.6 days (0.61 standard deviation) for wild type cells (which is faster than previously reported rates likely due to improved reactor design) and was 5.5 days for Δ*pgcA* (standard deviation 0.18)(Figure 3). Δ*pgcA* cells reached a total current density, j, of 557 $\mu A/cm^2$ (standard deviation 97.7 $\mu A/cm^2$) which is not statistically different from wild type containing vector control cells. Complementation of Δ*pgcA* in trans did not hinder growth of cells on the electrode. These results indicate that the role of PgcA is specific to metal oxides such as ferrihydrite and birnessite. The phenotype is not related to the acceptor potential because birnessite and ferrihydrite have enough potential separation to generate a phenotypic difference (as observed previously in other mutants (Zacharoff, Chan, and Bond 2015; Levar et al. 2014). The phenotype of ΔpgcA cells is not related to the distance terminal electrons have to travel. If this was the case, it would be expected that electrode respiration at high and low potentials would also be impaired.

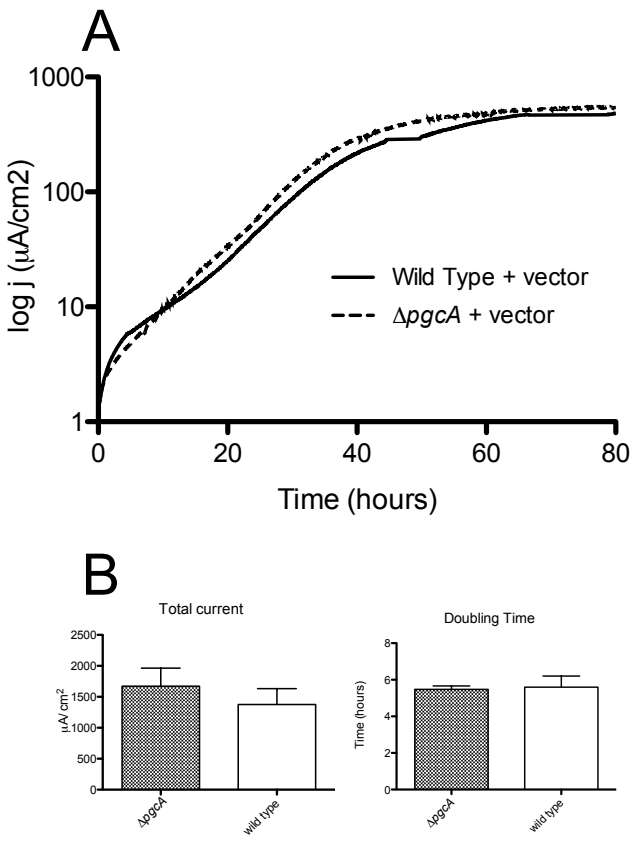

Figure 5.3 *Respiration of Δ*pgcA *and wild type* G. sulfurreducens *biofilms graphite electrodes.* A. Working electrodes were poised at 0.24 mV vs. SHE. Total current density, j, in μA/cm^2 is displayed during the course of biofilm growth in hours. B. Total current is the end point averages of all four bioreactors.

Geobacter strains lacking extracellular matrix components are often characterized by an ability to attach to positively and negatively charged surfaces. In the case of mutants in the *xap* gene cluster (such as GSU1501) hyper attachment to negatively charged surfaces of 96 well plates correlated to a normal ability in iron oxide reduction and an inability to adhere to poised graphite electrodes (Rollefson, Levar, and Bond 2009; Rollefson et al. 2011). As what might be predicted based on the iron oxide reduction phenotype, binding to negatively charged surfaces was slightly diminished in the Δ*pgcA* cells (as determined by crystal violet attachment assay). Compared to wild type vector control cells, 79% of Δ*pgcA* cells bound to

Nunclon polystyrene 96 well cell culture plates. This phenotype is almost opposite to the phenotype of mutants lacking the *xap* genes.

5.4.3 Biochemical assessment of PgcA

In order to investigate the biochemistry of this protein, PgcA was purified. To simplify expression and purification, PgcA was expressed in the host organism *Shewanella oneidensis*, a gamma-proteobacterium. While this organism respires insoluble metal using multiheme cytochromes (Richardson et al. 2012) it also can respire aerobically. In this study, *S. oneidensis* proved capable of generating PgcA in microaerobic conditions. Heme incorporation was determined by pyridine hemochrome assay (see supplemental method 5.7 and supplemental figure 5.2) and by mass spectrometry. The extinction coefficient at 408 nm was determined to 137,000 $M^{-1}cm^{-1}$. It was found that three hemes were incorporated. It was also determined that PgcA exists in a truncated, processed state. Amino acids 1 to 127 were cleaved, leaving a protein the size of 41 kDa. This is consistent with the size of a protein Lovley observed in the extracellular matrix in 1999 (Supplemental Figure 1).

The visible spectrum of PgcA has an absorbance maximum at: 405 nm in the oxidized state. Maxima of the reduced protein are centered at 417 nm (γ or Soret), 518 nm (β), 552 nm (α), (Figure 5.4A). Hemes of PgcA were capable of oxidization and reduction by ferricyanide and sodium dithionite, respectively. PgcA has a high redox potential range that would favor accepting electrons in the extracellular environment (Figure 5.4B). Comparatively, other extracellular multiheme cytochromes of *Geobacter sulfurreducens* have been found to have low midpoint potentials. The *c*-type hemes of OmcZ range in potential from -420 to -60 mV (Inoue, 2010). OmcS hemes have the reported potential range of -340 to -40 mV (Qian, 2011).

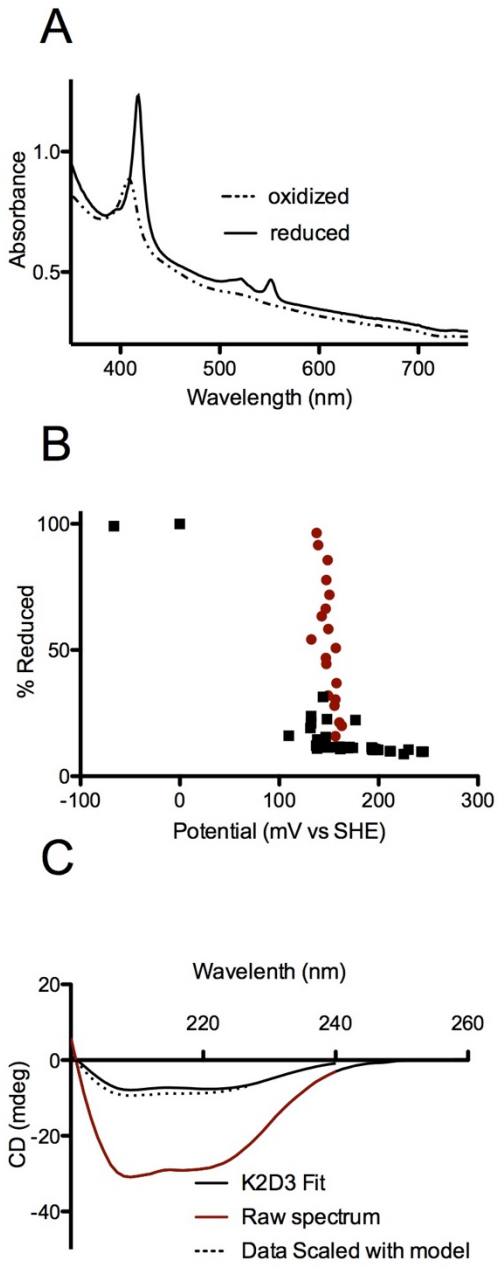

Figure 5.4 *Biochemical characterization of* G. sulfurreducens *PgcA as purified from host* S. oneidensis*.* A. Oxidized and reduced electronic absorption spectroscopy in the visible region. B. Reduction oxidation titration. 100% reduced defined by maximum peak height at 552 nm. Red points indicate data recorded during oxidation. Black points indicate data collected during reduction. C. Circular dichroism. Modeled spectrum generated from K2D3 program.

Proline rich proteins such as collagens have a unique triple helical structure and set some precedence for the ability proline to create unique structures (Greenfield, 2007).) Circular dichroism was used to investigate PgcA secondary structures since a structure of a protein containing PT_x repeats and fuzzy tandem repeats of this nature has not been resolved. Circular dichroism is sensitive to such secondary structures makes the technique ideally suited to studying unique secondary structures of proteins while in solution. It was found that this protein is composed of 70.55% alpha helical character and 5.24% of beta-sheet character (Figure 5.4C). This was determined using K2D3 program (Pellegrini et al. 2015)(Reviewed by (Greenfield 2007). Millidegrees (mdeg) were recorded from 200-240 nanometer wavelengths. No evidence of intrinsic disorder was observed. Determining secondary structure of heme proteins using circular dichroism is not commonly done. In order to determine if hemes contribute to the signal in the UV regions horse heart cytochrome *c* was used as a control. It was determined that horse heart cytochrome *c* contains 93.45%/0.18% alpha helix/beta-sheet, consistent with what is known from the crystal structure (Jordan, 1995). The beta sheet and alpha helical composition of is consistent with the alpha helical bias observed with *c*-type cytochromes (Smith, Kahraman, and Thornton 2010).

5.4.4 Purified PgcA can restore iron reduction capabilities of Δ*pgcA* cells to wild type levels

The purified PgcA was used in an assays to determine if PgcA could complement a Δ*pgcA* mutant extracellularly to restore iron oxide reduction. Previous mass spectrometry papers indicate that PgcA fragments were found in the periplasm (Ding et al. 2006) hence the indicator “periplasm” in the name PgcA. However, these results are not surprising given that all cytochromes begin and complete maturation in the periplasm. Just because a cytochrome is identified in the periplasm does not mean that the periplasm is where the cytochrome performs a function. Operating as a soluble shuttle extracellularly is one possible function of

PgcA. To test this, PgcA was compared with a known electron shuttle, flavin mononucleotide (Kotloski and Gralnick 2013; Hartshorne et al. 2007). Resting mutant and wild type cells were inoculated into nongrowth ferrihydrite and Fe (II) was monitored at time of inoculation, four hours post inoculation and 20 hours post inoculation. In a span of 20 hours wild type *G. sulfurreducens* will generate 3.4 mM ferrous iron. The Δ*pgcA* mutant, however, only generated 0.13 mM Fe(II)(Figure 5.5). Background levels or Fe(II) were also monitored (Supplemental Figure 5.3). Next, resting cells were inoculated into nongrowth ferrihydrite medium containing 0, 10, 50, 100 or 200 mM of flavin mononucleotide (Supplemental Figure 5.4). The reduction of ferrihydrite could not be increased by FMN concentrations above 50 mM. Addition of 10 mM flavin to Δ*pgcA* generated iron reduction levels comparable to wild type. Resting mutant and wild type cells were then inoculated into nongrowth ferrihydrite medium containing purified PgcA, 50 mM flavin mononucleotide or a combination of both. Two different concentrations of PgcA were tested, one physiological (0.02 μM) and one in excess (20 μM). The concentration of 0.02 μM was chosen because this was the protein concentration used in the Loyd and Lovley shuttling assay (1999). Δ*pgcA* iron reduction was recovered with the addition of purified PgcA. Iron reduction of both wild type and Δ*pgcA* could be increased by spiking medium with PgcA, FMN, or PgcA and FMN together. The highest amount of iron reduction in 20 hours was seen in the Δ*pgcA* strain with the combination of FMN and PgcA. It was found that the amount of iron that Δ*pgcA* could possibly reduce in the presence of FMN was saturated at 50 mM FMN. When PgcA was added in addition to 50 mM FMN, 6 mM of iron was reduced. This suggests that the iron that is being accessed by FMN and PgcA is different, for example different potentials. Or it is possible that the mode of action of the FMN and PgcA is different. It could be that PgcA is making more iron accessible to reduction by FMN or vice versa.

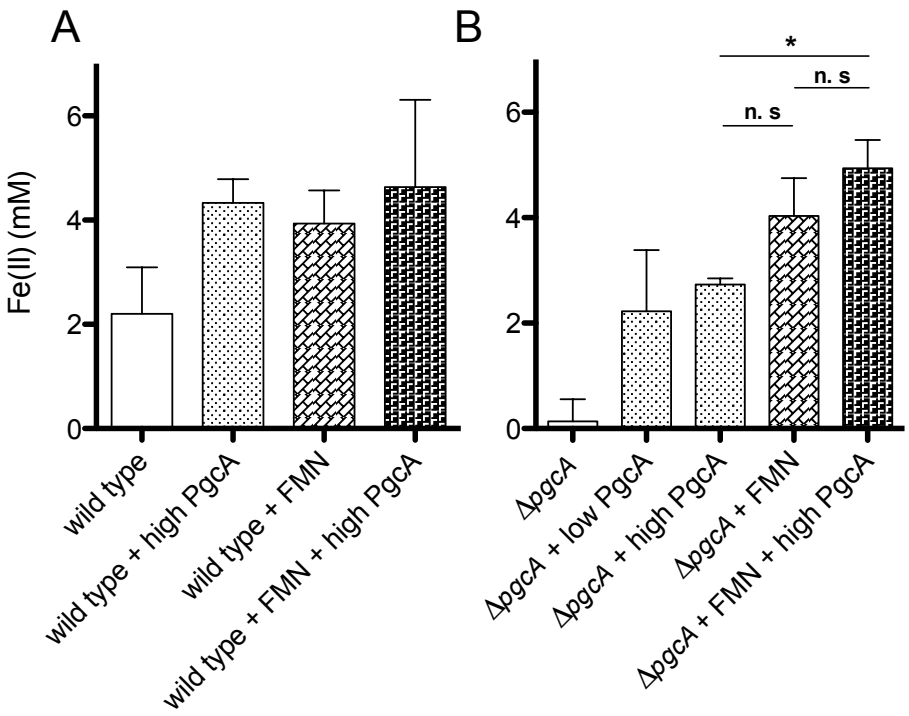

Figure 5.5 *Resting cell assays of PgcA extracellular actions.* A. Resting cells wild type cells were spiked into nongrowth iron oxide. Endpoint iron reduction was analyzed. Cells were treated with flavin mononucleotide (FMN), bovine serum albumin (BSA), horse heart cytochrome *c*, PgcA or a combination of two of the above. B. The same procedure repeated for Δ*pgca* cells. Standard deviations are +/- replicates of three.

5.5 Discussion

G. sulfurreducens is usually classified as a dissimilatory metal reducing organism that uses a “direct contact” method of metal reduction. This is in contrast to organisms that use redox active shuttles to reduce iron, such as *S. oneidensis* and *Geothrix fermentens*. The data presented here on the triheme cytochrome, PgcA makes this distinction less straightforward. PgcA as a soluble electron shuttle is a reasonable explanation for the phenotypes of cells lacking *pgcA* and for biochemical data on PgcA. However, other explanations should be explored, such as the possibility that PgcA is improving contact of cells to insoluble metals.

Aside from the three heme groups of PgcA, the other interesting feature of this protein is the repetitive domains. Repeats of such low complexity are a means to concentrate a particular property, which is why repetitive domains work so well in adhesion in nature and in the laboratory (for instance six-histidine tagged amino acids). Multiple repetitive sequences are common to structural and adhesion proteins in the extracellular space in both prokaryotes and eukaryotes. Bacteria have a precedence in modifying the local extreme extracellular environment with repetitive proteins. Ice nucleation proteins and antifreeze proteins contain larger repetitive regions with simpler repeat amino acid sequences nested within, as with PgcA. The smallest repeating unit of nucleation and antifreeze proteins is TXT (Kobashigawa et al. 2005). These proteins can produce thermal hysteresis as needed by the bacterium.

Ferrouginous soils and sediments harbor the danger of bacteria becoming encrusted in the byproducts of their own metabolism. Electron microscopy and extended x-ray fine structure spectroscopy (EXAFS) have been the methods of choice to mark crystallization patterns of vivianite and siderite forming as seeding crystals from bacterial EPS. This seeding process is one of the sources of bacterial

encrustation. While this crystallization has been documented for a number of organisms, encrustation processes have not been observed in *G. sulfurreducens*. This is true for both natural settings, and laboratory studies involving *Geobacter sulfurreducens* (Lloyd et al. 2010; J. R. Lloyd and Renshaw 2005).

Acknowledgments
Biophysical Resource Center at the University of Minnesota for providing time and training on the JASCO-J815 circular dichroism spectropolarimeter.

5.7 Summary and Future Directions

PgcA has a long history. It has been mentioned in the literature (Tremblay et al. 2011; Smith et al. 2014; Yi et al. 2009a) and has been identified by transposon mutagenesis a handful of times (Bond lab, unpublished). This makes the fact that it has a phenotype not surprising. However, the uniqueness of this protein can only fully be appreciated when time and care is taken to focus on phenotypes specific to this protein. The next experiments to be done should include the effects that this protein can have on metal respiration of other organisms such as *S. oneidensis*. If PgcA does not enhance metal respiration of *S. oneidensis* then the role of PgcA must involve specific interactions with one or more *G. sulfurreducens* proteins. A particularly interesting experiment would be to use *S. oneidensis* strains that do not secrete flavins. One such strain, Δ*bfe* lacks a flavin transporter and has no detectable iron reduction capabilities (Kotloski and Gralnick 2013). If PgcA can recover even some iron reduction by Δ*bfe*, the case for an electron shuttle would be supported.

Whether or not the repetitive sequence of PgcA serves an important function in metal reduction should also be investigated. As shown in Figure 5.1, PgcA homologs contain different repetitive elements and therefore make a reasonable starting point to determine the importance of these repeats. One intriguing

possibility is that PgcA can bind to Fe(III) oxides but not to Fe(II) oxides. This is suggested to be the case by the data shown in Figure 5.6. Purified PgcA was incubated for 10 minutes at room temperature with 55mM Fe(III) oxides and 55 mM Fe(II) oxides. The iron was then pelleted (4,000 × *g*) and the visible electronic absorbance spectrum of the supernatant was measured. Almost 100% of PgcA was pelleted with Fe(III) oxides while 80% of PgcA remained in the supernatant of the Fe(II) oxides sample.

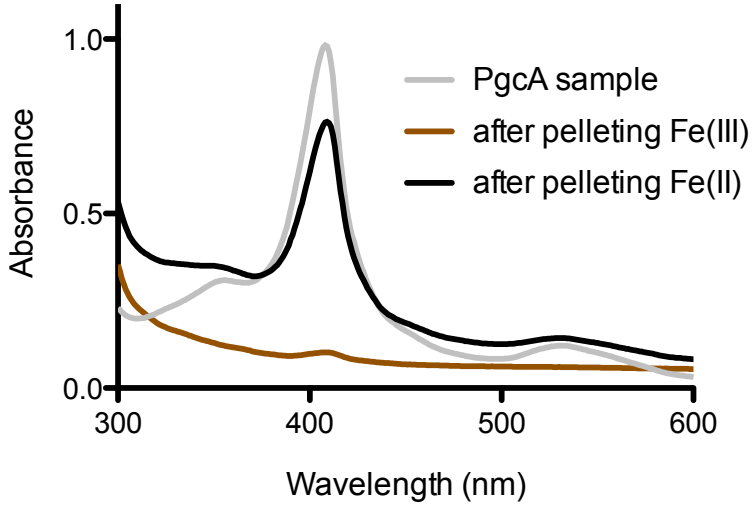

Figure 5.6 *PgcA has a stronger affinity for Fe(III) oxides compared to Fe(II) oxides.* PgcA was spiked into tubes containing either Fe(III) or Fe(II) oxides. The gray trace is the electronic absorbance spectrum of purified PgcA. Black and brown traces are the spectra from the supernatant after pelleting iron species.

5.6 Supplemental Figures

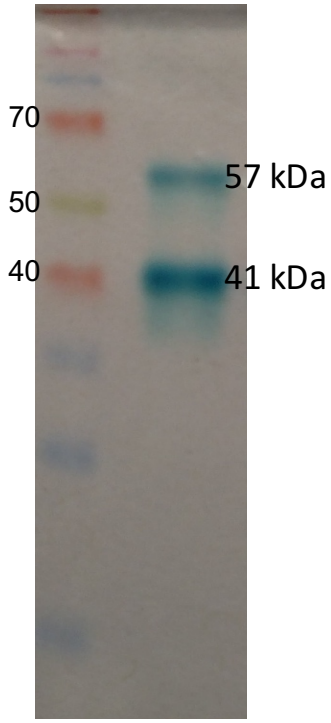

Supplemental Figure 5.1 *Purification of PgcA led to the identification of a smaller version of PgcA*. Heme stain of sample PgcA purified from nickel affinity column. The larger band is confirmed to be the 57 kDA unprocessed version of PgcA. The smaller version is confirmed to be the 41 kDa version of PgcA.

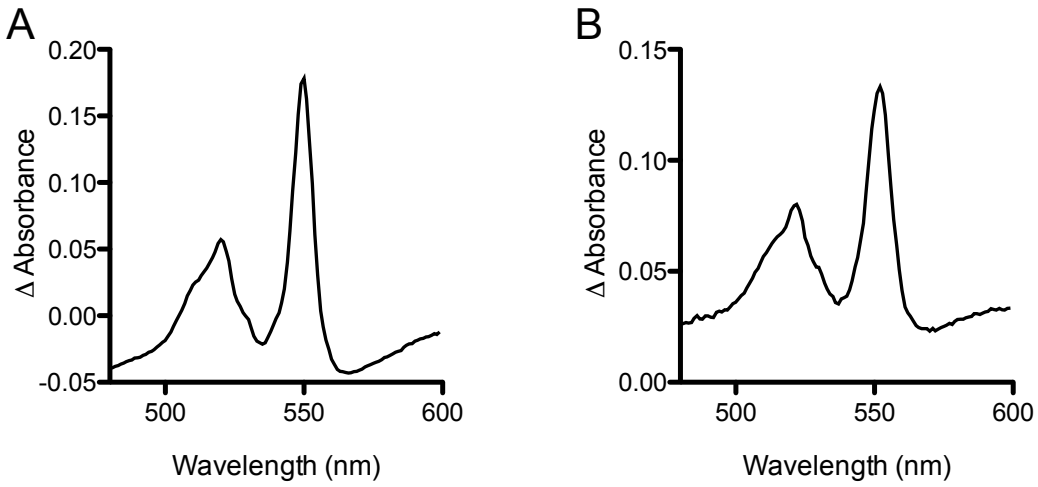

Supplemental Figure 5.2 *Pyridine hemochrome assay.* Cytochrome samples were treated with sodium hydroxide (75 mM final concentration) and pyridine (2.6 mM final concentration). Absorbance differences are oxidized spectra subtracted from reduced pyridine treated samples. A. Electronic absorbance spectrum differences of horse heart cytochrome *c.* B. Electronic absorbance spectrum differences of PgcA.

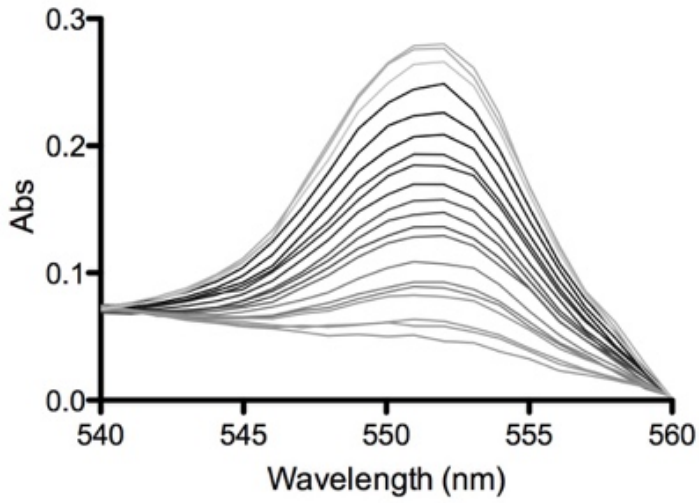

Supplemental Figure 5.3 *Region of UV/Vis spectra used to calculate peak height and percent of PgcA reduced*. Isosbestic points were used to generate a baseline that was subtracted from all peaks.

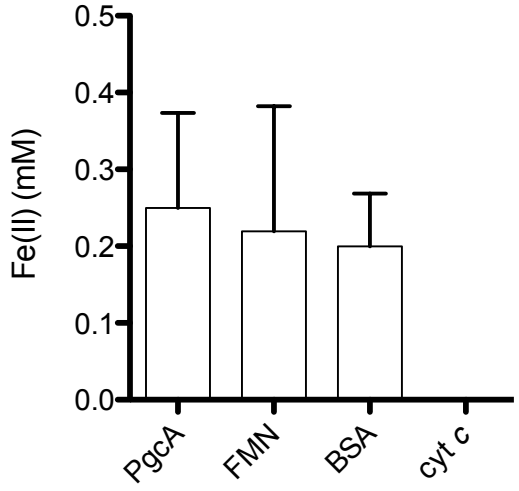

Supplemental Figure 5.4 *No cell control for nongrowth iron oxide experiments*. Concentration are 20 μM PgcA, BSA and horse heart cytochrome *c* (cyt *c*)(Sigma Aldrich, St. Louis, MO) and 200 μM FMN.

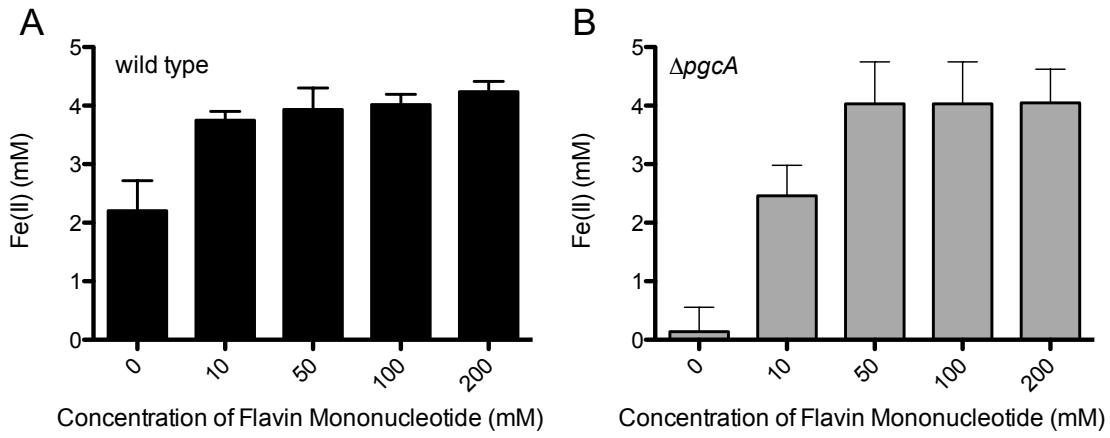

Supplemental Figure 5.5 *Iron reduction in the presence of different concentrations of flavin mononucleotide.* A. Wild type *G. sulfurreducens*. B. Δ*pgcA*.

5.7 Supplemental method – pyridine hemochrome assay and calculations

Reference: Berry, E.A., Trumpower, B.L., Simultaneous determination of hemes-*a*, hemes-*b*, and hemes-*c* from pyridine hemochrome spectra. Anal. Biochem. 161,1–15

For the purpose of biochemical techniques it is of utmost importance to qualify and quantify the number of hemes and the types of hemes that have been incorporated into the multiheme protein of interest. There are three major complications confronted in ultra violet/ visible field spectroscopy when studying multiheme cytochromes. First, even with one protein, and certainly across proteins, heme to heme, extinction coefficients can vary and have an unresovable degree of overlap. This holds true even if the comparison is from *c* type heme, to *c* type heme and also still possible if the axial ligations are also the same, for example. The second problem is that the protein purified protein may not have incorporated all of the hemes that amino acid sequence predicted. And finally, if there are any *a* or *b* type hemes present then the amino acid sequence is less reliable to predict the existence of these heme cofactors.

Trumpower et al, came up with a solution to these problems. The molecule pyridine is a heterocylic compound where the conjugated ring system is composed of five carbons and one nitrogen. In the presence of heme this compound will replace any axial ligands present. (Note on historical nomenclature: when the heme iron is hexacoordinated by nitrogenous bases in both the axial positions, in addition to nitrogens contributed by porhyrin, a hemochrome is said to be formed. Ferroporphyrins are thus hemochromes (haemochromes) and ferriporphyrins are thus hemichromes (heamichromes) (Falk, 1964). Spectroscopically, the result of this is that every heme in a protein will have the same extinction coefficient maxima. The ferricyanide oxidized spectrum is subtracted from the sodium dithionite reduced spectrum. This procedure is performed on a reference protein,

such a the monoheme horse heart cytochrome *c*, as well as the protein of interest. The extinction coefficient is then calculated from the following equation

Assay

For both samples, cytochrome *c* and unknown protein perform the following.

First, prepare 2.5 mL of sample such that A_{410} = 1.0. To this sample add 0.5 mL 0.6M NaOH and 0.68mL of 12.2mM pyridine. Split the samples. 1.7 mL into 2 cuvettes. Add excess sodium dithionite to one, add excess ferricyanide to the other. Collect the electronic absorbance spectra of reduced and oxidized samples. The extinction coefficient ($M^{-1}cm^{-1}$) can then be determined using the mathematical steps that follow.

Calculations

Step 1: Determine the amount of cytochrome *c* (cyt*c*) present in the ferricyanide oxidized sample.

This is done with the previously determined extinction coefficient ($\varepsilon_{\lambda 408nm}$) of 106,000 $M^{-1}cm^{-1}$ and Beer's law (Equation 5.1), solving concentration.

$$\varepsilon_{\lambda 408nm} = \frac{A_{408nm}}{[cytc]\times 1cm} \qquad \text{(Eq 5.1)}$$

Step 2: Subtract the spectra of the oxidized pyridine treated from the spectra of the reduced pyridine treated sample (see supplemental Figure 5.2).

Step 3: For the cytochrome *c* sample, calculate the extinction coefficient difference from the subtracted spectra as follows (Equation 5.2). The absorbance values in Equation 5.2 are from the reduced – oxidized spectrum created in step 2.

$$\Delta\varepsilon_{cytc} = \frac{A_{550}-A_{535}}{[cytc]} \qquad \text{(Eq. 5.2)}$$

Step 4: The change in absorbance for the unknown sample should now be calculated. Using the oxidized – reduced spectrum previously generated, $\Delta A_{unk.} = A_{550} - A_{535}$.

Step 5: The concentration of the unknown cytochrome (unk.) sample can now be calculated using Equation 5.4. Where ℓ is the path length and is usually 1 cm. n is the number of heme groups that are assumed. This equation is solved for the concentration of the known protein.

$$n[unk.] = \frac{\Delta A_{unk.}}{\Delta \varepsilon_{cytc} \times \ell} \quad \text{(Eq. 5.3)}$$

Step 6: Finally, the extinction coefficient for the unknown protein at a wavelength of 408 nm can be calculated (Equation 5.5). The absorbance used in this equation is from the oxidized pyridine treated unknown sample.

$$\varepsilon_{408\ nm} = \frac{A_{408\ nm}}{[unk.] \times \ell} \quad \text{(Eq. 5.4)}$$

The results of this equation can then be compared to the protein concentration of the unknown (which can be determined using a total protein assay, such as a Bradford assay or the absorbance at 280 nm).

Chapter 6: Dissertation conclusions and future work

6.1 On CbcL and the inner membrane of *Geobacter sulfurreducens*

This work is only the beginning of making a case for the involvement of CbcL in the generation of energy maintenance. When this dissertation was first started in 2012, there were no proposed mechanism for inner membrane proteins involved in extracellular electron transfer (Butler, 2010). Now there are two. And the responsivity of these proteins to extracellular electron acceptor potential had not been considered.

Chapter 2 demonstrated that the electrochemical measurement is reflective of the Δ*cbcL* mutants deficient in respiring terminal electron acceptors with relatively low potentials. This ability of CbcL to alter growth and electron transfer properties is followed up in Chapter 3. Mutations in CbcL can recover respiration using high potential electron acceptors in a strain otherwise lacking the capacity to respire to high potential acceptors. The interplay of CbcL and ImcH during metal respiration has generated many hypotheses.

What is the mechanism of CbcL?

To understand the function of CbcL the list of protein biochemistry that needs to be done include: determining the involvement of CbcL in menaquinone cycling, determining why CbcL does not function in respiration to high potential acceptors, and of course, being able to draw a line of electrons entering CbcL and leaving CbcL in a specific sequence of steps. Cyclic voltammetry of purified CbcL could be performed to detect differences in responses to electrical potential. This technique has successfully characterized the kinetics of CymA (McMillan et al. 2012). Comparing electrochemical profiles of CbcL to the profiles of CbcL variants identified in Chapter 3 would demonstrate if CbcL exhibits reversible inactivation.

How is proton motive force maintained and balanced in metal reducing organism in general?

Put another way: what is number of protons pumped per metabolic electron generated. And is there a difference in the amount of energy produce between CbcL and ImcH dependent pathways? Membrane potential sensitive dyes can detect differences in the inner membrane of bacteria. These difference in membrane charge can be detected either by microscopy or by flow cytometry. The balance of ATP/ADP in cells lacking *cbcL* and *imcH* would also be informative of the efficiencies of these pathways. This could be compared to the amount of protein that these mutants are capable of making under different respiratory conditions.

Do these proteins have similar functions in other metal respirers?

Given the widespread nature of these two proteins it seems likely that these mechanisms are more widespread in the bacterial world (Figure 6.1). Other dissimilatory metal reducing bacteria have homologs of *cbcL* and *imcH*. In the genome of *Desulfuromonas soudanensis*, for instance, *cbcL* and *imcH* are only separated by one gene (Badalamenti et al. 2016). Like *G. sulfurreducens*, *D. soudanensis* can respire electrodes. Cyclic voltammetry performed on this organism identified a midpoint potential that is 100 mV more positive than the dominant midpoint potential of *G. sulfurreducens.* Deletion mutants of *cbcL* should be created in *D. soudanensis* to see if CbcL is similarly involved in *D. soudanensis* respiration. Additionally, growth and respiration studies should be conducted on Δ*imcH* and Δ*cbcL* strains to see if these genes have the same specificity to high and low potentials of terminal electron acceptors. This comparison leads to the interesting hypothesis that organisms that have *cbcL* and *imcH* are capable of forming biofilms on poised electrodes.

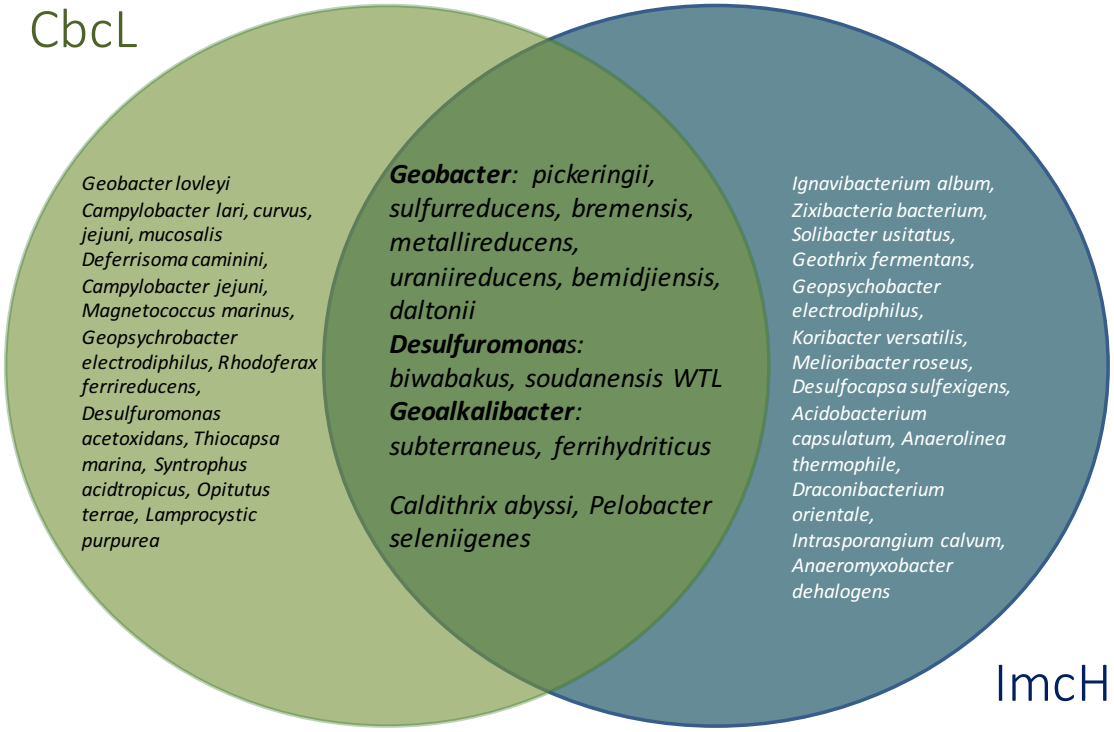

Figure 6.1 *Distribution of CbcL and ImcH in bacteria.* The center of the Venn diagram is a list of organisms that contain a copy of both *imcH* and *cbcL*.

6.2 On the extracellular matrix and PgcA

PgcA has been longed discussed and never studied. The idea that this protein is specific to metals leads to questions about protein mechanism. Chapter 5 characterizes *Geobacter sulfurreducens* mutants lacking *pgcA.* PgcA is demonstrated to be involved in the extracellular respiration of insoluble metals. Some of the characteristics of this protein are similar to that of known redox active shuttles.

Several experiments could be performed to determine the role of PgcA. Microscopy has been used in previous studies to determine the degree to which wild type and mutant *G. sulfurreducens* associate with insoluble iron oxides

(Rollefson et al. 2009). Agar containing cells and insoluble iron oxides were adhered to a coverslip. DAPI, a dye that fluoresces when bound to DNA, was then used to image cells. This is the first experiment that should be done with Δ*pgcA* mutants. The second, experiment recommended would test the ability of PgcA to complement redox shuttling deficient strains of other organisms, such as the *S. oneidensis Δbfe* mutant.

The experiments mentioned above, as well as those performed in Chapter 5 should be repeated with different homologs of PgcA. Since homologs of the PgcA have different repetitive regions and heme content this would help determine what aspect of these domains is important to metal respiration.

Finally, PgcA has been shown to have a stronger affinity for Fe(III) oxides then Fe(II) oxides. Insoluble metals exist in complexes with other each and with other molecules. These metals change potential and forms while being reduced (Nealson and Saffarini 1994). If the experimental means existed, the ability of PgcA to reversibly bind insoluble metal surfaces should be further investigated. This might be alluding to how *G. sulfurreducens* interacts with highly complex metal oxides without the danger of encrustation within the byproducts of respiration.

6.3 Big picture questions that remain to be answered about *G. sulfurreducens* metal respiration

As mentioned in the introduction, there are three energetic challenges involved the respiration of insoluble metals via the direct contact method of *G. sulfurreducens*.

1. The energy that is available to provide a driving force for respiration is relatively small.
2. The distance that electrons have to travel during respiration is far.
3. The terminal electron acceptors themselves are highly complex.

This work has increased the understanding of the three mysteries of *G. sulfurreducens* respiration (Figure 6.2). First, the energy that is available to provide a driving force for respiration is relatively small. In other words, the available free energy based on the electrons acceptor (iron oxides range from -0.3 V to 0.3 V). Energy conservation at the inner membrane has to be highly efficient. This dissertation provides demonstration that the inner membrane protein CbcL is the favored respiratory pathway when the acceptor potential is relatively low. When relatively high metal potentials are available, *G. sulfurreducens* uses an ImcH dependent pathway. The rate limiting step of extracellular respiration is the step that couples electron transfer to energy harvesting. This work also explains *G. sulfurreducens* approach complicated metal oxides.

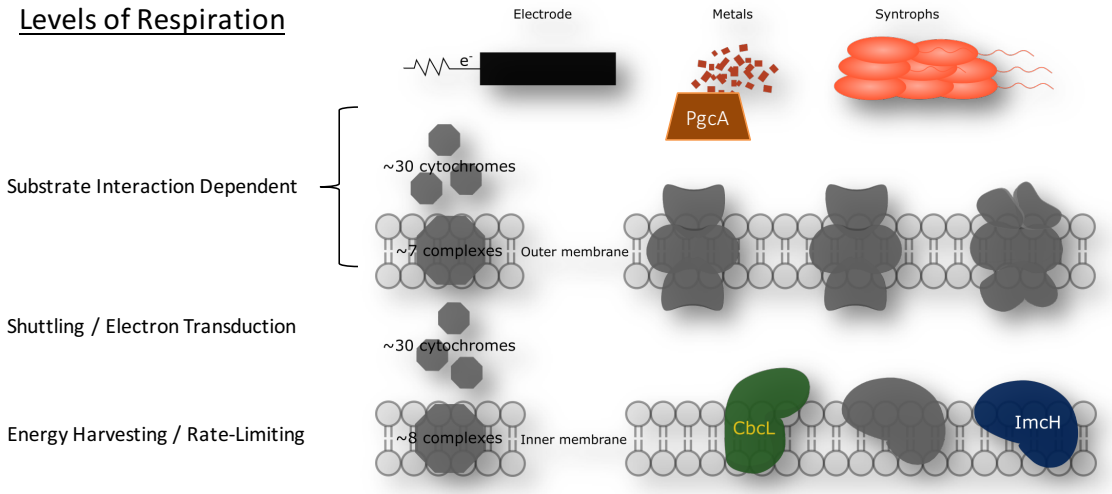

Figure 6.2 *A new prediction of the molecular mechanism of metal respiration in* G. sulfurreducens.

Figure 6.2 illustrates what was identified in this dissertation as well as highlighting that this is just a small fraction of the questions that still remain. At the inner membrane, there must be other proteins that are capable of transferring electrons out of the inner membrane. This is based on cyclic voltammetry data presented in Chapter 2. There are 3 other *cbc* gene operons that has not been presented in this

dissertation. Gene deletion studies of these proteins should be carried on. While early studies on these genes have been ambiguous (Ding 2008; Aklujkar 2013) it would be interesting to revisit these proteins in light of the data presented here. For instance, in the present day, genetic manipulation of *G. sulfurreducens* now includes a scarless gene deletion strategy and complementation vectors specifically designed for *G. sulfurreducens.* This new system allows for gene deletions to be stacked. This will eliminate the complication of "pathway overlap." For example, the *cbc* gene operons all contain a gene encoding a periplasmic *c* type cytochrome. By deleting one of these it might be possible for another to compensate for the deleted cytochrome.

Finally, poised electrodes were long called a "proxy" terminal electron acceptor for insoluble metals. Since it is now clear that *G. sulfurreducens* can discern between poised electrodes and metals, there must be an additional reason for why *G. sulfurreducens* is capable of forming biofilms on electrodes. The ability of *G. sulfurreducens* to form syntrophic relationships (Shrestha et al. 2013) is an exciting new condition to test for respiratory phenotypes in the inner membrane and in the extracellular matrix.

References

Aklujkar, M., Coppi, M.V., Leang, C., Kim, B.C., Chavan, M.A, Perpetua, L.A., Giloteaux, L., Liu, A., and Holmes, D.E. 2013. Proteins involved in electron transfer to Fe(III) and Mn(IV) oxides by *Geobacter sulfurreducens* and *Geobacter uraniireducens*. Microbiology. 159: 515-535.

Aklujkar, M., and Lovley, D.R. 2010. Interference with histidyl-tRNA synthetase by a CRISPR spacer sequence as a factor in the evolution of *Pelobacter carbinolicus*. BMC Evolutionary Biology. 10: 230.

Armstrong, F. A. 1999. Electron transfer and coupled processes in protein film voltammetry. Biochemical Society Transactions 27 (2): 206–10.

Badalamenti, J. P., Summers, Z. M., Chan, C. H., Gralnick, J. A., and Bond, D. R. 2016. Isolation and genomic characterization of *Desulfuromonas soudanensis* WTL, a metal- and electrode-reducing bacterium from anoxic deep subsurface brine. Frontiers in Microbiology. 7 (June): 913.

Berry, E.A., Trumpower, B.L., Simultaneous determination of hemes-*a*, hemes-*b*, and hemes-*c* from pyridine hemochrome spectra. Anal. Biochem. 161,1–15

Bird, L., Bonnefoy, V., Newman, D.K. 2011. Bioenergetic challenges of microbial iron metabolisms. Trends in Microbiology 19 (7): 330–40.

Blöthe, M., and Roden, E.E. 2009. Microbial iron redox cycling in a circumneutral-pH groundwater seep. Applied and Environmental Microbiology 75 (2): 468–73.

Bond, D.R., Holmes, D.E., Tender, T.M., and Lovley, D.R. 2002. Electrode-reducing microorganisms that harvest energy from marine sediments. Science. 295: 483-485.

Brune, A., and Schink, B. 1990. Pyrogallol-to-phloroglucinol conversion and ather hydroxyl-transfer reactions catalyzed by cell extracts of *Pelobacter acidigallici*. Journal of Bacteriology 172 (2): 1070–76.

Butler, J. E., Young, N. D., and Lovley, D. R. 2010. Evolution of electron transfer out of the cell: comparative genomics of six *Geobacter* genomes. Bmc Genomics 11: 40.

Bowman, SEJ, and Bren, KL. 2008. The chemistry and biochemistry of heme *c*: functional bases for covalent attachment. Natural Product Reports 25 (6): 1118–30.

Breuer, M., Rosso, K.M., Blumberger, J., and Butt, J.N. 2015. Multi-haem cytochromes in *Shewanella oneidensis* MR-1: structures, functions and opportunities. Journal of the Royal Society Interface. 12 (102): 20141117.

Butler, J.E., Young, N.D., and Lovley, D.R. 2010. Evolution of electron transfer out of the cell: comparative genomics of six *Geobacter* genomes. Bmc Genomics 11: 40.

Caccavo, F., Lonergan, D. J., Lovley, D.R., Davis, M., Stolz, J.F., and McInerney, M.J. 1994. *Geobacter sulfurreducens* sp. nov., a hydrogen- and acetate-oxidizing dissimilatory metal-reducing microorganism. Applied and Environmental Microbiology 60 (10): 3752–59.

Caccavo, F., Lonergan, D. J., Lovley, D. R., Davis, M., Stolz, J. F., and Mcinerneyl, M. J. 1994. Oxidizing dissimilatory metal-reducing microorganism. Microbiology 60 (10): 3752–59.

Canfield, E., Rosing, T.M., and Bjerrum, C. 2006. Early anaerobic metabolisms. Philosophical Transactions of the Royal Society of London. Series B, Biological Sciences 361 (1474): 1819–34; discussion 1835–36.

Canstein, v. H., Ogawa J., Shimizu S., Lloyd J. R. 2008. Secretion of flavins by *Shewanella* species and their role in extracellular electron transfer. Applied and Environmental Microbiology. 74:615–623.

Chan, C.H., Levar, C.E., Zacharoff, L., Badalamenti, J.P., Bond, D.R. 2015. Scarless genome editing and stable inducible expression vectors for *Geobacter sulfurreducens*. Applied and Environmental Microbiology 81 (20): 7178–86.

Compton, R.G, Banks, C. E., Understanding Voltammetry. 153-188 (2007). World Scientific Publishing. Singapore.

Commault, S.A., Lear, G, Packer, M., and Weld, R.J. 2013. Influence of anode potentials on selection of *Geobacter* strains in microbial electrolysis cells. Bioresource Technology 139: 226–34.

Coursolle, D, and Gralnick, JA. 2012. Reconstruction of extracellular respiratory pathways for iron (III) reduction *in Shewanella oneidensis* strain MR-1. Frontiers in Microbiology 3: 1–11.

Ding, Y., Hixson, K.K., Aklujkar, M.A., Lipton, M.S., Smith, R.D., Lovley, D.R., and Mester, T. 2008. Proteome *of Geobacter sulfurreducens* grown with Fe(III) oxide or Fe(III) citrate as the electron acceptor." Biochimica et Biophysica Acta 1784 (12): 1935–41.

Ding, Y., Hixson, K.K., Giometti, C.S., Stanley, A., Esteve-Núñez, A., Khare, T., Tollaksen, S.L. 2006. The proteome of dissimilatory metal-reducing microorganism *Geobacter sulfurreducens* under various growth conditions. Biochimica et Biophysica Acta 1764 (7): 1198–1206.

Einsle, O., Stach, P., Messerschmidt, A., Simon, J., Kroger, A., Huber, R., Kroneck, P.M. 2000. Cytochrome *c* nitrite reductase from *Wolinella succinogenes*. Journal of Biological Chemistry 275 (50): 39608–16.

Falk, J. E. 1964. Porphyrins and metalloporphyrins: their general, physical and coordination chemistry, and laboratory methods, Volume 2. Elsevier Publishing Company. Amsterdam, Netherlands.

Fleige, S., and Pfaffl, M.W. 2006. RNA integrity and the effect on the real-time qRT-PCR performance. Molecular Aspects of Medicine 27: 126–39.

Fufezan, C., Zhan, J., Gunner, M. R. 2008. Ligand preference and orientations in *b*- and *c*-type heme binding proteins. Proteins. 73 (3): 690–704.

Glockner, A. B., and Zumft, W.G. 1996. Sequence analysis of an internal 9.72-kb segment from the 30-kb denitrification gene cluster of *Pseudomonas stutzeri*. *Biochimica et Biophysica Acta* 1277: 6–12.

Grant, M.R., Tymon, L.S., Helms G.L., Thomashow, L.S., Keller, K. and Harsh, J.B. 2016. Biofilm adaptation to iron availability in the presence of biotite and consequences for chemical weathering. Geobiology. Ahead of print.

Gray, H. B., and Winkler, J. R. 2009. Electron flow through proteins. Chemical Physics Letters. 483 (1-3) 1–9.

Greenfield, NJ. 2007. Using circular dichroism spectra to estimate protein secondary structure. Nature Protocols. 6: 2867-90.

Hamelers, H., Heijne, A.T., Stein, N., Rozendal, R., and Buisman, C.J.N. 2011. Butler-Volmer-Monod model for describing bio-anode polarization curves. Bioresource Technology 102 (1): 381–87.

Hartshorne, R. S., Jepson, B. N., Clarke, T. A., Field, S. J., Fredrickson, J., Zachara, J., Shi, L., Butt, J. N., and Richardson, D. J. 2007. Characterization of *Shewanella oneidensis* MtrC: a cell-surface decaheme cytochrome involved in respiratory electron transport to extracellular electron acceptors. Journal of Biological Inorganic Chemistry. 12 (7): 1083–94.

Hartshorne, R. S., Reardon, C.L., Ross, D., Nuester, J., Clarke, T.A., Gates, A.J., Mills, P.C. 2009. Characterization of an electron conduit between bacteria

and the extracellular environment. Proceedings of the National Academy of Sciences of the United States of America 106 (52): 22169–74.

Ishii, S., Suzuki, S., Norden-krichmar, T.M., Tenney, A., Chain, P.S.G, Scholz, M.B., Nealson, K.H. and Bretschger, O. 2013. A novel metatranscriptomic approach to identify gene expression dynamics during extracellular electron transfer. Nature Communications. (4)1601:1–10.

Inoue, Kengo, Xinlei Qian, Leonor Morgado, Byoung-Chan Kim, Tünde Mester, Mounir Izallalen, Carlos a Salgueiro, and Derek R Lovley. 2010. Purification and characterization of OmcZ, an outer-surface, octaheme *c*-type cytochrome essential for optimal current production by *Geobacter sulfurreducens*. *Applied and Environmental Microbiology* 76 (12): 3999–4007.

Jormakka, M., Törnroth S., Byrne B., Iwata S. 2002. Molecular basis of proton motive force generation: structure of formate dehydrogenase-N. Science 295: 1863–68.

Katti, M.V., Sami-Subbu, R., Ranjekar, P.K., and Gupta, V.S. 2000. Amino acid repeat patterns in protein sequences: their diversity and structural-functional implications. Protein Science. 9 (6): 1203–9.

Kellenberger, C.A., Wilson, S.C., Hickey, S.F., Gonzalez, T.L., Su, Y., Hallberg, Z.F., Brewer, T.F. 2015. GEMM-I riboswitches from *Geobacter* sense the bacterial second messenger cyclic AMP-GMP. Proceedings of the National Academy of Sciences. 112 (17): 5383-8.

Kim, B.-C., Postier, B.L., Didonato, R.J., Chaudhuri, S.K., Nevin, K.P., and Lovley, D.R. 2008. Insights into genes involved in electricity generation in *Geobacter sulfurreducens* via whole genome microarray analysis of the OmcF-deficient mutant. Bioelectrochemistry. 73 (1): 70–75.

Kleingardner, J.G.., and Bren, K.L. 2015. Biological significance and applications of heme *c* proteins and peptides. Accounts of Chemical Research. 48(7):1845-52.

Klimes, A., Franks, A.E., Glaven, R.H., Tran, H., Barrett, C.L., Qiu, Y., Zengler, K., and Lovley, D.R. 2010. Production of pilus-like filaments in *Geobacter Sulfurreducens* in the absence of the type IV pilin protein PilA. FEMS Microbiology Letters 310 (1): 62–68.

Kobashigawa, Y., Nishimiya, Miura, K., Ohgiya, S., Miura, A., Tsuda, Sakae. 2005. Part of ice nucleation protein exhibits the ice-binding ability. FEBS Letters 579: 1493-1497.

Kotloski, N.J., and Gralnick, J.A. 2013. Flavin electron shuttles dominate extracellular electron transfer by *Shewanella oneidensis*. mBio 4 (1): 10–13.

Leang, Ching, M V Coppi, and D R Lovley. 2003. OmcB, a *c*-type polyheme cytochrome, involved in Fe(III) reduction in *Geobacter sulfurreducens*. Journal of Bacteriology. 185 (7): 2096–2103.

Leang, Ching, Xinlei Qian, Tünde Mester, and Derek R Lovley. 2010. Alignment of the c-Type Cytochrome OmcS along Pili of *Geobacter sulfurreducens*. Applied and Environmental Microbiology. 76 (12): 4080–84.

Lebedev, N., Strycharz-Glaven, S. M., and Tender, L. M. 2014. Spatially resolved confocal resonant raman microscopic analysis of anode-grown *Geobacter sulfurreducens* Biofilms. *Chemphyschem*. January, 1–9.

Levar, C.E., Chan, C.H, Mehta-Kolte, M.G., and Bond, D.R. 2014. An inner membrane cytochrome required only for reduction of high redox potential extracellular electron acceptors. mBio. 5 (6): 1–9.

Lies, D. P., Hernandez, M. E., Kappler, A., Mielke, R. E., Gralnick, J. A., Newman, J. K. 2005. *Shewanella oneidensis* MR-1 uses overlapping pathways for iron reduction at a distance and by direct contact under conditions relevant for biofilms. 71 (8): 4414-26.

Liu, Y., Bond, Daniel. 2012 Long-distance electron transfer by *G. sulfurreducens* biofilms results in accumulation of reduced *c*-type cytochromes. ChemSusChem Communications. 5 (7): 1047-1053.

Liu, J., Chakraborty, S., Hosseinzadeh, P., Yu, Y., Tian, S., Petrik, I., Bhagi, A., and Lu, Y. 2014. Metalloproteins containing cytochrome, iron-sulfur, or copper redox centers. Chemical Reviews. 114 (8): 4366–69.

Liu, Y., Wang, Z., Liu, J., Levar, C., Edwards, M. J., Babauta, J. T., Kennedy, D. W., Shi, Z., Beyenal, H., Bond, D. R., Clarke, T. A., Butt, J. N., Richardson, D. J., Rosso, K. M., Zachara, J. M., Fredrickson J. K., Shi, L. 2014. A trans-outer membrane porin-cytochrome protein complex for extracellular electron transfer by *Geobacter sulfurreducens* PCA. Environmental Microbiology Reports. 2014 6(6):776-85.

Liu, Y., Kim, H., Franklin, R. R., Bond, D. R. 2011. Linking spectral and electrochemical analysis to monitor c-type cytochrome redox status in living *Geobacter sulfurreducens* biofilms. Chemphyschem. 12 (12): 2235–41.

Leang, C., Qian, X., Mester, T., Lovley, D. R. 2010. Alignment of the *c*-type cytochrome OmcS along pili of *Geobacter sulfurreducens*. Applied Environmental Microbiology. 76:4080–4084.

Lloyd, J. R., and Renshaw, J. C. 2005. Bioremediation of radioactive waste: radionuclide–microbe interactions in laboratory and field-scale studies. Current Opinion in Biotechnology. 16 (3): 254–60.

Lloyd, K. G., Albert, D.B., Biddle, J.F., Chanton, J.P., Pizarro, O. and Teske, A. 2010. Spatial structure and activity of sedimentary microbial communities underlying a *Beggiatoa* spp. mat in a Gulf of Mexico hydrocarbon seep. PloS One 5 (1): e8738.

Londer, Y. Y., Dementieva, I. S., D'Ausilio, C. A., Pokkuluri, P. R., Schiffer, M. 2006. Characterization of a *c*-type heme-containing PAS sensor domain from Geobacter sulfurreducens representing a novel family of periplasmic sensors in *Geobacteraceae* and other bacteria. FEMS Microbiology Letters. 258 (2): 173–81.

Lovley, D. R., Phillips, E. J., Lonergan, D. J., Widman, P. K. 1995. Fe(III) and S0 reduction by *Pelobacter carbinolicus*. Applied Environmental Microbiology. 61 (6): 2132–38.

Lovley, D.R., and Phillips, E.J.P. 1986. Organic matter mineralization with reduction of ferric iron in anaerobic sediments organic matter mineralization with reduction of ferric iron in anaerobic sediments. Applied Environmental Microbiology. 51 (4): 683–89.

Lusk, B.G., Badalamenti, J.P., Parameswaran, P., Bond, D.R., and Torres, C. 2015. Draft genome sequence of the gram-positive thermophilic iron reducer *Thermincola ferriacetica* strain Z-0001T. Genome. A 3 (5): 1072–73.

Mahadevan, R., Bond, D.R., Butler, J.E., and Coppi, M.V. 2006. Characterization of metabolism in the Fe (III) -reducing organism *Geobacter sulfurreducens* by constraint-based modeling. Applied and Environmental Microbiology. 72 (2): 1558–68.

Majzlan, J. 2012. Minerals and aqueous species of iron and manganese as reactants and products of microbial metal respiration. In Microbial Metal Respiration; from Geochemistry to Potential Applications, edited by Gescher, J. and Kappler, A.

Marritt, S. J., Lowe, T. G., Bye, J., McMillan, D. G., Shi, L., Fredrickson, J., Zachara, J., Richardson, D. J., Cheesman, M. R., Jeuken, L. J., Butt, J. N. 2012.

A functional description of CymA, an electron-transfer hub supporting anaerobic respiratory flexibility in *Shewanella*. *The Biochemical Journal* 444 (3): 465–74.

Marritt, S. J., McMillan, D. G., Shi, L., Fredrickson, J. K., Zachara, J. M., Richardson, D. J., Jeuken, L., Butt, J. N. 2012. The roles of CymA in support of the respiratory flexibility of *Shewanella oneidensis* MR-1*. Biochemical Society Transactions.* 40 (6): 1217–21.

Marsili, E., Baron, D.B, Shikhare, I.D., Coursolle, D., Gralnick, J. G., and Bond, D.R. 2008. *Shewanella* secretes flavins that mediate extracellular electron transfer. Proceedings of the National Academy of Sciences of the United States of America 105 (10): 3968–73.

Marsili, E., Rollefson, J.B., Baron, D.B., Hozalski, R.M., and Bond, D.R. 2008. Microbial biofilm voltammetry: direct electrochemical characterization of catalytic electrode-attached biofilms. Applied and Environmental Microbiology 74 (23): 7329–37.

Marsili, Sun and Bond 2010). Voltammetry and Growth Physiology of Geobacter sulfurreducens Biofilms as a Function of Growth Stage and Imposed Electrode Potential. Electroanalysis. 22:865–874.

McMillan, D. G., Marritt, S. J., Butt, J. N., and Jeuken, L. 2012. Menaquinone-7 is a specific cofactor in tetraheme quinol dehydrogenase CymA. Journal of Biological Chemistry*.* 287 (17): 14215–25.

McMillan, D. G., Marritt, S. J., Firer-Sherwood, M. A, Shi, L., Richardson, D. J., Evans, S. D., Elliott, S. J., Butt, J. N., Jeuken, L. 2013. Protein-protein interaction regulates the direction of catalysis and electron transfer in a redox enzyme complex. Journal of the American Chemical Society. 135 (28): 10550–56.

Mehta-Kolte, M. G., and Bond, D.R. 2012. *Geothrix fermentans* secretes two different redox-active compounds to utilize electron acceptors across a wide range of redox potentials. Applied and Environmental Microbiology 78 (19): 6987–95.

Mehta T, Coppi MV, Childers SE, Lovley DR. 2005. Outer membrane *c*-type cytochromes required for Fe(III) and Mn(IV) oxide reduction in Geobacter sulfurreducens. Applied Environmental Microbiology. 71:8634–8641.

Merkley, E. D., Wrighton, K., Castelle, C.J., Anderson, B. J., Wilkins, M. J., Shah, V., Arbour, T. 2015. Changes in protein expression across laboratory and field experiments in *Geobacter bemidjiensis*. Journal of Proteome Research, 14 (3): 1361 - 1375.

Methé, B. A., Nelson, K. E., Eisen, J. A., Paulsen, I. T., Nelson, W., Heidelberg, J. F., Wu, D. Wu, M., Ward, N., Beanan, M. J., Dodson, R. J., Madupu, R., Brinkac, L. M., Daugherty, S. C., DeBoy R. T., Durkin, A. S., Gwinn, M., Kolonay, J. F., Sullivan, S. A., Haft, D. H., Selengut, J., Davidsen, T. M., Zafar, N., White, O., Tran, B., Romero, C., Forberger, H. A., Weidman, J., Khouri, H., Feldblyum, T. V., Utterback, T. R., Van Aken, S. E., Lovley, D. R., Fraser, C. M. 2003. Genome of *Geobacter sulfurreducens*: metal reduction in subsurface environments. *Science.* 302 (5652): 1967–69.

Millo, Diego. 2012. Spectroelectrochemical analyses of electroactive microbial biofilms. Biochemical Society Transactions. 40 (6): 1284–90.

Mitchell, P. 1979. Keilin's respiratory chain concept and its chemiosmotic consequences. Science 206 (4423): 1148–59.

Mitchell, P. 1961. Coupling of phosphorylation to electron and hydrogen transfer by a chemiosmotic type of mechanism. Nature 191:144–148.

Morgado, L., Bruix, M., Londer, Y., Pokkuluri, R., Schiffer, M., and Salgueiro, C. A. 2007. Redox-linked conformational changes of a multiheme cytochrome from *Geobacter sulfurreducens*. Biochemical and Biophysical Research Communications 360: 194–98.

Morgado, L., Paixão, V. B., Schiffer, M., Pokkuluri, P. R., Bruix, M., Salgueiro, C. A.. 2012. Revealing the structural origin of the redox-Bohr effect: the first solution structure of a cytochrome from *Geobacter sulfurreducens*. The Biochemical Journal. 441 (1): 179–87.

Munro, A. W., Girvan, H. M., McLean, K., J., Cheesman, M. R., Leys, D.. 2009. Tetrapyroles: Birth, life and death, edited my Warren, M. J., Smith, A. G. Chapter 10: Heme and Hemoproteins. Landes Bioscience and Springer Science + Business Media.

Myers C. R., Myers, J.M. 1997. Cloning and sequence of *cymA*, a gene encoding a tetraheme cytochrome *c* required for reduction of iron(III), fumarate, and nitrate by *Shewanella putrefaciens* MR-1. Journal of Bacteriology. 179:1143–1152.

Nealson, K H, and D Saffarini. 1994. Iron and manganese in anaerobic respiration: environmental significance, physiology, and regulation. Annual Review of Microbiology 48: 311–43.

Neumann, H., and Zillig, W. 1990. Structural variability in the genome of the *Thermoproteus* Tenax virus TTV1. Molecular and General Genetics. 222 (2-3): 435–37.

Neumann, H., and Zillig, W. 1990. The TTV1-Encoded Viral Protein TPX: Primary Structure of the Gene and the Protein. 18 (1): 1990.

Nevin, K. P., Richter, H., Covalla, S. F., Johnson, J. P., Woodard, T. L., Orloff, A. L., Jia, H., Zhang, M., and Lovley, D. R. 2008. Power output and columbic efficiencies from biofilms of *Geobacter sulfurreducens* comparable to mixed community microbial fuel Cells. Environmental Microbiology. 10 (10): 2505–14.

Nevin, K. P., Lovley, D. R. 2002. Mechanisms for accessing insoluble Fe(III) oxide during dissimilatory Fe(III) reduction by *Geothrix fermentans*. Applied Environmental Microbiology. 68:2294–2299

Nevin, K. P., Lovley, D. R. 2002. Mechanisms for Fe(III) oxide reduction in sedimentary environments. Geomicrobiology Journal. 19:141–159.

Nevin, K. P., Lovley, D. R. 2000. Lack of production of electron-shuttling compounds or solubilization of Fe(III) during reduction of insoluble Fe(III) oxide by *Geobacter metallireducens*. Applied Environmental Microbiology. 66:2248–2251.

Nevin, K. P., Kim, B.-C., Glaven, R. H., Johnson, J. P., Woodard, T. L., Methe, B. A., DiDonato, R. J., Covalla, S. F., Franks, A. E., Liu, A., Lovley, D. R. 2009. Differences in physiology between current-producing and fumarate-reducing biofilms of *Geobacter sulfurreducens*: identification of a novel outer-surface cytochrome essential for electron transfer to anodes at high current densities. PLoS One 4:e5628.

Nicholls, David, and Ferguson, S. 2002. Bioenergetics 3. Amsterdam: Academic Press.

Pellegrini, M. 2015. Tandem Repeats in Proteins: Prediction Algorithms and Biological Role. Frontiers in Bioengineering and Biotechnology. 3 (143).

Pellegrini, M., Renda, E. M., and Vecchio, E. 2012. Ab initio detection of fuzzy amino acid tandem repeats in protein sequences. BMC Bioinformatics. 13 (Suppl 3): S8.

Perez-Iratxeta C., Andrade-Navarro, M. A. 2007. K2D2: estimate of protein secondary structure from circular dichroism spectra. *BMC Structural Biology*, **8**-25.

Pirbadian, S., and El-Naggar, M. 2012. Multistep hopping and extracellular charge transfer in microbial redox chains. Physical Chemistry Chemical Physics. DOI: 10.1039/c2cp41185g

Pocaznoi, D., Erable, B., Delia, M.-L., and Bergel, A. 2012. Ultra microelectrodes increase the current density provided by electroactive biofilms by improving their electron transport ability. Energy and Environmental Science. 5 (1): 5287.

Polizzi, N. F., Skourtis, S. S., and Beratan, D. N. 2012. Physical constraints on charge transport through bacterial nanowires. Faraday Discussions 155: 43.

Prangishvili, D., Vestergaard, G., Häring, M., Aramayo, R., Basta, T., Rachel, R., and Garrett, R. A. 2006. Structural and genomic properties of the hyperthermophilic archaeal virus ATV with an extracellular stage of the reproductive cycle. Journal of Molecular Biology 359 (5): 1203–16.

Qian, X., Mester, T., Morgado, L., Arakawa, T., Sharma, M. L., Inoue, K., Joseph, C., Salgueiro, C. A., Maroney, M. J., and Lovley, D. R. 2011. Biochemical characterization of purified OmcS, a *c*-type cytochrome required for insoluble Fe(III) reduction in *Geobacter sulfurreducens*. Biochimica et Biophysica Acta. 1807 (4): 404–12.

Qiu, Y., Cho, B.-K., Park, Y. S, Lovley, D., Palsson, B. Ø., and Zengler, K. 2010. Structural and operational complexity of the *Geobacter sulfurreducens* Genome. Genome Research 20 (9): 1304–11.

Qiu Y, Nagarajan H, Embree M, Shieu W., Abate, E., Juarez, K., Cho, B. K., Elkins, J. G., Barret, C. L., Lovley, D. R., Palsson, B. O., Zengler, K. 2013. Characterizing the interplay between multiple levels of organization within bacterial sigma factor regulatory networks. *Nature Communications.* 4:1755.

Rabaey, K., Boon, N., Siciliano, S. D., Verstraete, W., and Verhaege, M. 2004. Biofuel cells select for microbial consortia that self-mediate electron transfer. Applied Environmental Microbiology 70 (9): 5373–5358.

Reguera, G., Nevin, K. P., Nicoll, J. S., Covalla, S. F., Woodard, T. L., Lovley, D. R. 2006. Biofilm and nanowire production leads to increased current in *Geobacter sulfurreducens* fuel cells. Applied Environmental Microbiology. 72 (11): 7345–48.

Richardson, D. J., Edwards, M. J., White, G. F., Baiden, N., Hartshorne, R. S., Fredrickson, J., Shi, L. Zachara J, Gates, A. J., Butt, J. N/, Clarke, T.A. 2012. Exploring the biochemistry at the extracellular redox frontier of bacterial mineral Fe(III) respiration. Biochemical Society Transactions. 40 (79): 493–500.

Richardson, D., and Sawers, G. 2002. PMF through the redox loop. Science 295. 1842.

Richter, H., Nevin, K. P., Jia, H., Lowy, D. A., Lovley, D. R., and Tender, T.M. 2009. Cyclic voltammetry of biofilms of wild type and mutant *Geobacter sulfurreducens* on fuel cell anodes indicates possible roles of OmcB, OmcZ, type IV pili, and protons in extracellular electron transfer. Energy and Environmental Science 2 (5): 506–16.

Rollefson, J. B., Levar, C. E., and Bond, D. R. 2009. Identification of genes involved in biofilm formation and respiration via mini-himar transposon mutagenesis of *Geobacter sulfurreducens.* Journal of Bacteriology. 191 (13): 4207–17. d

Rollefson, J.B., Stephen, C. S., Tien, M., and Bond, D. R. 2011. Identification of an extracellular polysaccharide network essential for cytochrome anchoring and biofilm formation in *Geobacter sulfurreducens*. Journal of Bacteriology 193 (5): 1023–33.

Rose, N. D., and Regan, J. M. 2015. Changes in phosphorylation of adenosine phosphate and redox state of nicotinamide-adenine dinucleotide (phosphate) in *Geobacter sulfurreducens* in response to electron acceptor and anode potential variation. Bioelectrochemistry. 06(Pt A): 213-20.

Salas, E. C., Berelson, W. M., Hammond, D. E., Kampf, A. R., and Nealson, K. H. 2011. The impact of bacterial strain on the products of dissimilatory iron reduction. Geochim Cosmochim Acta. 74 (May 2009): 574–83.

Schafer, A., Tauch, A., Jager, W., Kalinowski, J., Thierbach, G., and Puhler, A. 1994. Small mobilizable multi-purpose cloning vectors derived from the *Escherichia coli* plasmids pK18 and pK19: selection of defined deletions in the chromosome of *Corynebacterium glutumicum*. Gene. 145: 69–73.

Sharma, S., Cavallaro, G., Rosato, A. 2010. A Systematic investigation of multiheme *c*-type cytochromes in prokaryotes. Journal of Biological Inorganic Chemistry. 15 (4): 559–71.

Schrott G. D., Ordoñez, M. V., Robuschi, L., Busalmen, J. P. 2014. Physiological stratification in electricity-producing biofilms of *Geobacter sulfurreducens*. ChemSusChem. 7:598–603.

Sharma, S., Cavallaro, G., Rosato, A. 2010. A systematic investigation of multiheme *c*-type cytochromes in prokaryotes. Journal of Biological Inorganic Chemistry. 15 (4): 559–71.

Shrestha, P. M., Rotaru, A.-E., Aklujkar, M., Liu, F., Shrestha, M., Summers, Z.M., Malvankar, N., Flores, D. C., and Lovley, D. R. 2013. Syntrophic growth

with direct interspecies electron transfer as the primary mechanism for energy exchange. Environmental Microbiology Reports. 5 (6): 904–10.

Simon, R., Priefer, U., Puhler, A. 1983. A broad host range mobilization system for in *vivo* genetic engineering: transposon mutagensis in Gram negative bacteria. *Biotechnology* 1: 784–91.

Silberberg, M.S., 2003. Chemistry: The molecular nature of matter and change. 3rd edition. McGraw-Hill. New York, NY.

Simon, R., Priefer, U., Puhler, A. 1983. A broad host range mobilization system for in vivo genetic engineering: transposon mutagenesis in gram negative bacteria. Biotechnology. 1: 784–91.

Simon, J, van Spanning, R. J. M., and Richardson, D. J. 2008. The organisation of proton motive and non-proton motive redox loops in prokaryotic respiratory systems. Biochimica et Biophysica Acta. 1777 (12). Elsevier B.V.: 1480–90.

Simpkin, D., Palmer, G., Devlin, F. J., McKenna, M. C., Jensen, G.M., and Stephens, P. J. 1989. The axial ligands of heme in cytochromes: a near-infrared magnetic circular dichroism study of yeast cytochromes *c*, *c*1, and *b* and spinach cytochrome *f*. Biochemistry. 28 (20): 8033–39.

Smith, D. M. A., and Rosso, K. M. 2014. Possible dynamically gated conductance along heme wires in bacterial multiheme cytochromes. Journal of Physical Chemistry. B 118 (29): 8505–12

Smith, Dayle M A, and Kevin M. Rosso. 2014. Possible dynamically gated conductance along heme wires in bacterial multiheme cytochromes. *Journal of Physical Chemistry. B* 118 (29): 8505–12.

Smith, J. A., Tremblay, P. L., Shrestha, P. M., Snoeyenbos-West, O. L., Franks, A. E., Nevin, K. P., Lovley, D. R. 2014. Going wireless: Fe(III) oxide reduction without pili by *Geobacter sulfurreducens* strain JS-1. Applied and Environmental Microbiology. 80 (14): 4331–40.

Smith, J. A., Aklujkar, M., Risso, C., Leang, C., Giloteaux, L., Holmes, D. E. 2015. Mechanisms involved in Fe(III) Respiration by the hyperthermophilic archaeon *Ferroglobus placidus*. Applied and Environmental Microbiology. 81 (8): 2735–44.

Smith, L. J., Kahraman, A., Thornton, J. M. 2010. Heme proteins--diversity in structural characteristics, function, and folding. *Proteins* 78 (10): 2349–68.

Snider, R. M., Strycharz-Glaven, S. M., Tsoi, S. D., Erickson, J. S., and Tender, L. M. 2012. Long-range electron transport in *Geobacter sulfurreducens* biofilms Is redox gradient-driven. Proceedings of the National Academy of Sciences of the United States of America. 109 (38): 15467–72.

Straub, K. L., Hanzlik, M., and Buchholz-Cleven, B. E. 1998. The use of biologically produced ferrihydrite for the isolation of novel iron-reducing bacteria. Systematic and Applied Microbiology 21 (3): 442–49.

Straub, K. L., and Schink, B. 2004. Ferrihydrite reduction by *Geobacter* species is stimulated by secondary bacteria. Archives of Microbiology 182 (2-3): 175–81.

Strycharz-Glaven, S. M., Snider, R. M., Guiseppi-Elie, A., and Tender, L. M. 2011. On the electrical conductivity of microbial nanowires and biofilms. Energy and Environmental Science. 4 (11): 4366–79.

Strycharz, S. M., Malanoski, A. P., Snider, R. M., Yi, H., Lovley, D. R., and Tender, L. M. 2011. Application of cyclic voltammetry to investigate enhanced catalytic current generation by biofilm-modified anodes of *Geobacter sulfurreducens* strain DL1 vs. variant strain KN400. Energy and Environmental Science. 4 (3): 896–913.

Torres, C. I., Marcus, A. K., Rittmann, B. E. 2008. Proton transport inside the biofilm limits electrical current generation by anode-respiring bacteria. Biotechnology and Bioengineering. 100 (5): 872–81.

Torres, C. I., Marcus, A. K., Lee, H.-L., Parameswaran, P., Krajmalnik-Brown, R., Rittmann, B. E. 2010. A kinetic perspective on extracellular electron transfer by anode-respiring bacteria. *FEMS Microbiology Reviews* 34 (1): 3–17.

Torres, C. I.. 2014. On the importance of identifying, characterizing, and predicting fundamental phenomena towards microbial electrochemistry applications. *Current Opinion in Biotechnology. 27* (June): 107–14.

Tremblay, P.-L., Summers, Z., M., Glaven, R. H., Nevin, K. P., Zengler, K., Barrett, C. L., Qiu, Y., Palsson, B. Ø., and Lovley, D. R. 2011. A *c*-Type cytochrome and a transcriptional regulator responsible for enhanced extracellular electron transfer in *Geobacter sulfurreducens* revealed by adaptive evolution. Environmental Microbiology. 13 (1): 13–23.

Venkateswaran, K., Moser, D., Dollhopf, M., Lies, D., Saffarini, D., MacGregor, B., Ringelberg, D., White, D., Nishijima, M., Sano, H., Burghardt, J., Stackebrandt, E., Nealson, K. 1999. Polyphasic taxonomy of the genus *Shewanella* and description of *Shewanella oneidensis sp*. nov. International Journal of Systematic Bacteriology. 49:705-724.

Vincent, K. A., Parkin, A., Lenz, O., Albracht, S. P., Fontecilla-Camps, J. C., Cammack, R., Friedrich, B., Armstrong, F. A. 2005. Electrochemical definitions of O2 sensitivity and oxidative inactivation in hydrogenases. Journal of the American Chemical Society. 127 (51): 18179–89.

Virdis, B., Harnisch, F., Batstone, D. J., Rabaey, K., and Donose, B. C. 2012. Non-invasive characterization of electrochemically active microbial biofilms using confocal raman microscopy. Energy & Environmental Science. 5 (5): 7017–24.

Voet and Voet, 2011. Biochemistry, 4th Edition. John Wiley and Sons, Inc. Hoboken, NJ. U. S. A.

Wall, Judy D, and Lee R Krumholz. 2006. Uranium Reduction. Annual Review of Microbiology. 60: 149–66.

Weber, K. A., Achenbach, L. A., and Coates, J. D. 2006. Microorganisms pumping iron: anaerobic microbial iron oxidation and reduction. Nature Reviews Microbiology. 4 (10): 752–64.

Weber, K. A., Urrutia, M. M., Churchill, P. F., Kukkadapu, R. K., and Roden, E. E. 2005. Anaerobic redox cycling of iron by freshwater sediment microorganisms. Environmental Microbiology. 8 (1): 100–113.

Yi, H., Nevin, K. P., Kim, B.-C., Franks, A. E., Klimes, A., Tender, L. M., and Lovley, D. R. 2009. Selection of a variant of *Geobacter sulfurreducens* with enhanced capacity for current production in microbial fuel cells. Biosensors and Bioelectronics 24 (12): 3498–3503.

Yoho, R. A., Popat, S. C., and Torres, C. I. 2014. Dynamic potential-dependent electron transport pathway shifts in anode biofilms of *Geobacter sulfurreducens*. ChemSusChem. 7 (12): 3412-9.

Zacharoff, L., Chan, C. H., and Bond, D. R. 2015. Reduction of low potential electron acceptors requires the CbcL inner membrane cytochrome of *Geobacter sulfurreducens*. Bioelectrochemistry. 107: 7- 13.

Zhu, X., Yates, M. D., Hatzell, M. C., Rao, H. A., Saikaly, P. E., and Logan, B. E. 2014. Microbial community composition is unaffected by anode potential. Environmental Science & Technology. 48: 1352 – 1358.